UNIVERSITY OF READING

DEPARTMENT OF METEOROLOGY

Improving the Simulation and Understanding of Biologically Driven Carbon Pumps in Marine Ecosystems using an Ensemble-Based Data Assimilation Method

Thesis submitted for the degree of Doctor of Philosophy

DAVID SURSHAM

JULY 2018

In Collaboration with the Plymouth Marine Laboratory

Abstract

The transfer of carbon dioxide between the ocean and the atmosphere, and within the ocean interior, can be described by constituent "carbon pumps". These carbon pumps are driven by biological and physical processes. The biological components can be separated into the "biological carbon pump", which describes the cycling of carbon in the upper layers driven by photosynthesis in phytoplankton, and the "microbial carbon pump", which describes the bacterial transformation of dissolved organic carbon into a slowly degradable form in the deep ocean. Understanding these processes requires both sophisticated marine ecosystem models and observations of the ocean carbon cycle.

This thesis proposes that the simulation and understanding of the carbon pumps can be improved through data assimilation. Data assimilation is the process of incorporating observations (data) into a dynamic model to improve the accuracy of the simulations. This thesis makes use of ocean colour observations obtained by satellite imaging, assimilated into the marine ecosystem model ERSEM.

The first objective of this study is to provide evidence that assimilating ocean colour data into a marine ecosystem model improves the simulation of carbon fluxes in the ocean, which is supported by results from identical twin experiments. The second objective is to improve the understanding of the biological and microbial carbon pumps and their variability across different marine locations. This was achieved by comparing the results of ocean colour data assimilation reanalyses at a nutrient rich coastal site and a nutrient-poor open-ocean site.

A major finding of this study is that nutrient concentrations control the strength of the biologically driven carbon pumps, with the microbial carbon pump showing dominance in nutrient poor environments.

Acknowledgements

I would first like to thank the Plymouth Marine Laboratory, where I spent the majority of my time during this PhD, for facilitating my research. In particular I thank my supervisor, Dr Stefano Ciavatta, for his continuous support throughout my PhD and for being available whenever possible to answer questions and work through any problems. I would also like to thank Professor Peter Jan van Leeuwen, for many useful discussions and for helping me to understand theoretical data assimilation concepts, particularly related to particle filtering. I am also grateful for Dr Luca Polimene, for sharing his knowledge on the microbial carbon pump and for helping out with the interpretation of the results relating to the carbon pumps. I also extend my thanks to Dr Phil Browne who was managing the EMPIRE data assimilation framework at the time of this work, for his help with integrating EMPIRE with the ERSEM model.

On a personal note, I would like to thank my mother, who has continuously supported me in my efforts and has always been there to help me. I would also like to thank my partner Jena, for her much appreciated company and support during my time working on this PhD.

Declaration

I confirm that this is my own work and the use of material from other sources has been properly and fully acknowledged.

Signed: David Sursham

Contents

Chapter 3

Twin Experiments

Chapter 4

Ocean Colour Assimilation at Station L4

Chapter 5

Ocean Colour Assimilation at BATS

Chapter 1

Introduction

1.1. Overview and Motivation

Atmospheric concentrations of carbon dioxide have increased since the industrial revolution, and are now the highest they have been in 800,000 years (IPCC Fifth AR 2013). The ocean has absorbed about 30% of anthropogenic CO_2 emissions, which has placed an importance on the understanding of ocean carbon fluxes in recent scientific research. While the rate of this uptake is relatively well constrained (2.2 ± 0.3 Pg C per year), the processes responsible for carbon sequestration in the ocean are not well understood.

While many physical and chemical processes are important drivers of the ocean carbon fluxes, biologically driven processes also make a significant contribution. This study will focus on the biological components of the carbon fluxes, with a primary focus on the roles of phytoplankton and bacteria.

Phytoplankton are microscopic marine plants. They are predominantly single-celled and are mostly confined to the surface layers of the ocean due to their dependence on sunlight for survival. They absorb light to undergo photosynthesis by means of pigments called chlorophyll, which influences the colour of the ocean surface. This can be detected from space using satellite imaging (e.g. Zhang et al., 2017) in a product known as "ocean colour", which is now routinely monitored by several space agencies worldwide.

The global distribution of chlorophyll concentration, which can be inferred directly from ocean colour data, varies annually due to spatial and seasonal variations of the phytoplankton community biomass in the marine environment. This is driven by changes in solar irradiance, temperature, spatial gradients of nutrient availability, and grazing by secondary producers. Figure 1.1 illustrates

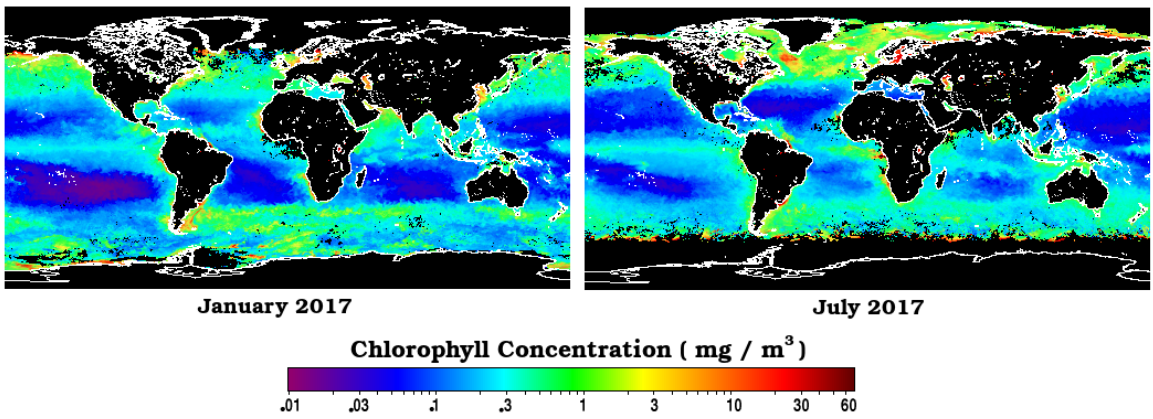

Figure 1.1: A comparison of the global distribution of chlorophyll for January and June of 2017. Data shown was retrieved from MODIS, a remote sensing instrument launched by NASA[DOI: https://oceancolor.gsfc.nasa.gov/cgi/browse.pl].

these variations from a NASA data set. In this figure, a higher chlorophyll concentration is observed in coastal waters compared the deep ocean due to an increase in nutrient availability. Higher concentrations are also typically seen in the northern hemisphere in the summer months, as well as the southern hemisphere in winter months, due to the differences in average daily exposure to sunlight during different seasons.

Chlorophyll concentration is an indicator of phytoplankton biomass (carbon content). However, the ratio between the carbon and chlorophyll concentration within the phytoplankton cells is not constant but varies as a function of irradiance, temperature and nutrient concentration (Geider et al., 1987). Therefore, monitoring the concentration of chlorophyll across the year allows us to obtain information about the phytoplankton contributions to many ocean carbon fluxes, such as primary production, predator-prey interactions between zooplankton and phytoplankton, the sinking of dead phytoplankton cells, and the seasonal variability of such processes. These possibilities provide a basis for using surface chlorophyll data from ocean colour to gain an insight into carbon cycling in marine ecosystems.

In addition to phytoplankton, bacteria are another key biological contributor to the ocean carbon fluxes. They are also micro-organisms, but unlike phytoplankton, maintain their presence in the deeper ocean. Bacteria compete with phytoplankton for uptake of nutrients, particularly nitrate, phosphate and ammonium (Caron, 1994). However, due to their nutrient uptake efficiency, they are mostly dominant in oligotrophic (nutrient-poor) regions, where bacterial biomass is similar to that of phytoplankton. They play a pivotal role in marine carbon cycling due to their interactions with dissolved organic matter (DOM), including its consumption and processing of the DOM. Much of this matter is cycled through the oceans by transportation and remineralisation at greater depths.

It is possible to infer bacterial processes by observing DOM (Kähler et al., 1997), through a means similar to that of phytoplankton processes and ocean colour. However, the availability of DOM data is currently low. Despite this, modelling bacterial processes is still necessary for the understanding of carbon cycling in the deep ocean, and is therefore a vital inclusion in marine ecosystem models (Polimene et al., 2012).

The roles of phytoplankton and bacteria in the cycling of carbon are incorporated into two mechanisms known as the biological carbon pump (BCP; Falkowski, 2012) and the microbial carbon pump (MCP; Jiao, et al., 2010). These pumps will be outlined here, but are explained in more detail in section 1.3.1.

The BCP describes the transport of organic matter in both dissolved and particulate form due to gravitational sinking and vertical mixing. This is enabled through primary production at the surface and the subsequent trophic interactions in the deeper layers of the ocean. Current estimates suggest that the BCP exports 5-12 Pg C y^{-1} from the euphotic zone (the region at the surface where sunlight is sufficient for photosynthesis) to the "twilight zone" (the region in the

deep ocean where carbon is sequestered on time scales up to millennia; Siegel et al. 2016).

The MCP, which was only recently conceptualised, describes the bacterially mediated transformation of dissolved organic carbon from labile (easily degradable) to recalcitrant (slowly degradable) forms. Modern estimates of the current rate of recalcitrant dissolved organic matter (RDOM) production range from 0.07 to 0.6 Pg C per year, indicating a critical one-order magnitude of uncertainly for this process (Jiao et. al., 2010).

The relative dominance of BCP and MCP is thought to be dependent on seasonal and inter-annual climate variability and nutrient gradients in the global ocean (Jiao et. al., 2013). However, high uncertainty in the relative influence of the two pumps remains due to the difficulty of observing the organic and inorganic carbon stocks and fluxes in the ocean. There is also a poor understanding of the patterns of the variability of biological carbon fluxes in relation to climate oscillations and trophic gradients in the ocean.

Marine biogeochemical models such as the European Regional Seas Ecosystem Model (ERSEM; Blackford et al., 2004, Butenschön et al., 2016) are now able to simulate many of the biological processes involved in these pumps. They have been used to quantify carbon fluxes and budgeting in the ocean (e.g Wakelin et al., 2012), and recent efforts towards the integration of ocean-colour data into marine ecosystem models has led to revised estimates of carbon fluxes in the ocean through assimilation algorithms (e.g. Ciavatta et al., 2016). Carbon pumps in marine models are explained in more detail in section 1.3.2, with an in-depth description of the ERSEM model in section 2.2.1.

There are now opportunities to take the approach of data incorporation in marine models further due to the recent availability of high frequency data from remote sensing projects (e.g. ESA OC-CCI) (Zibordi et al., 2010). There are also

comprehensive in-situ datasets from diverse monitoring sites of the global ocean (e.g. station L4 in the North West European shelf and BATS in the oligotrophic North Atlantic gyre). By integrating marine ecosystem models with ESA OC-CCI data, there is potential for a better understanding of the global variability of the BCP and MCP.

The process of combining models with data is known as "data assimilation" (DA) (see section 1.3.3 for more details). This is a huge area of research in its own right, and subsequently DA techniques are often applied to models without a thorough exploration of the benefits of using alternative DA techniques. This thesis incorporates a discussion of the operational side of DA and experiments with a newer techniques, in addition to the discussion of its outcomes in this application. This is included in light of the well-documented challenges that marine biogeochemical models such as ERSEM face when applying DA methods, which is due to the high-dimensionality, non-linear and positive-definite nature of many of the biogeochemical variables (Dowd et al., 2014).

Potential problems with applying DA in this area still persist when using conventional methods such as the Ensemble Kalman Filter, particularly as it assumes that the model error covariances form a Gaussian (and therefore linear) distribution. This problem increases further when the degree of non-linearity of the relationships between state variables changes depending on particular spatial dynamics, such as the position of the mixed layer depth in the water column. This argues for a closer examination of alternative non-linear DA techniques (Van Leeuwen, 2009), which is explored as a potential alternative in this thesis in the identical twin experiments presented in Chapter 3.

1.2. Objective and Procedure

The aim of this project is to improve the understanding and simulation of carbon pumps in the ocean by assimilating ocean colour data into marine ecosystem models. This was achieved by applying an ensemble-based DA method to the marine ecosystem model ERSEM. To this end, two distinct monitoring sites were considered for DA application to capture the variability in the carbon pumps (BCP and MCP) across different parts of the ocean.

The first step made to satisfy this objective was to identify the most effective DA method for providing the best representation of the carbon fluxes. For this, two different DA methods, the Ensemble Transform Kalman Filter (ETKF) and the Implicit Equal Weights Particle Filter (IEWPF), were applied in controlled twin experiments. These experiments have three main aims: (1) to support the case that assimilating ocean-colour can improve the simulation of carbon fluxes, (2) to assess the suitability of competing DA techniques, (3) to tune the parameters of the selected DA algorithm for its subsequent application in real ecosystem simulations. Chapter 3 is dedicated to describing these twin experiments and their results.

Then, the assimilation of ESA OC-CCI ocean colour data was performed with the objective to quantify the inter-annual variability of the carbon fluxes in two environmentally distinct regions of the global ocean. These areas were chosen based on the availability of data and so that they would encompass both open ocean and coastal regions, as well as nutrient rich and nutrient poor locations, to investigate the impact of different nutrient regimes on the relative intensity of fluxes involved in the BCP and MCP. Therefore, the assimilation of ocean colour was considered at two sites: Station L4 and the site for the Burmuda Atlantic Time-Series Study (BATS). The location of these sites is shown in figure 1.2.

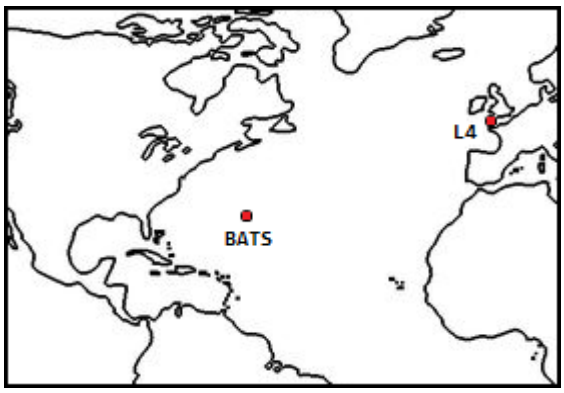

Figure 1.2: The location of Station L4 and BATS in relation to the North Atlantic

To validate the assimilation of ocean colour at these sites, available in-situ measurements of other biogeochemical variables were used to examine the "closeness" of the assimilation ensemble to these data compared to a simulation without assimilation. The results of this validation are outlined in Chapter 4 (for Station L4) and Chapter 5 (for BATS).

The results were then post-processed in Chapter 6 to explain the differences in the MCP and BCP in relation to the nutrient regimes at the two sites. This provides a key result for this thesis, showing that the DA reanalyses can help in efforts to understand complex ecosystem processes.

In summary, this thesis makes a case for the inclusion of the assimilation of ocean colour in efforts to calculate the carbon fluxes and understand the carbon pumps in the oceans. It presents estimates for the extent of improvement of the carbon flux representation on the basis of the twin experiments, and provides evidence of improvements at sites with different biogeochemical properties. From the results it is possible to see the benefit of DA in terms of improved accuracy and to infer some dynamic properties of the ecosystem.

The remainder of this chapter includes a literature review of the background material that this project intends to build upon. Chapter 2 will discuss the methodological details of the model, observations and DA methods. Chapter 3

will show the results of the twin experiments, and discuss how they can be used to inform the real data-assimilation products. Chapter 4 will present results from ocean-colour assimilation at station L4, and Chapter 5 will do the same for BATS. Chapter 6 will provide a comparison of the variability of the dominance of the carbon pumps between the sites, which will be based on the results provided by the previous two chapters. Finally chapter 7 will summarise the achievements of this project and outline possible future directions.

1.3. Background Material

1.3.1 Understanding the Ocean Carbon Pumps

The term "carbon pump" describes a mechanism that transports carbon dioxide (CO_2). This idea was explored in an ocean context by Volk and Hoffert, (1985), who defined and investigated different types of carbon pumps. They defined an ocean carbon pump as "a process that depletes the ocean surface of CO_2 relative to the deep-water CO_2". Following this, they reasoned that the global ocean carbon pump can be described as a system of component pumps. Their proposition was that the ocean pump should be separated into three constituents: the "soft-tissue pump", the "solubility pump", and the "carbonate pump".

The "soft-tissue" pump describes the vertical redistribution of CO_2, both by its incorporation into phytoplankton cells, and by the subsequent gravitational sinking of particulate organic carbon (POC) into the deeper ocean. This process now forms the basis of what is known as the "biological carbon pump" (BCP) (Figure 1.3), a term which in more recent years has become a partial replacement to the term "soft-tissue", as examined by Sigman and Haug, (2003). They suggest that the BCP is a consideration of all biologically driven sequestration of CO_2, and therefore the soft-tissue pump could be considered a subcategory of this. Falkowski et al., (2012) discusses some of the additional processes that now comprise the BCP, such as the breakdown of the organic carbon in phytoplankton by its predators (e.g. zooplankton) and the decomposition of dead organic matter by bacteria.

The "solubility pump" (SCP) describes the physio-chemical processes in the ocean. This term is still widely used, and is discussed by Falkowski et al., (2000), where it is said to be primarily driven by the increased solubility of CO_2 in lower temperatures and higher salinity. Further transportation is provided through the dynamics and thermohaline circulation. While the SCP is an essential component

of the global carbon cycle, it is largely omitted from this thesis to maintain a focus on the biological contributions.

The remaining "carbonate pump" named by Volk and Hoffert, (1985), first emerged as an additional process that was subtracted from the combined signal of the solubility and soft-tissue pumps. This pump, studied extensively in Ridgewell and Zeebe, (2006), is driven by the mineral calcium carbonate ($CaCO_3$), the precipitation of which results in an increase in pCO_2 (partial pressure of CO_2) due a re-partitioning of undissolved carbon in favour of aqueous CO_2. This pump consists of many biological factors, particularly due to the use of calcium carbonate as a protective shell in many types of plankton, but this is outside the scope of this thesis.

A comparison of the relative contributions of these pumps was performed by Cameron at al., (2005), which used a factorial analysis to conclude that the soft-tissue, solubility and carbonate pump contribute around 63%, 24% and 6% respectively to variations in atmospheric CO_2, using an Earth system model of intermediate complexity.

Recent studies have revealed a further biologically-driven pump, the "microbial carbon pump" (MCP) (Figure 1.4), which has been classified separately from the well-established BCP. The mechanism behind this pump was proposed by Jiao et al., (2010). This introduces the MCP by suggesting that a proportion of dissolved organic matter produced by primary production is not re-mineralised, but instead transformed by marine bacteria into refractory (slowly degradable) forms which may persist in the ocean for extended time scales, perhaps up to millenia (Hansell 2013). Although many experimental works seem to support this hypothesis (e.g. Biddanda et al., 1997), the mechanisms underpinning the MCP remain largely unknown

A comprehensive look at the relative contributions of the BCP and the MCP can be found in Legendre et al., (2015). Here, the magnitude of the MCP is defined quantitatively as being the rate of production of DOC with an average lifetime greater than 100 years. They estimate that the MCP contributes an average of 0.2 Pg C to the World Ocean each year, whereas the BCP magnitude could be placed somewhere between 0.3 and 0.7 Pg C per year.

Jiao et al. (2014) proposed an integration of the BCP and MCP, but this requires a better understanding of the interplay of the carbon fluxes between the two pumps. They hypothesise that an increased nutrient availability within an ecosystem decreases the efficiency of carbon storage by the MCP, which in turn increases the dominance of the BCP in the system (Figure 1.5). This hypothesis was supported by Polimene et al., 2016, through model simulations which showed a relationship between carbon pump dominance and the carbon to nutrient ratios in phytoplankton.

This thesis explores this hypothesis further and aims to quantify the relative importance of the BCP and MCP in relation to the availability of nutrients in the water column. This is achieved by simulating the relevant carbon fluxes at two sites in the ocean representative of nutrient-poor gyre conditions and nutrient-rich coastal conditions.

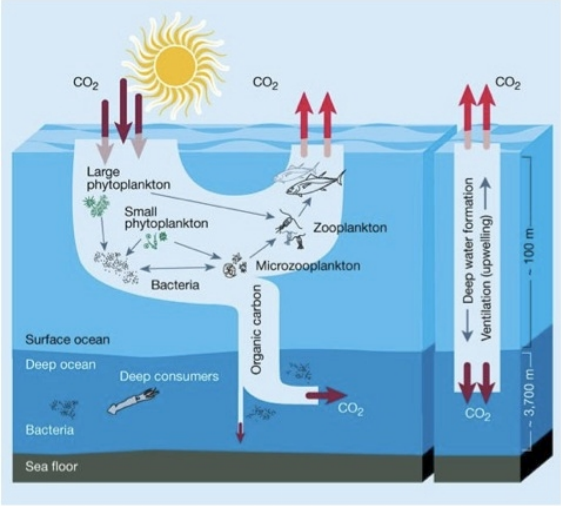

Figure 1.3: Diagram of the BCP, from Chisolm et al., 2000 (Nature). Here, phytoplankton and zooplankton are split into two categories by size, to represent the dependence of length scale on their interactions.

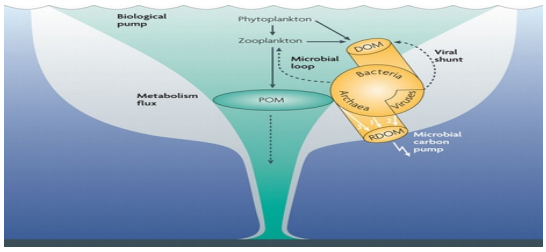

Figure 1.4: Diagram of the MCP, from Jiao et al., 2010

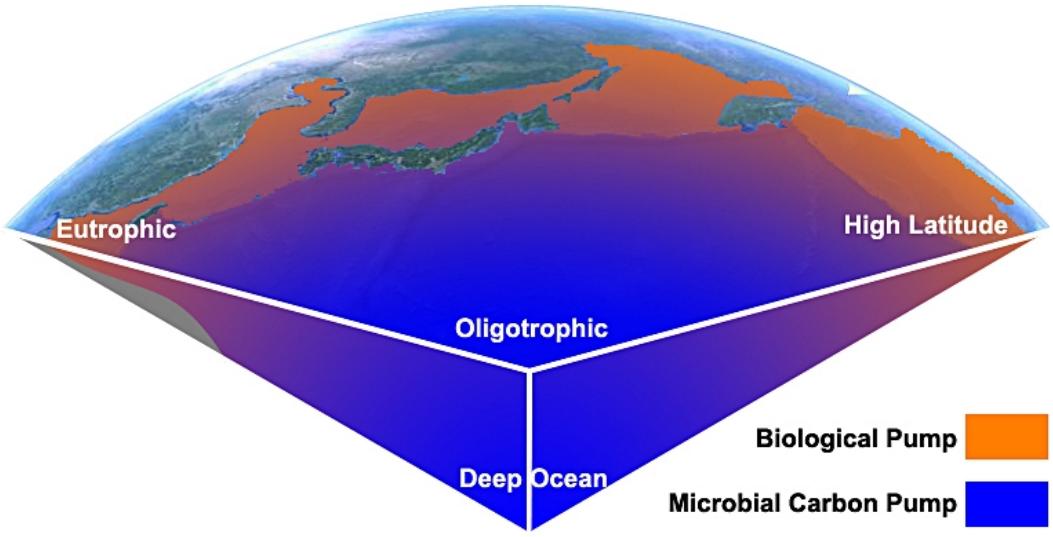

Figure 1.5. An illustration demonstrating the main environmental conditions that accompany the dominance of the BCP and MCP – nutrient availability for the BCP and depth for the MCP. Figure is taken from Jiao et al., 2014

1.3.2 Carbon Fluxes in Marine Ecosystem Modelling

Ecosystem models are mathematical representations of the processes driving the spatial-temporal evolution of ecological variables that characterise the state of a natural environment. In an effort to simulate ocean carbon fluxes, this work considers biogeochemical marine ecosystem models that describe the processes driven by the plankton community. Fasham et al., (1990), outlines an early example of this in a nitrogen-based plankton model. This used a "low trophic level" model, meaning that it focussed on primary producers and micro-organisms (e.g. bacteria, phytoplankton, zooplankton), while incorporating essential nutrients such as carbon and nitrogen.

Low trophic level models give an essential insight into the biologically driven carbon fluxes due to their representation of primary production (PP), which is the basis of the BCP. In the model provided by Fasham et al., (1990), the annual net PP was estimated by adjusting the phytoplankton mortality rate while adhering to a ratio of carbon : nitrogen : phosphate that is equal to the value of 106 : 16 : 1 proposed by Redfield (1934) (which was subsequently known as the "Redfield ratio"). This is not the only method of estimating PP, as many studies infer this from productivity irradiance (P-E) curves, such Furuya et al, 1998. These are examples of "static" approaches, meaning that PP is assumed to be approximately constant. Later studies, such as Macedo et al., (2006), argue for a dynamic approach, motivated by an effort to avoid the overestimation of photo-inhibition that is observed when using a static model.

Improvements to the simulations of PP were also facilitated by a number of innovations to dynamic marine ecosystem modelling. For example, the representation of a variable stoichiometric ratio was examined by Geider et al., (1997), which proposed a chlorophyll-*a* to carbon ratio regulated by alterations in light exposure, nutrient-limitation and temperature. Furthermore, there is the

introduction of the plankton functional types (PFTs) into the model used by Baretta et al., (1995). Here, zooplankton and phytoplankton are separated into subgroups to distinguish between trophic interactions that are specific to those groups. An example of this is the incorporation of silicate into diatom shells, which does not occur in the other phytoplankton types. Le Quere et al., (2005) provided a more in-depth examination into the characteristic traits of each PFT, and proposed a set of 10 PFTs based on a set of physiological, environmental and nutrient requirements that regulate their biomass and productivity.

Most contemporary models include complex relations between the PFT sizes and essential BCP dynamics. For example, the selective grazing of zooplankton may vary depending on its size, prompting the need for a separation of zooplankton based on the relative length scale of each group (Le Quere et al., 2005). Similarly, the sinking of particulate organic carbon is also a function of the size, which in turn depends on the size of the organisms (phytoplankton or zooplankton) from which the particles derive.

By simulating primary production, grazing, and various other trophic interactions, models have started to quantify the BCP in the global ocean. A notable example is Giering et al., (2014), wherein the first carbon budget calculation in the mesopelagic regions was made. They concluded that prokaryotes (such as bacteria) provided the dominant sink for organic carbon, and are responsible for around 70 to 92 per cent of remineralisation in the deeper ocean region.

For the simulation of MCP, an explicit representation of bacteria is required. This has only been achieved in more recent model simulations. Allen et al., (2004) examined a water column in the North Sea with the inclusion of bacterial biomass and the dissolved organic carbon (DOC), which drives the bacterial production. They deduced that changes in the stratification of the water column

influences the development of the microbial loop. Polimene et al., (2006), introduced the bacterially-mediated formation of recalcitrant DOM and investigated the dynamics leading to DOM accumulation, particularly in regions where the microbial-loop is dominant.

Despite these advancements, there is a lot of work required for the modelling of the MCP. Current models are still incapable of providing the key fluxes involved in the MCP that have been outlined in literature accounts. Models are also unable to keep up with the newer theoretical additions to bacterial communities, such as those outlined by Polimene et al., (2017).

This research uses an updated version of the European Regional Seas Ecosystem Model (ERSEM), a case study of which is provided by L. De Mora et al., 2016. In addition to simulating the BCP, this model is also capable of simulating key processes of the MCP due to its inclusion of bacteria and the production of recalcitrant DOC (Polimene et al., 2017).

1.3.3 Data Assimilation

Data assimilation (DA) is the process of incorporating observations of a system into a model describing the system. This is useful because both observations and models are uncertain representations, and so an analysis that combines the two (while appropriately accounting for these uncertainties) is capable of producing a more accurate representation of the system.

DA is typically applied for one of two major purposes: parameter estimation, which adjusts model parameters to best fit the observations, or state estimation, which updates the model states based on the observations during a model run. This thesis will proceed to discuss state estimation, as it most effectively provides a reanalysis (a refining of an existing analysis) of the carbon fluxes.

The state estimation DA process can be interpreted as an application of the stochastic filtering process, as outlined in Jazwinski (1970). In this context, filtering is the method of determining a best estimate for the true state of a system from a potentially noisy set of observations. This process can be expressed mathematically through Bayes' Theorem, where the posterior pdf (probability density function) is used to provide the best estimate and the uncertainty of the state:

$$p\langle x|y\rangle = \frac{p(x)p\langle y|x\rangle}{p(y)} \tag{1}$$

Where x is the state vector, y is the observation vector, $p(x|y)$ is the posterior pdf, $p(x)$ is the prior pdf and $p(y|x)$ is the observed pdf.

A further distinction that is often made is the categorisation of modern DA methods into "variational" and "sequential" techniques, although hybrids between the two are becoming more popular.

Variational DA methods rely on the calculus of variations to find the mode of the posterior pdf by minimizing a cost function, typically assuming a Gaussian prior pdf. "3D-Var" is an early type of variational technique developed by Sasaki (1958), which assumes that observations are static in time, so the x and y in Bayes Theorem above are only valid at a specific time. A more complex version of this, known as "4D-Var", was later developed by Le Dimet and Talagrand (1986), which considered the distribution of the observations in a time window, so that the observation vector in Bayes Theorem depends on time. A further classification within variational techniques is that if a state is required to satisfy a deterministic dynamical model, it is called a "strong-constraint" problem, meaning x is the state at the beginning of the assimilation window, and otherwise it is called "weak-constraint", in which x denotes a model trajectory inside the observation window.

Variational approaches have been applied in BGC DA in a strong constraint form (e.g. Matear 1995, Freidrichs et al., 2007), but are problematic due to the lack of consideration for the contribution of model error. Furthermore, the approach relies on a linearisation of the model equations and its adjoint, which is an issue when the dynamics are strongly non-linear. Due to these drawbacks, this thesis does not explore variational techniques and instead examines sequential DA.

Sequential DA methods rely on forward propagation of the model in time until an observation is reached, whereupon it performs its "analysis step". Perhaps the simplest method of a sequential method would be optimal interpolation, introduced by Gandin (1963), which weights each observation based on statistical information about their errors. This method is not typically used in sophisticated models as it fails to propagate error covariances.

The most popular types of sequential DA stem from the original Kalman Filter (KF) proposed by Kalman, (1960). The KF is an algorithm that makes use of a set

of noise-prone observations to estimate a combined probability distribution through Bayesian inference. For complex high-dimensional models, the KF is now performed with ensembles (a grouping of dispersed model runs, assumed to be representative of model uncertainty), as proposed by Evensen, (1994). This is known as the Ensemble Kalman Filter (EnKF).

The EnKF proceeds by propagating an ensemble of states with the fully non-linear model while assuming a Gaussian probability distribution. To represent the error statistics in the analysis step, the EnKF performs an ensemble of parallel data assimilation cycles. At the analysis step, the update equation for one ensemble member is:

$$x_k = x_{k|k-1} + \hat{K}_k\left(y_k - H x^f_{k|k-1}\right) \tag{2}$$

Here x_k is the state vector at time k, H is the observation matrix and y_k is the observation at time k, which is subject to a perturbation given by:

$$y_k = y_k + v_k \tag{3}$$

Where v_k is a random variable with a normal distribution.

The Kalman Gain is denoted by $\hat{K}_k$. This is the weight, or relative importance, given to the current state estimate which is achieved through a comparison of the covariance update between timesteps. A higher Kalman gain indicates that the filter is placing a higher importance to recent measurements. This is given by:

$$\hat{K}_k = P_{k|k-1} H_k^T \left(H_k P_{k|k-1} H^T + R_k\right)^{-1} \tag{4}$$

Where R is the observation covariance matrix and $P_{k|k-1}$ is the covariance update between timesteps $k-1$ and k, which can be written as:

$$P_{k|k} = \left(I - K_k H_k\right) P_{k|k-1} \left(I - K_k H_k\right)^T + K_k R_k K_k^T \tag{5}$$

This is known as the Joseph form for the update covariance matrix. Note that I is the identity matrix. This can be simplified further when choosing the optimal Kalman Gain, which gives the following equation:

$$P_{k|k}=\left(I-K_k H_k\right)P_{k|k-1} \tag{6}$$

Since its introduction the EnKF has received many improvements and exists in many augmented variations. Notably, there is the Localised Ensemble Transform Kalman Filter (LETKF; Hunt et al., 2007) which includes localisation to minimise spurious correlations between model variables that arise from the relatively small ensemble sizes that can be afforded in real applications, and to enhance the rank of the ensemble covariance matrix. This implementation also includes inflation, enabling the spread of the ensemble to be adjusted. The form of EnKF used in this thesis is a similar implementation of the form outlined in Hunt et al. (2007), without localisation (ETKF), and is discussed further in 2.3.1.

Another alternative to the EnKF method is to use a sequential data assimilation method that attempts to solve Bayes' Theorem directly, without making the Gaussian assumption for any of the variables. An example of this is particle filtering (PF) (Del Moral, 1996), and is reviewed extensively in a geophysical context by van Leeuwen, (2009). It represents the model probability distribution function as an ensemble of particles, each with an assigned weight (relative importance). It resamples the particles at the analysis step based on their predictive performance.

PFs assume that the prior $p(x)$ can be written as the sum of delta functions:

$$p(x)=\sum_{i=1}^{N_e}\delta\left(x-x_i\right) \tag{7}$$

These delta functions centre on the particles x_i , and each particle is a model state, as in an EnKF. Together they form a posterior pdf that is not constrained by any assumption of its shape.

While full non-linearity is an advantage of PFs, a disadvantage has been the inability to perform well in high-dimensional systems (called the "curse of dimensionality"), due to a rapid loss of the statistical information of the particles when the number of independent observations is large. The introduction of the Equivalent Weights Particle Filter (EWPF), suggested by Van Leeuwen, (2010), offers a solution to this by exploiting the "proposal density", a method which ensures that particles will be relatively close to the observations. In this method, every ensemble member is reassigned to have an equal weight (relative importance) at the analysis step. Zhu et al. (2016), extended this further into the Implicit-Equal Weights Particle Filter (IEWPF), which proceeds by sampling implicitly with a different covariance for each particle, resulting in equal particle weights by construction. More details on these methods are given in Section 2.3.2.

One final note on the model error considerations for both of the sequential DA methods outlined is that the model state is propagated forward between timesteps with a random forcing factor β_k :

$$x_k = f(x_{k-1}) + \beta_k \tag{8}$$

where k is the timestep and f denotes the deterministic model. The nature of this forcing factor is chosen to reflect the model uncertainty, and can therefore be set up to depend on a model error covariance matrix, known as the Q matrix. This determines the error covariance between each state variable. The implementation of this matrix in the set-up of the perturbations used in this project will be described further in Sections 2.3.3 and 3.2.2.

1.3.4 Data Assimilation in Biogeochemical Marine Models

Marine Biogeochemistry (BGC) is now an essential component of many marine modelling platforms. It is a field that is clearly set to benefit from DA due to the recent surge in availability of remotely sensed data as well as the strong relationships that exist between the BGC and the observable physical environment, which is discussed by Gehlen, (2015).

An early example of sequential DA in BGC marine models was performed by Ishizaka (1990), which used an optimal interpolation method to assimilate ocean colour into a coupled physical-biological model in the South-east US continental shelf. While somewhat beneficial, this method omitted many sources of error, and the corrections due to assimilation were often overpowered by the dynamics of a free model run. Semovski and Wozniak (1995) used a similar method with chlorophyll assimilation in a model of the North Atlantic and Baltic Sea, while comparing their output with in-situ data as a means of validation. While the representation of the phytoplankton seasonal cycle was improved, there were some undesired side-effects such as an erroneous increase in zooplankton biomass. They concluded that further DA work needed to incorporate a more complete representation of ecosystem dynamics, noting representations of primary production estimates and the inclusion of dissolved organic carbon as examples.

Ensemble methods were later applied to account for the multivariate nature of the BGC models. Eknes and Evensen (2002) demonstrated the potential of the EnKF through its implementation into a 1D BGC model. They conducted twin experiments using 100 ensemble members with phytoplankton biomass as the assimilated variable. They revealed that the evolution of the whole model state could be controlled with this method, including critical unobserved variables such as zooplankton and the nutrients. Allen (2003) used this technique in a more

complex model (ERSEM) by assimilating in situ chlorophyll and nutrients into a 1D model in the Cretan Sea. They a found a marked improvement in the model's ability to hindcast chlorophyll, but emphasized the need for high frequency data due to a maximum predictability window of two days.

Further examples of EnKF approaches include Torres (2006), who assimilated chlorophyll and nutrient data into a 1D ERSEM representation of the Ria de Vigo estuary, and Ciavatta (2011), who assimilated chlorophyll data into a 3D ERSEM representation for the Western English Channel using data collected from station L4. Both studies report improvements to the representation of chlorophyll as well as a number of unobserved variables, although the improvements to the forecasting ability were limited. Ciavatta (2014) extended work from the previous study with an updated version of ERSEM, this time assimilating light attenuation. This resulted in improvements to the carbon flux simulation, plankton trophic dynamics, and even some bacterial dynamics, which were included in the model to provide initial insight into the MCP. This showed that EnKF techniques were potentially useful alongside recent developments in ecosystem understanding. These studies, among many others, helped to establish the EnKF techniques as the leading sequential DA method in marine BGC.

The other main class of ensemble methods that has seen some success in marine BGC are the PF methods. Sequential importance resampling (SIR), the standard PF technique, was the first method of this kind to be applied to a marine BGC model by Losa, (2003). However, this was only a 0D model and was found to experience difficulties with model stability due to filter degeneracy. Dowd (2007) used a Markov Chain Monte Carlo (MCMC) approach in an attempt to avoid the degeneracy seen in the SIR filter, and managed to produce results that were comparable to the EnKF for state estimation in a 0D model. A different approach was taken by Mattern (2013), which used the SIR filter in a 3D model of the Middle Atlantic Bight. By making a series of modifications to the SIR method,

such as state augmentation and smoothing to deal with observation outliers, they achieved an improved model-data fit compared to an optimised model simulation, which showed the potential for PF methods in surface chlorophyll assimilation. While some success has been demonstrated, there are still many unexplored areas of PF techniques in a marine BGC context.

Despite all the advances in the aforementioned techniques, there are still many statistical challenges that arise from applying DA in marine BGC. These challenges include: highly non-linear relationships that govern the dynamic BGC models, the large number of dimensions required by these models, the positive-definite nature of many BGC variables as well as physical complications such as the geometric boundary conditions that constrain the models (e.g. coastlines).

On top of this, many of the parameters are uncertain, with a wide range of values reported in literature. This is exemplified by Parslow, (2013), with regards to trajectories involving phytoplankton blooms and nitrate depletion. There are further uncertainties in the ocean circulation models that drive BGC models, which are discussed by Toyoda et al., (2013) in their effort to improve state estimations of lower trophic ecosystems. There are currently no DA methods that can account for all these problems simultaneously, and so the most successful methods have attempted to find a compromise.

Dowd (2014) provides a detailed account of potential DA techniques for marine BGC modelling, in both variational and sequential DA. This thesis will focus on some of the sequential methods, specifically EnKF and PF techniques, as potential candidates.

The main problem experienced by the EnKF application in marine BGC, is that the variables are highly non-linear in both distribution and uncertainty, which the EnKF does not explicitly address. This also extends to the observed fields, such as chlorophyll that is distributed logarithmically, as determined by

Campbell (1995). From this, there is a solution, which is executed by Ciavatta et al., (2011) and Ford et al., (2012) among others, which is to log-transform chlorophyll prior to its assimilation at each analysis step. Another anamorphic transformation to transform non-Gaussian distributed variables to Gaussian variables is used by Lenartz et al, (2007), also with the EnKF. While these solutions do not completely resolve this problem, they show that the EnKF methods are capable of producing desired results for ocean colour assimilation, which has motivated the examination of a filter of this kind in this project.

Particle filters are the fully non-linear solution to this problem, but in turn they typically struggle from a separate issue - "curse of dimensionality", as described in the previous section. This is a problem as most dynamic marine BGC models operate in a high number of dimensions, resulting from their fine resolutions in space and time and the complexity of the underlying equations. For this reason, standard particle filter methods, such as the SIR filter, often lead to a poor representation of the targeted distribution, as the filter degenerates with even a small number of members, which is shown by Snyder et al., (2008). This is why the recently proposed updates to particle filtering which offer potential solutions to the high-dimension problem, such as Van Leeuwen (2010) and Zhu, (2016), are of interest within this field. While there are currently no literature accounts of the equivalent weight particle filter methods in BGC marine modelling, they are examined as a second method of interest within this project.

Chapter 2

Methods

2.1. Overview

This chapter presents a description of the general methods applied in this project, including details of the model, data and set-up for the assimilative simulations.

Firstly, the ecosystem model will be described. This is a coupling of the ocean biogeochemical model ERSEM (European Regional Seas Ecosystem Model), with the 1D ocean physical model GOTM (General Ocean Turbulence Model). This model is used to represent the carbon fluxes that are involved in the biological and microbial carbon pumps (BCP and MCP) such as primary production, respiration, zooplankton grazing and particle sinking for the BCP, as well as bacterial DOC production for the MCP. The most recent description of ERSEM is provided by Butenschon et al., (2016). The coupled model ERSEM-GOTM has been applied in many previous studies, such as Blackford et al. (2007) which estimated biogeochemical dynamics at two sites in the global ocean. GOTM will be described in less depth than ERSEM due to the biological focus of this thesis. A brief discussion of the mixed layer depth consideration in GOTM-ERSEM is also included as a reference point for later discussion.

Then, the data assimilation algorithms will be described. Two techniques were chosen for examination: the Ensemble Transform Kalman Filter (ETKF), and the Implicit Equal Weights Particle Filter (IEWPF). There are major differences in these approaches arising from fundamentally different assumptions on the distribution of data and model states, which will be discussed. These methods were applied using the DA framework EMPIRE (Employing MPI for Researching Ensembles). While this is the first application of the ETKF and the IEWPF with

ERSEM, some DA methods have already been applied to ERSEM-GOTM such as Torres, (2006), with the Ensemble Kalman Filter (EnKF). It is worth mentioning that ERSEM with the EnKF has also been applied in three-dimensional assimilative applications by Ciavatta et al., (2011, 2014 and 2016). Further successful examples of DA within ERSEM include the use of the Singular Evolutive Interpolated Kalman filter (SEIK) by Triantafyllou et al., (2003), Korres et al., (2012), Triantafyllou et al., (2013), as well as the Singular Evolutive Extended Kalman filter (SEEK), by Hoteit et al., (2003), Hoteit et al., (2004), and Korres et al., (2012).

The skill metrics that were applied to assess and compare the performances of the reference and assimilative simulations are also presented in this chapter. This will primarily focus on the interpretation of the root-mean squared deviation (RMSD) between the means of the two simulations.

Finally, an account of the type of observational data assimilated in this work, i.e. remotely sensed ocean-colour data, will be provided. This is the surface chlorophyll concentration provided by the ESA's Ocean Colour Climate Change Initiative (OC-CCI). This was used for the assimilation at the two ocean sites (station L4 and BATS), as well as for the characterisation of the artificial observations in the twin experiments. Previous works have made use of assimilation with these data, including Ford and Barciela, (2017) and Ciavatta et al., (2016), with ERSEM.

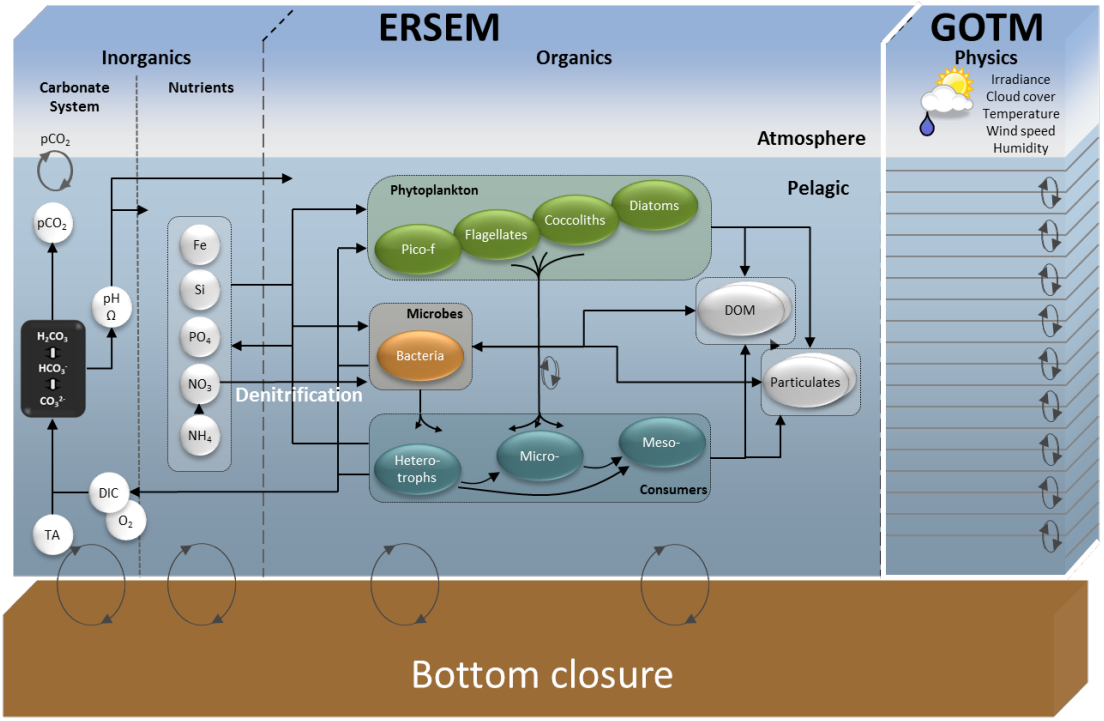

Figure 2.1. Schematic of the combined model. The structure of ERSEM is on the left with the main components of GOTM shown on the right.

2.2. The Model: ERSEM-GOTM

The full ecosystem model chosen for this project consists of two component models: the 0-dimensional model ERSEM, which simulates the trophic dynamics that drive the BGC variables, and the 1-dimensional model GOTM, which describes the vertical transport of the variables and the physical processes determining the vertical profiles of temperature and salinity. A diagram showing the main features of this model is shown in Figure 2.1.

2.2.1 The biogeochemical model: ERSEM

ERSEM is designed to simulate the biogeochemical dynamics of a realistic marine ecosystem (Baretta et al., 1995). Since its initial development the model has received regular updates, and this project makes use of the recent version presented by Butenschön et al., (2016). In this work, the model state vector includes the following:

4 phytoplankton functional types: ERSEM uses a functional type approach to model the dynamics of the low trophic levels of the ecosystem, and so the primary producers are split into four phytoplankton functional types (PFTs). These include three categories based on relative size – picophytoplankton, nanophytoplankon and microphytoplankton – in addition to diatoms, which are included separately due to their unique incorporation of silicate. Each PFT has four corresponding variables that represent the content of its constituents: chlorophyll, carbon, nitrate and phosphate. The diatom PFT has an extra variable for its silicate content. The PFTs are characterized by stoichiometric ratios of nutrients-to-carbon and chlorophyll-to-carbon, which may vary dynamically (Geider et al., 1997; Baretta-Bekker et al., 1997) between individual ranges defined

in the model parameterization by Blackford et al. (2004). The PFTs differ because of the different values of the parameters characterizing the specific lysis rates (rate of cell disintigration) and specific rest respiration. The processes relating to phytoplankton in the ecosystem model are shown in Figure 2.2 (left).

3 zooplankton functional types: the zooplankton functional types (ZFTs) consist of mesozooplankton, microzooplankton, and heterotrophic nanoflagellates. These are also separated by relative size, because this determines the type of PFT they graze on and the relative size of particulate organic matter they excrete. Each ZFT is represented by a variable corresponding to its biomass (carbon content), as well as nitrate and phosphate content for the two larger types (microzooplankton and heterotrophic nanoflagellates). The processes relating to zooplankton in the ecosystem model are shown in Figure 2.2 (middle).

1 bacterial functional type: this is the main driver of the microbial loop. It is responsible for the production and recycling of dissolved organic matter (DOM) in labile, and recalcitrant forms, and drives the regeneration of inorganic nutrients in the water column (Polimene et al., 2006; Hansell, 2013). There are variables corresponding to the bacterial content of carbon, nitrate and phosphate. Bacteria contribute to cycling of not only inorganic nutrients, but also labile, semi-labile and recalcitrant DOM. The processes relating to bacteria in the ecosystem model are shown in Figure 2.2 (right).

6 inorganic components: this includes five inorganic dissolved nutrients (carbon dioxide, nitrate, ammonia, phosphate and silicate), and dissolved oxygen. The model configuration applied here includes a carbonate system module, which regulates the air-sea flux of carbon dioxide (Butenschön et al., 2016).

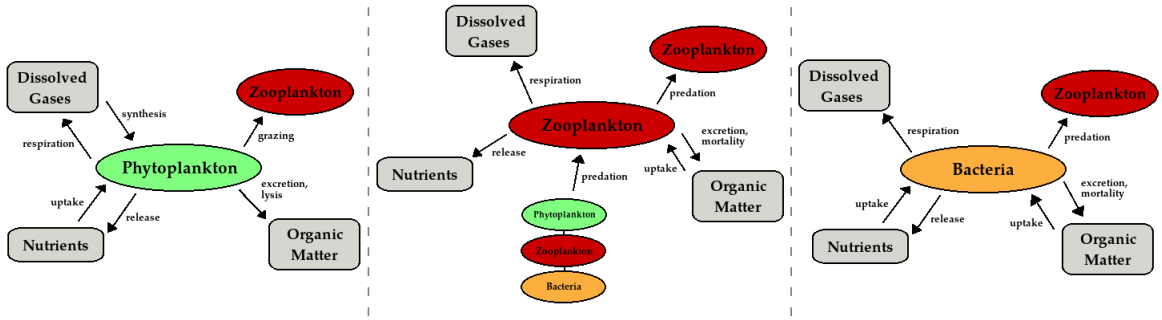

Figure 2.2. Diagram of phytoplankton, zooplankton and bacteria interactions. For phytoplankton: synthesis of dissolved gases includes photosynthesis which uses carbon dioxide. Uptake of nutrients includes nitrate, phosphate and ammonium, as well as silicate for diatoms only. Organic matter from excretion takes the form of particulate organic matter, that undergoes sinking and uptake by bacteria. For zooplankton: Predation occurs both on phytoplankton, zooplankton and bacteria, and well as by zooplankton themselves. Organic matter is produced both by excretion and mortality (dead matter). For bacteria: cycling of nutrients as well as organic matter produced by the PFTs and ZFTs.

These variables can be combined and used in equations to examine fluxes pertaining to the BCP and the MCP. This project considers a total of five carbon fluxes. This is comprised of three relevant fluxes for the BCP: (1) primary production, (2) zooplankton grazing and (3) the sinking of particulate organic carbon, and one relevant flux for the MCP: (4) net bacterial production. In addition, a final flux describing CO_2 exchange between the ocean and atmosphere, (5) the air-sea flux, is also considered due to its implications for the global carbon budget. The representation of these five fluxes in ERSEM will now be explained in further detail.

(1) Primary production (PP): in marine ecosystems this is the net gain or loss in the synthesis of organic compounds from phytoplankton. To represent this, ERSEM considers the combined effects of carbon uptake, excretion and respiration by the PFTs (Figure 2.2). The uptake of carbon removes CO2 from the surroundings, whereas excretion and respiration both export CO2 to the surroundings. The

mathematical formulation of PP in ERSEM is based on the work of Baretta-Bekker et al. (1997). Here, the gross carbon uptake is treated separately from the uptake of nitrogen and phosphorus. This is because the cellular nutrient uptake of newly fixed carbon is affected more by the nutrient limitation than by photosynthesis. From this, it is assumed that the gross primary production (GPP) consists of both a photosynthetic component (through cellular uptake) and an unused, excreted component (resulting in nutrient limitation). This approach was also used by Falkowski and Raven (2007). Overall, the ERSEM computation of the mass-specific phytoplankton GPP is complex and considers the chlorophyll-*a* to carbon quota of each PFT, the metabolic response to temperature of each PFT, as well as silicate and iron limitation factors, photosynthetic rates, and photoinhibition.

(2) Zooplankton grazing: this describes the consumption of primary producers by predators, and may also be referred to as zooplankton predation. In ERSEM, this is performed by all 3 of the ZFTs mentioned previously. The model dynamics are based on work by Baretta-Bekker et al. (1995), Broekhuizen et al. (1995), and Heath et al., (1997). An important consideration is that the type of phytoplankton that each ZFT may consume is variable, as predation capability depends on size. In ERSEM, this uses type II Michaelis-Menten-type uptake capacities (Chesson, 1983; Gentleman et al., 2003). Zooplankton also graze on bacteria and even exhibit cannibalism, and so the governing equations must include the ZFTs themselves as potential prey.

ERSEM represents the total prey available to zooplankton as the following:

$$Pr^{\chi}_{C,N,P} = \sum_{\Psi} f_{pr} | Z^{\chi}_{\Psi} \frac{\Psi'_{C}}{\Psi'_{C} + h^{\chi}_{min}} \Psi'_{C,N,P} \tag{9}$$

where χ are the ZFTs, Ψ are the individual prey types, f_{pr} are the food preferences and h_{min} is a food half-saturation constant based on the detection capacity of predators.

(3) The sinking of particulate organic carbon (POC): this describes the effects of gravity on the carbon by-products of microbial, PFT and ZFT excretion, mortality and grazing. ERSEM makes three distinctions between the relative sizes of POC (small, medium and large) based on the size of the PFT or ZFT that it originates from. The sinking of the POC model states is achieved by passing them to a physical driver, which considers the velocity of sinking. This velocity is connected by:

$$\omega_{sed}^{\chi} = \omega_{0}^{\chi} + \omega_{lim}^{\chi} \max\left(0, p_{sink}^{\chi} - l_{<\mathrm{NP}>}^{\chi}\right) \tag{10}$$

where ω are the sinking velocities subject to different conditions ("sed" - sedimentation, "0" – a constant relating to the POC type, and "lim" - nutrient limited), χ are the phytoplankton states, p_{sink} is the threshold for nutrient limitation, and $l_{<\mathrm{NP}>}^{\chi}$ is the combined nitrogen-phosphorus limitation factor.

(4) Net bacterial production: this refers to the carbon output from bacterial decomposition and the modulation of particulate and dissolved organic matter (DOM). In ERSEM, bacteria feeds on labile dissolved organic matter, and produce semi-labile and recalcitrant forms of DOM, which are those with longer degradation timescales. This is the primary driver of the microbial loop dynamics in the model. The rate of the bacterial uptake of DOM is regulated by temperature, nutrient and oxygen conditions. Following this, the nutrient status of bacteria controls the labile DOM. The ERSEM formulation of this process includes the mechanism for the production of recalcitrant DOC mediated by

bacteria as described by Hansell, (2013). This provides the model with the outline of the MCP, despite the exclusion of recalcitrant DOC with lifetimes much greater than a year. The sub-model for these processes is provided by Polimene et al., (2007).

The formulation in ERSEM of the bacterial uptake of particulate and dissolved organic matter is given by:

$$\widetilde{R} = R_{C,P,N}^{lab} + q^{slab} R_{C,P,N}^{slab} + q^{srefr} R_{C,P,N}^{srefr} + q^{small} R_{C,P,N}^{small} + q^{med} R_{C,P,N}^{med} + q^{large} R_{C,P,N}^{large} \quad (11)$$

where q is the turnover rate corresponding to turnover of the organic matter R. $R_{C,P,N}$ relates to the carbon, phosphate and nitrate content of each type of dissolved organic matter, with "lab" - labile, "slab" - semi-labile, "srefr" - semi-refractory, and "small", "med" and "large" meaning different categorical sizes.

(5) Air-sea flux: this is the exchange of carbon dioxide at the interface between ocean and atmosphere. This flux is driven physically and is based on the differences between the partial pressures of both mediums. The pCO_2 in the water both influences and is influenced by the BCP and MCP, and therefore the exchange is also considered in this work. This exchange is also crucial to the global carbon cycle.

The air-sea flux for carbon dioxide in ERSEM is given by:

$$F_C\big|_{sea}^{air} = \rho_{sea} k_{airC}\left(T, u_{wind}\right)\left(p_{CO_2} - p_{CO_2}^{air}\right) \quad (12)$$

where F is the flux, ρ_{sea} is the sea density, T is the temperature, u_{wind} is the wind speed, p is pressure and k is an empirical gas transfer coefficient taken from Nightingale et al., (2000).

2.2.2 **The physical model: GOTM**

The General Ocean Turbulence Model (GOTM; Burchard et al., 1999) is a one-dimensional physical model that is used to represent the vertical mixing of hydrodynamic variables in a water column. Forcing functions for this model, include wind, temperature, irradiance, cloud cover and relative humidity. The fluxes of ecosystem components are determined between adjacent boxes and/or layers. The procedure of coupling of ERSEM and GOTM is discussed in Allen et al. (2004).

The model is capable of calculating temperature, salinity, velocities, turbulence momentum and fluxes between the atmosphere and the sea. The sensible and latent heat fluxes are calculated from the formulae in Casterllari et al., (1998), and the long wave back-radiation is calculated using the May formulation (Budyko, 1974). The surface stress is calculated from the wind stress, and the formulae for this were chosen based on a sensitivity study of surface heat flux formulation on the model response (Siddorn and Allen, 2003).

Some of these parameters can be adjusted to test for different regimes, for example in the use of a Mellor–Yamada (Mellor and Yamada, 1974) type k-L or a k-ε type turbulence closure scheme. Routines for nudging observations also exist in GOTM, which were applied here to relax the simulation towards the profiles of salinity and water temperature. This form of relaxation was used in prior successful GOTM-ERSEM simulations (e.g. Blackford et al., 2004; Torres et al., 2006; Polimene et al., 2012; 2014; 2016, Butenschön et al., 2016).

2.2.3 Representation of the Mixed Layer Depth in ERSEM-GOTM

The mixed layer depth (MLD) in a marine system is the depth above which the physical and BGC properties of the water column are homogeneous due to turbulence. This section is included to help inform the interpretation of results in Chapter 3.

The MLD is relevant to plankton dynamics because it regulates the availability of nutrients in the upper layers, where the light availability enables primary production. In the idealised site set-up for station L4, the time evolution of the MLD is driven by the spring/summer warming of the upper layer (by solar irradiance that determines stratification) and the autumn/winter mixing of the whole water column due to wind-induced turbulence. The variation of the MLD position in a GOTM-ERSEM simulation configured for station L4 is shown in Figure 2.3. Note that 50 metres is the full depth modelled by the set-up shown in the figure, so when the MLD is below this point the entire column is considered mixed.

The effect of the MLD on the correlations between variables at different depths is demonstrated in Figure 2.4, which shows the correlation between the surface layer chlorophyll concentration and the bottom layer POC. The left plot uses the daily values for each variable taken when the water column is fully mixed, and the right plot uses the daily values when the water column is stratified. Here, it can be seen that when there is nutrient mixing in the water column (in late autumn and winter), these variables are correlated linearly. When the water column is stratified (in late spring and summer), there is far more scattering with no discernible trends. Despite this, the linear regression is smaller in the fully mixed case because the two points of linear behaviour are far apart, taking the plot away from the regression line.

The seasonally-altering nature of these correlations as revealed by the MLD incorporation in GOTM-ERSEM are a source of the non-linearity that are typically encountered in BGC Marine DA. This shows that the non-linear behaviour in these models may be situational depending on the season.

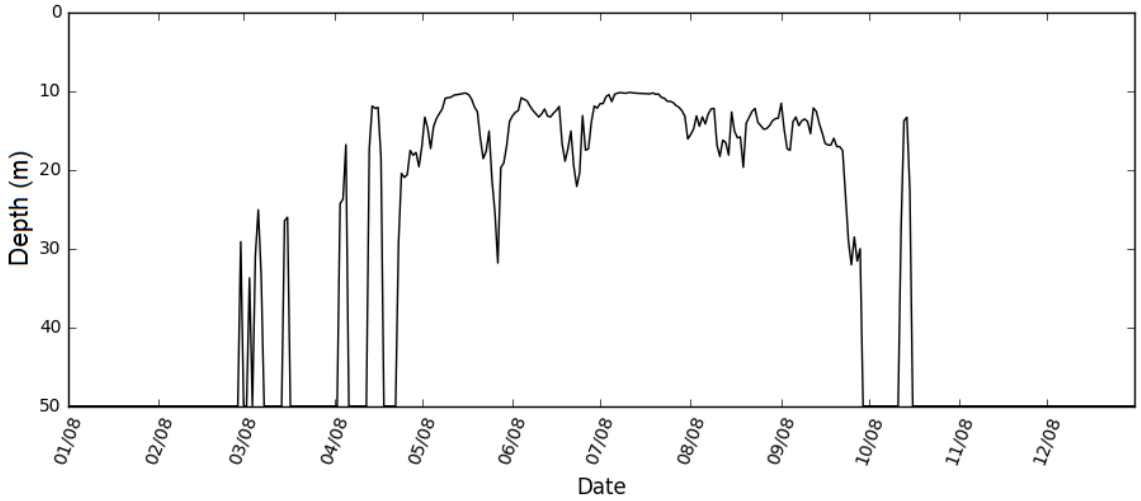

Figure 2.3: Evolution of the simulated mixed layer depth at station L4. A depth of 50 metres indicates that the water column is fully mixed. The MLD is calculated here based on the depth locations at which vertical gradients in temperature and salinity profiles experience sharp changes.

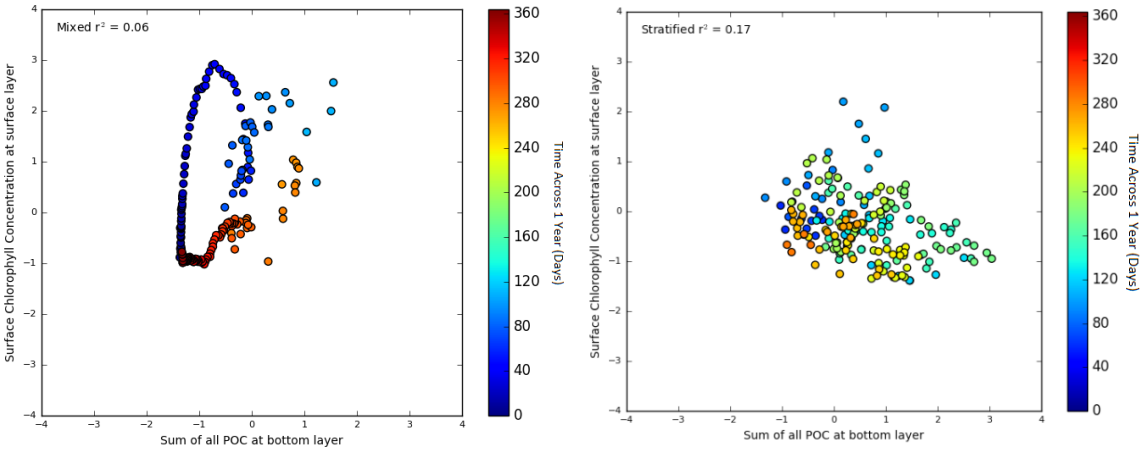

Figure 2.4: A scatter plot of chlorophyll concentrations in the surface layer against the POC concentration at the bottom layer in a 1 year ERSEM simulation at station L4. The plot on the left includes each day where the entire water column is mixed (i.e. mixed layer depth is below 50 metres) and the plot on the right includes each day where the water column is partially stratified (mixed layer depth < 50 metres). The r^2 value shown in the top left of each plot is the coefficient of determination of the linear regression. The colour map shows the progression of daily values, from blue (day 0) to red (day 365) The values shown here are normalised, and so they may take negative values.

2.3 Data Assimilation

These sections will describe in more depth the two DA methods explored for this work: the Ensemble Transform Kalman Filter (ETKF) and the Implicit-Equal Weights Particle Filter (IEWPF). Both of these methods are sequential ensemble-based approaches.

2.3.1 Ensemble Transform Kalman Filter (ETKF)

This is an extension of the Ensemble Kalman Filter (EnKF), which propagates an ensemble of states with the full non-linear model, while assuming a Gaussian probability distribution of the model states during analysis times (see figure 2.5). The update equation of the Ensemble Kalman Filter is given by equation 2 in section 1.3.3.

The implementation of the ETKF used in this thesis draws from a set-up of the LETKF (Hunt B. R. et al., 2007), without the use of localisation. The LETKF is so-called as it draws from both the Local Ensemble Kalman Filter (LEKF; E. Ott et al., 2005) and the Ensemble Transform Kalman Filter (ETKF; Bishop et al., 2001). The LEKF was introduced to fulfil a need for a grid point by grid point analysis, due to rapidly growing background errors (Kalnay and Toth, 1994). This was achieved through a localisation algorithm which ensured that the data assimilated at a grid point would influence the adjacent grid points appropriately. The ETKF attempted to improve the EnKF accuracy through a different approach – using an ensemble transformation which removes the need to update each ensemble member individually, improving efficiency. Its main strength was found to be its computational efficiency in high-dimensional systems. The ETKF was the method used in this thesis, adapted from an implementation of the LETKF described by Hunt et al., 2007, without localisation.

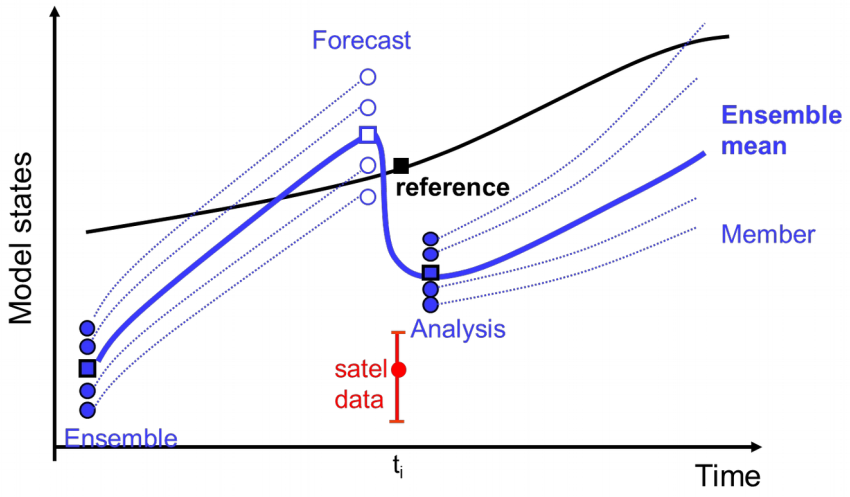

Figure 2.5. Diagram of the EnKF applied using satellite data. The blue lines are the ensemble members, which progress in non-linear propagation until the timestep with a satellite observation, shown in red. Here, the analysis step occurs, in which ensemble members are reassigned values based on the magnitude and error of the observation using Gaussian error covariances. The black line indicates a reference model simulation (without assimilation).

The ETKF uses inflation to allow the user to adjust for the individual model case. The inflation parameter is the proposed solution to the under-estimation of the background error covariance, which arises from often unavoidable omissions of various sources of error in the background ensemble, and from the fact that the ensemble only spans part of the state space. It was first included as a parameter to EnKF methods by Anderson et al. (1999), and in its simplest form operates by inflating the distance of each ensemble member from the ensemble mean by a constant factor, which in turn increases the ensemble variance by the square of this factor. This form of inflation was explored by Sarcher and Barthello (2008), who determined that the sampling errors in the estimates of the Kalman gain should be proportional to the Kalman gain itself. From this, Whitaker and Hamill (2012) introduced a new formulation for the inflation factor, given by:

$$\rho=\alpha\left(\sigma_b-\frac{\sigma_a}{\sigma_b}+1\right) \tag{13}$$

Where σ_b is the background error standard deviation, σ_a is the analysis error standard deviation, and α is an adjustable parameter. If α is zero, there is no inflation, and at α = 1, the analysis variance is equivalent to the background variance. This inflation method is called a "relaxation to prior spread" scheme, as it inflates the posterior ensemble proportional to the amount that the ensemble variance is reduced by the assimilation.

2.3.2 Implicit Equal-Weights Particle Filter (IEWPF)

The IEWPF builds on the particle filtering (PF) methods, which provide a fully non-linear DA method by solving Bayes' theorem explicitly. It represents the model probability distribution function as an ensemble of particles, each with an assigned weight (relative importance). It resamples the particles at the analysis step based on their predictive performance. A diagram illustrating each step in the PF is shown in Figure 2.6.

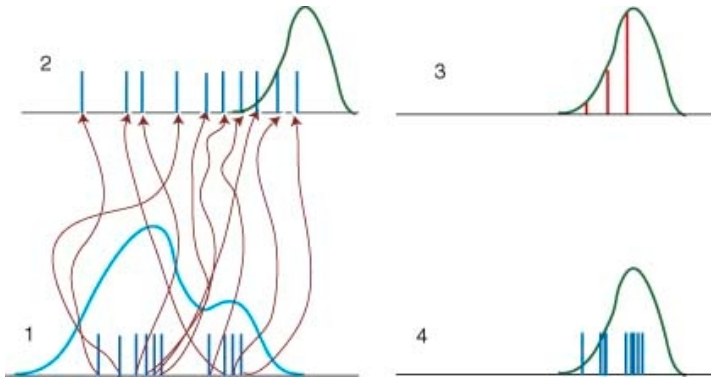

Figure 2.6. Diagram of the standard PF. Here, 10 particles sample the prior pdf, shown as vertical bars in (1), where the height indicates their weight. The particles are propagated forward in time using full non-linear equations resulting in a redistribution as shown in (2), where the pdf of the observations is given by the green curve. At the analysis step (3), Bayes' Theorem is applied and the bars and the observation pdf are multiplied. This results in new weights of the particles, indicated by the red bars. After the resampling step, the procedure is repeated with 10 equally weighted particles (4). This figure is available at: wileyonlinelibrary.com/journal/qj.

The classical PF methods are only efficient for small-dimensional problems, which makes them unsuitable for most models in the geosciences. This prompted the introduction of the Equivalent Weights Particle Filter (EWPF; van Leeuwen, 2010). Here, the PF method can be applied to higher dimensional systems by exploiting the concept of a *proposal density*.

The proposal density arises from the formulation of the expectation value of a function of the state vector. This effectively makes use of a series of mathematical arguments to arrive at a rewritten version of Bayes' theorem, in which an additional probability density function may be included (*q)*:

$$p\left(x^n|y^n\right)=\frac{1}{N}\sum\frac{p\left(y^n|x^n\right)p\left(x^n|x^{n-1}\right)q\left(x^n|x^{n-1},y^n\right)}{p\left(y^n\right)q\left(x^n|x^{n-1},y^n\right)} \tag{14}$$

Here, x^n is the state vector at time n, y^n is the observation vector at time n, N is the number of ensemble members, p are the pdfs and q is the proposal density.

As equation 14 shows, there is a multiplication and division of the proposal density q. This means that the form of the proposal density is of no consequence to the overall solution of Bayes' theorem, but allows for a choice of any form which may be advantageous to the assimilation procedure when the ensemble size is small, as it is in realistic applications. In light of the high-dimensionality problem in the PF, the proposal density is often used as a means of directing the particles towards the future observations, because it ensures that each particle contains relevant statistical information.

This filter also reduces any loss of information due to straying particles by means of re-sampling at each analysis step. In the EWPF method, the particles are propagated forward in time driven by the full non-linear model equations while

also propagating an extra variable known as a "weight" which is assigned to each of these particles. This weight is used as a measure of the relative importance of the particles as probability density changes. Due to the tendency of these weights to vary significantly in magnitude (which corresponds to a statistically insignificant representation by low-weight particles), the re-sampling stage in the EWPF proceeds by abandoning low weight particles while duplicating high-weight particles to take their place. This results in an ensemble of particles of equal weight, as it was in its initialisation, and avoids the issue of filter degeneracy. Doucet and Tadić (2003), and van Leeuwen (2009) provide a review of specific methods of implementing the resampling.

The IEWPF is very similar in form to the EWPF, but manages to achieve equal weights through implicit (or indirect) means (Zhu et al., 2016). Here, samples are drawn implicitly from proposal densities with a specific covariance assigned to each particle, and this ensures that the particle weights will be equal by construction at the analysis step. This method allows for consistency in ensemble spread for various unobserved variables and grid points, which is a complication often experienced using the EnKF.

As part of the proposal density used between observation times, the *nudging factor* is a key parameter for the IEWPF which will require tuning based on the specifications of the applied system. Nudging is the term given to the operation by which a system of particles is pushed deterministically towards an area of state space where the likelihood is expected to be high (Akyıldız and Míguez et al., 2017). In the EWPF and IEWPF, this is performed by applying a forcing function in the form of a relaxation term towards the value of the next observation, before the ensemble has reached the time of the next observation. This results in two parameters, as both the magnitude of this nudging factor, as well as its relative location in time between the observations dates, can be

adjusted. Currently, the proposed optimal method of tuning these parameters is by trial of multiple runs while readjusting the values, in which a suitable performance diagnostic is examined (Ades and van Leeuwen, 2015). This diagnostic can be the root-mean squared deviation between the mean truth state if tuned within a twin experiment approach. It can also be considered through a rank histogram approach as used by Ades and van Leeuwen (2015).

2.3.3 Stochastic perturbation of model states

Data assimilation requires a representation of the uncertainty attached to the model. This is challenging because there are many contributing sources of uncertainty, such as limits in the formulation of the relevant ecosystem processes, uncertainty in the parametrizations and errors in the data representing the model forcing functions.

In previous applications of ensemble DA methods with marine models, model errors have been represented by means of stochastic perturbations of forcing functions, e.g. solar irradiance driving photosynthesis (Ciavatta et al., 2011, 2016) and other atmospheric functions (Natvik and Evensen, 2003; Simon and Bertino, 2009), or by means of stochastic perturbations of the model states during the model forecast steps (e.g. Torres et al., 2006) or prior to the analysis (e.g. Ciavatta et al., 2011; Ciavatta et al., 2016)

Stochastic perturbations of model states can be generated by a spectral method (Evensen 2003), which samples random numbers from a specified distribution. Browne and van Leeuwen (2015) represent the model evolution error by applying a random number based on a Gaussian distribution with zero mean (implying no model bias) at each time step. The covariance of this Gaussian was estimated based on the variances retrieved through a long model run. It is

important to note that stochastic perturbations can generate negative values for the model states, which are unrealistic for marine biogeochemical variables because these are mostly positive-defined, such as the concentrations (Natvik and Evensen, 2003). To prevent this issue, previous works have applied refined anamorphic transformations (e.g. Simon and Bertino, 2009, Fontana et al., 2012), log-transformations of the states (e.g. Nerger and Gregg, 2008, Ciavatta et al., 2011, 2014, Janjić et al., 2014) or clipping the negative values to zeros or small positive values (e.g. Natvik and Evensen, 2003).

In this work, stochastic perturbations were applied to multiple model states at each timestep of the model integration, to represent the uncertainties in the model while it is propagated in time. These perturbations were generated as pseudo-random values sampled from a multivariate Gaussian distribution with zero mean and cross-covariances among model states. This was computed from a preliminary 100-member ensemble of model runs.

The procedure for computing the stochastic perturbations of each model state is as follows: a pseudo-random value is generated for the total chlorophyll variable, after which this value is multiplied by the state-to-chlorophyll covariance to compute the perturbation of the model state. Then the perturbation of each model state is multiplied by a further parameter, Qsd (this acts as the standard deviation of the Q matrix). This parameter needs to be tuned in relation to the length of the integration time step, to prevent the ensemble from diverging to unrealistic values or collapsing towards the trajectory of a typical model simulation. When the stochastic perturbations generate negative values, they are clipped to an extremely low positive value (i.e. 10^{-14}) which is comparable to the approach by Natvik and Evensen (2003).

2.3.4 Implementation of the Data Assimilation Framework: EMPIRE

The DA methods were applied using EMPIRE (Employing MPI for Researching Ensembles), which is a data assimilation framework developed at the University of Reading (Browne and Wilson, 2015). EMPIRE is a framework that facilitates the coupling of mathematical models with a range of DA algorithms to assimilate data in real system simulations. The techniques included are based on their success in previous applications and research potential, such as in both twin experiments and real-system applications. A schematic of EMPIRE is shown in Figure 2.7.

EMPIRE also allows for the use of "twin experiments". In twin experiments, the model is integrated in time to produce "true" values of the biogeochemical states. This "truth" can also be perturbed to generate synthetic observations that can be used in assimilative experiments to assess and compare different DA methods.

The model GOTM-ERSEM was implemented into EMPIRE for the first time within this project. This ideal assimilative marine modelling framework was applied in both twin experiments and real-system simulations. This required modifications to the FORTRAN code to implement and test MPI routines within the GOTM-ERSEM git repository.

In particular, this work required:

- The implementation of MPI code within the main program of the model.
- The implementation of MPI code within the time loop of the ecosystem model integration.
- The representation of the observational operator to link the surface total chlorophyll observations into the sum of the chlorophyll concentrations of the four ERSEM PFTs.

- The accommodation of time irregularity of retrieval of assimilated data, which is typical in ocean-colour time series.
- The coding of Input/Output routines to compute the model error through the multivariate stochastic perturbations of the state variables.
- The coding of preventative controls for the negative values of model states generated by the stochastic perturbations and the assimilative analysis.
- The construction of a model error covariance matrix based on correlations between variables in an ensemble of model runs.

Each of these updates was made within the EMPIRE code using FORTRAN90 and MPI.

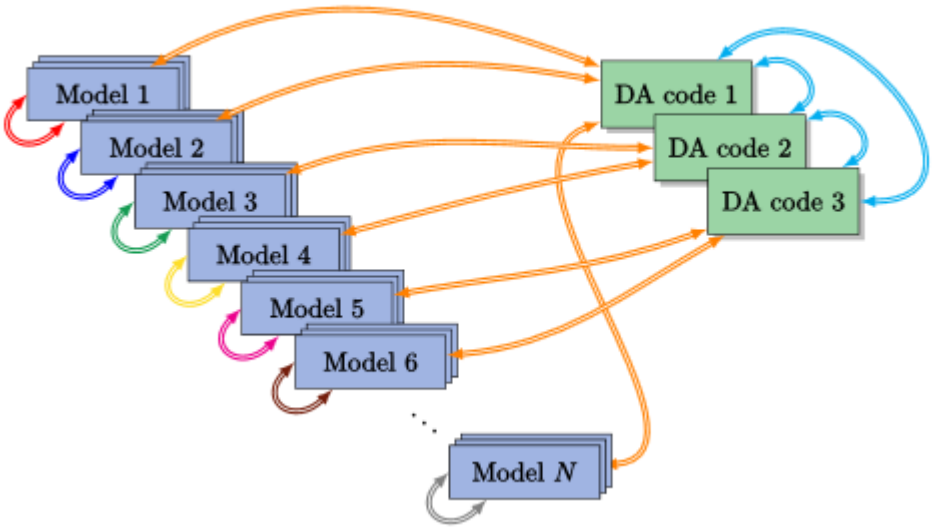

Figure 2.7. A schematic of the EMPIRE method

2.4. Skill metrics for assessing DA performance

The use of quantitative metrics is necessary for an objective assessment of the performance of the model simulation in representing observations of the marine ecosystems (Gregg et al., 2009). The same is true for the assessment and comparison of the suitability of DA methods applied in identical "twin experiments" (defined in the previous section).

Here, the primary means of assessment for model and assimilation performance is achieved through the calculation of the root-mean squared deviation (RMSD). This quantifies the extent of differences between the model (or analysis) output and the comparison benchmark (observations in real system simulation or simulated "synthetic observations" or "truth" in twin experiment simulations). This is given by the following equation:

$$RMSD = \sqrt{\frac{\sum_i \left(x_i - y_i\right)^2}{n}} \tag{15}$$

where *i* is an iteration of locations in time, x is the output, y is the comparison benchmark and n is the number of match-ups between the two. For comparison of the output to discrete observations, *i* represents the time steps where the data occurs and *y* represents the values of the observations. For comparison to another simulation continuous in time (i.e. the "truth" in twin experiments) *i* represents each model timestep and *y* represents the values of the other simulation.

The following sections will present the application of skill metrics in two separate parts – one for controlled twin experiments and one for DA applications in real ecosystem simulations, as there are important distinctions to be made for each approach.

2.4.1 DA skill assessment in controlled twin experiments

In controlled twin experiments, a model simulation is used to provide a representation of the real state we are attempting to emulate. In a twin experiment context, this is referred to as the "truth" run (Abarbanel, 2013). Therefore, the skill of the DA method can be assessed by examining the extent to which the temporal trajectories of state variables in the analysis resembles those of the state variables produced by the truth run.

The most direct method to achieve this is by calculating the average deviation of the DA ensemble mean from the truth run. This is the main technique used by Browne and van Leeuwen, (2015), among others. In this work, the calculation of this metric is given as a scalar RMSD value (equation 15). The skill of the DA methods can also be evaluated by looking at the absolute value of the difference between mean ensemble value and truth at each integration time step. This can be used to provide a continuous series of values that can be plotted to examine the variability of the DA method's performance in time.

Another useful metric to assess the twin experiments is rank histograms. These can be used to assess the likelihood of a set of observations (or a truth simulation) to remain confined to the spread of an ensemble of model simulations. It can also be used to assess the appropriateness of ensemble spread itself.

For twin experiments, a rank histogram is formed by systematically assigning a number to the truth run at each timestep. This represents the "ranking" of the value of the truth run within the values of the ensemble at these timesteps for a given variable (e.g. it is given a rank 0 if it is below every ensemble member or a value n if it is above n ensemble members). By presenting the frequency of the occurrence of each rank in a histogram, the quality of the truth simulation and the

ensemble dispersion can be determined. An ideal scenario will result in a flat rank histogram. The interpretation of rank histograms in illustrated in Figure 2.8.

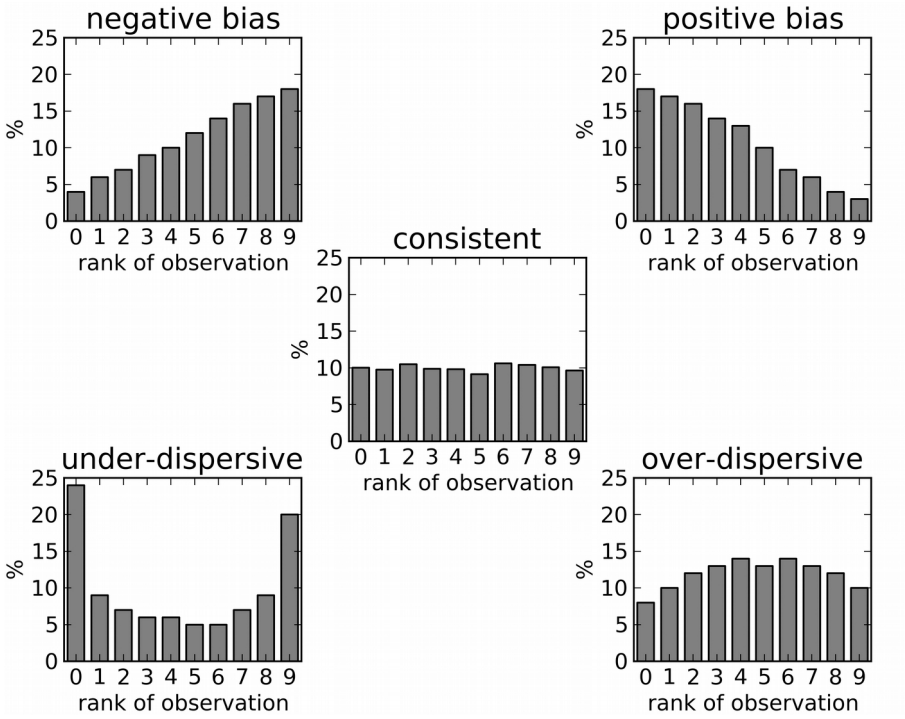

Figure 2.8. The interpretation of different rank histograms (here shown for the observation location in ensemble rather than truth run). The x-axis presents the observations rank among a 10-member ensemble and the y axis represents the proportion of time steps where the observation takes this rank. Figure was taken online from DOI: 10.5772/55699.

The top left histogram shows the distribution of bars skewed towards high values meaning that the truth is typically larger than most ensemble members, hence the ensemble is negatively biased. The top right histogram depicts the opposite situation, the truth is typically lower than most of the members, suggesting a positive bias in the ensemble. The bottom two graphs show the cases where the truth lies most often outside the ensemble or centred on the ensemble, which indicates that the ensemble dispersion is too low or too high.

2.4.2 DA skill assessment in real system simulations

It is more difficult to assess the performance of DA in real applications because there is no knowledge of the "true" state available for comparison. Here, the result itself is assumed to be the best possible estimate, so identifying a suitable skill metric is challenging (Gregg et al., 2009). The proximity of the analysis to the assimilated observations may be examined as a means to confirm the correct implementation of DA as the analysis should be closer to the data than the model.

However, it is possible to compare the analysis from a real DA implementation to a different set of unassimilated observations for the other state variables in the system. For example, Ciavatta et al., (2011, 2014) uses this method by assimilating remotely sensed ocean colour data, and then assessing the DA performance by examining its ability to reproduce the trends seen in a separate in-situ nutrient data set. It is also possible to compare different data of the same variable, as shown by Korres et al., (2012), with in-situ and satellite derived chlorophyll concentration data.

In this work, the assimilative output is compared with independent observations of biogeochemical variables measured in-situ at the sites of the real system simulations (station L4 in the English Channels and BATS in the Bermuda Sea). The multiannual assimilative output was matched-up with the observations in time and space (depth) and the RMSD in equation 15 was computed.

2.5. Ocean Colour Data

In this project, remotely sensed ocean colour data (for total chlorophyll concentration) was chosen as the assimilated variable. Assimilating ocean colour is advantageous because the satellite retrievals for data have high temporal frequency, and cover a large spatial area. Furthermore, the data have a strong connection to the BCP, as there is a close correlation between chlorophyll and phytoplankton biomass. Some representation of the MCP is also possible, but difficult due to the surface confinement of the assimilated variables and the implicit nature of the link to MCP processes. Many studies have already incorporated satellite ocean colour data in sequential DA techniques (e.g. Ciavatta et al., 2011, 2014 and 2016, Torres et al., 2006, Ford et al., 2012, Hemmings et al., 2008, Gregg, 2008, and many others).

This project uses remotely sensed ocean colour data provided by the Ocean Colour - Climate Change Initiative (OC-CCI) project of the European Space Agency (ESA) (Brewin et al., 2015). The data set was created by merging satellite data from the sensors MERIS, MODIS and SeaWiFS, after shifting the wavelength bands and correcting the bias between them. It consists of a global daily level 3 binned product provided on a sinusoidal grid at 4 km resolution.

Chlorophyll-a concentrations in the OC-CCI dataset are provided as daily products with a horizontal resolution of ~4km/pixel. The root-mean-square uncertainty and the bias in the chlorophyll-a concentration are also provided, based on comparison with match-up in-situ data. The availability of data depends on location – observations for station L4 typically occur every day, but there is often missing data due to complications such as cloud cover, so 5-day composites were used in this project.

The data comes with per-pixel error, and has been applied in previous DA works (Ciavatta et al., 2016). In this project, 30% is taken as an upper-bound for the uncertainty, for simplicity. However, in coastal waters the estimates of per-pixel error is much higher than in the open ocean (>30%), so the assimilation will have less effect in correcting the model simulation.

For the twin experiments, artificial observations were generated for chlorophyll concentration from an ERSEM model run, which uses uncertainties and retrieval frequencies matching those outlined for the OC-CCI data in the station L4 region. This was used to achieve a realistic emulation of the data sets that were later used for the DA at station L4, allowing for an accurate assessment of the capability of the DA methods. Further details on this will be provided in the twin experiments chapter.

2.6. Summary

The marine ecosystem model applied in this project is ERSEM-GOTM, which is able to describe the dynamics of various ocean carbon fluxes that relate to the BCP and MCP. The improvement that the assimilation of ocean colour data from the ESA's OC-CCI can make to the representation of these carbon fluxes will be investigated. Two ensemble-based DA methods, the ETKF and IEWPF, will be applied to tackle the dual challenges of non-linearity and high-dimensionality that BGC marine models present. They will be applied using the DA framework EMPIRE that was upgraded in this project to work with the marine ecosystem model.

The methods described here were adapted in two types of applications: controlled twin experiments, and real assimilation at the two sites, station L4 and BATS. As the results from the TEs are performed in an environment representative of station L4, they are more directly applicable to the real assimilation performed at this site. However, most outcomes of the TEs are dependent on model dynamics which are still present in a BATS simulation. The results of these applications will be described in Chapters 3, 4 and 5 respectively.

Chapter 3

Twin Experiments

3.1. Overview

This chapter presents the application of the DA methods in identical "twin experiments" (TEs). These are numerical experiments in which a model simulation is used as a representation of the "true" values of the biogeochemical (BGC) states. The capability of ensemble DA methods to reproduce similar BGC trajectories is then assessed by assimilating sub-sampled synthetic observations of this "truth" simulation. These pseudo-observations are generated from the truth run by means of stochastic perturbations of the output which are representative of a suitable observational error. While reliant on many approximations, the TEs are a useful method to quantify the expected improvement that can be made by DA methods when applied to model simulations. The sensitivity of the model to initialisation is also explored by producing a Stochastic Ensemble.

For this PhD project, the TEs are applied to pursue two objectives: (1) to quantify improvements in the representation of carbon fluxes by assimilating ocean colour data, and (2) to compare the performance of two sequential DA methods.

The chapter begins by outlining set-ups of the model and DA schemes used to perform the TEs. In particular, the tuning of the error covariance matrix representing the model error, the attainment of an appropriate observational error, and the tuning of the parameters specific to the ETKF and the IEWPF are described.

Then the results are presented. This will evaluate three ensemble simulations: the ETKF, the IEWPF and a stochastic ensemble (SE). The first two are DA methods, whereas the SE is simply an ensemble simulation of members starting from dif-

ferent initial conditions and perturbed stochastically. The SE does not make use of observations and is included here to test the sensitivity of the model to intial conditions, and is used as a benchmark to understand whether DA is beneficial with respect running an uncertain model simulation. The performance of the DA methods will then be compared in relation to the following five carbon fluxes involved in the BCP and MCP: air-sea flux, zooplankton predation on phytoplankton and bacteria, net ecosystem production, net bacterial production and the sinking of particulate organic carbon. The metric used here to assess the performance of each method is the average difference between the ensemble mean and the truth.

Finally, the results will be discussed and interpreted, with reference to the challenges that face both of the DA methods, such as non-linearity of marine systems and the need for an accurate representation of unobserved carbon fluxes, as described in chapter 1. Following the results of the TEs presented in this chapter, the most successful method will be chosen as the method to be applied in the subsequent assimilation of ocean colour in the real-system reanalyses.

3.2. Set-up

3.2.1 Model set-up

These TEs examined ocean colour DA within a coastal marine system. They were performed using a configuration of the water column, parameters, initial conditions, and atmospheric forcing for the marine model (GOTM-ERSEM) drawn from a previous model application at a coastal monitoring site by Butenschon et al. (2016). This coastal monitoring site is station L4 of the Western English Channel Observatory (Smyth et al., 2009).

A water column 50 meters deep was simulated, which is subdivided into 100 layers of variable thickness within the model (as there is a higher resolution at the surface and bottom of the column). At the bottom of this column, a benthic return module simulates the benthic fluxes at the sediment interface. Model initialisation makes use of meteorological surface forcing data supplied by a reanalysis of the European Centre for Medium-range Weather Forecasts (Dee et al., 2011). GOTM was set-up to nudge real data of temperature and salinity profiles at station L4 for a better simulation of the physical processes, such as vertical mixing, at the site.

The "truth" simulation spanned a period of two years, from the beginning of 2007 to the end of 2008. This included a spin-up period of one year. This was used to minimise the impact of initial conditions, and to achieve stable physical and biogeochemical conditions within the model configuration (Butenschon et al., 2016). The following year is where the assimilation takes place, and the truth simulation is taken as a potential ensemble member. In this year, model-generated observations of ocean-colour data were produced and assimilated. These were synthetic chlorophyll concentration pseudo-observations which were

generated based on the model trajectory of the total chlorophyll variable in the second year of the truth simulation. The analysis of the TEs will be focussed on this second year (2008).

The three ensemble simulations were also generated over two years. The ensemble members were initialised by perturbing the same initial conditions of the truth simulation, and proceeded subject to stochastic perturbations at each time step to represent the model uncertainty, as described in section 2.3.3.

Each ensemble - the SE, the ETKF and the IEPWF - contained 50 members, while using the same error covariance matrices to define the stochastic perturbations. In both the assimilative simulations, the pseudo-observations of chlorophyll were assimilated only in the second year of simulation, with a time step of five days. These factors were consistent to ensure a fair test between the methods. However, there were also some parameters characteristic to only one of each DA methods (such as localisation in the ETKF and nudging in the IEWPF), which were chosen based on the best performance in trial and error simulations.

3.2.2 Model errors and correlation

The development of a suitable model error covariance matrix (Q) to represent model error requires the consideration of the relationships between variables in ERSEM. This includes an understanding of the impact that incremental changes in the total chlorophyll variable can have on the full range of ERSEM variables, as well as the correlations between each variable. Note that the information for this covariance matrix is able to be represented through the use of a correlation matrix for all the model states since the correlation matrix is effectively the covariance matrix of the standardised variables. This can be then scaled according to the estimated uncertainties to represent the covariance matrix for the errors.

To construct the correlation matrix, the correlations between all state variables in ERSEM were determined. This was achieved by using a large stochastic ensemble (of 100 members) perturbed at each time-step and depth, and creating a matrix to store the values of each variable at time steps of 10 days throughout a one-year run. From this matrix, the correlations between the variables were computed for each time step using a correlation function in python. A time averaged value of the correlations is then taken over all the time steps to represent the average correlation between variables.

A graphical representation of the correlation matrix used in the TEs is shown in Figure 3.1. Here, a green square indicates that the variable was, on average, positively correlated with the corresponding variable. The purple squares indicate negative correlation. Each variable has a correlation with itself of 1. These correlations were all taken at the surface layer (the top layer) of the simulated water column, which is the depth at which the observations are assimilated. However, the perturbations were added at every layer.

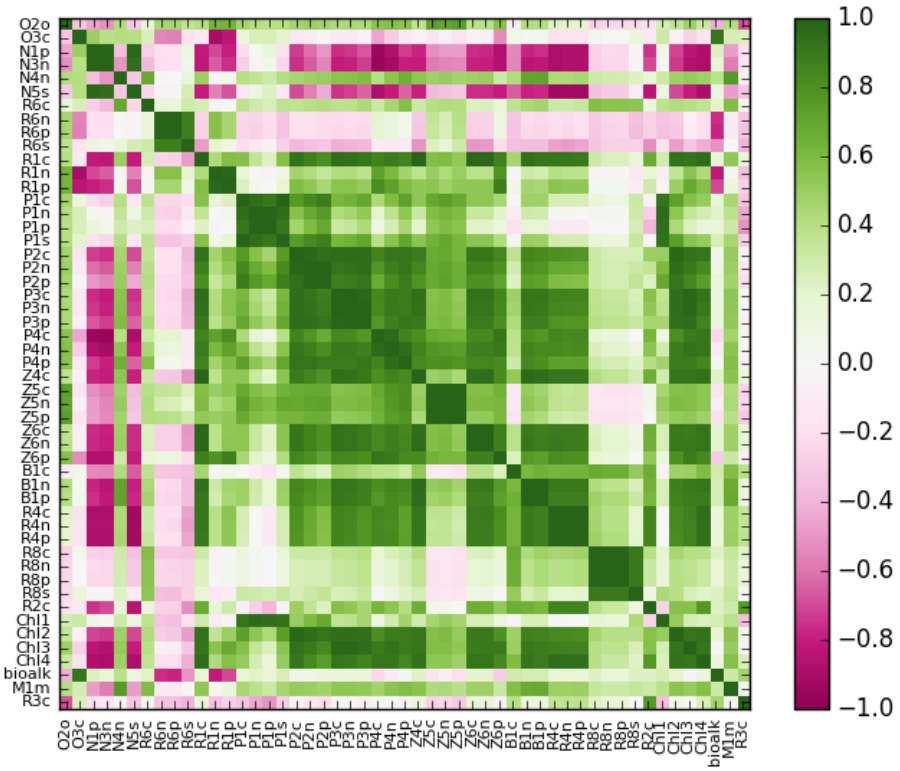

Figure 3.1. A visual representation of the correlation matrices for the 51 variables considered in the Q matrix based on the run of 100 ensemble members in the year 2008. The variable names are given by their codes in ERSEM; e.g. N = nutrient types, P = phytoplankton types, Z = zooplankton types, Chl = chlorophyll types, R = dissolved and particulate organic carbon; B =bacteria, O = gas compounds.

It should be noted that the correlations between variables are subject to change at different points in the year due to the annual solar cycle that drives plankton productivity. For this reason, the variability of the correlations in relation to the season was also investigated. Further correlation matrices are shown in Figure 3.2, which are split into four to approximately show different seasons throughout the year. These were taken as an average over three-month periods. In this figure, it can be seen that some of the positive correlations in the winter turn into negative correlations in the summer (e.g. for bacteria, the PFTs and ZFTs). The correlations are also overall smaller in magnitude in the summer, as shown by their faintness in the figure, which indicates values close to zero. The variability of the correlations illustrates one of the challenges of BGC data assimilation: the model error covariances are variable in time.

To evaluate if this variability could be accounted for in the twin experiments, a numerical experiment was performed consisting of a one-year long SE simulation in which the four Q matrices shown in Figure 3.2 were used in sequence to represent the errors in the different seasons. However, This lead to abrupt shifts of the ensemble dispersions at the cut-off points for each season, causing unrealistic discontinuities in the values of the biogeochemical variables. Therefore, it was decided to continue using the average correlation matrix taken over the full year (Figure 3.1) to compute the multivariate stochastic perturbations representing the model error. It should be highlighted that the temporal variability of the model-error covariances is still accounted for in the analysis steps of the DA methods applied here, despite the use of a constant Q matrix. For example, the ETKF computes the covariances from the ensemble distribution at each analysis step, and the IEWPF assigns low weights to particles that deviate considerably from the observations over time.

There is a similar issue of spatial variability of the correlations among BGC variables, which occurs in relation to the depth within the water column. The position of the mixed layer depth is responsible for this, as it results in the stratification of the water column and therefore weakening of the correlations among BGC trajectories in the surface and bottom layers. This effect is shown in Figure 3.3 for total chlorophyll, where there are two distinct regions of cross-correlations on either side of the mixed layer depth. For simplicity, this project considers a correlation matrix which is constant along the water column.

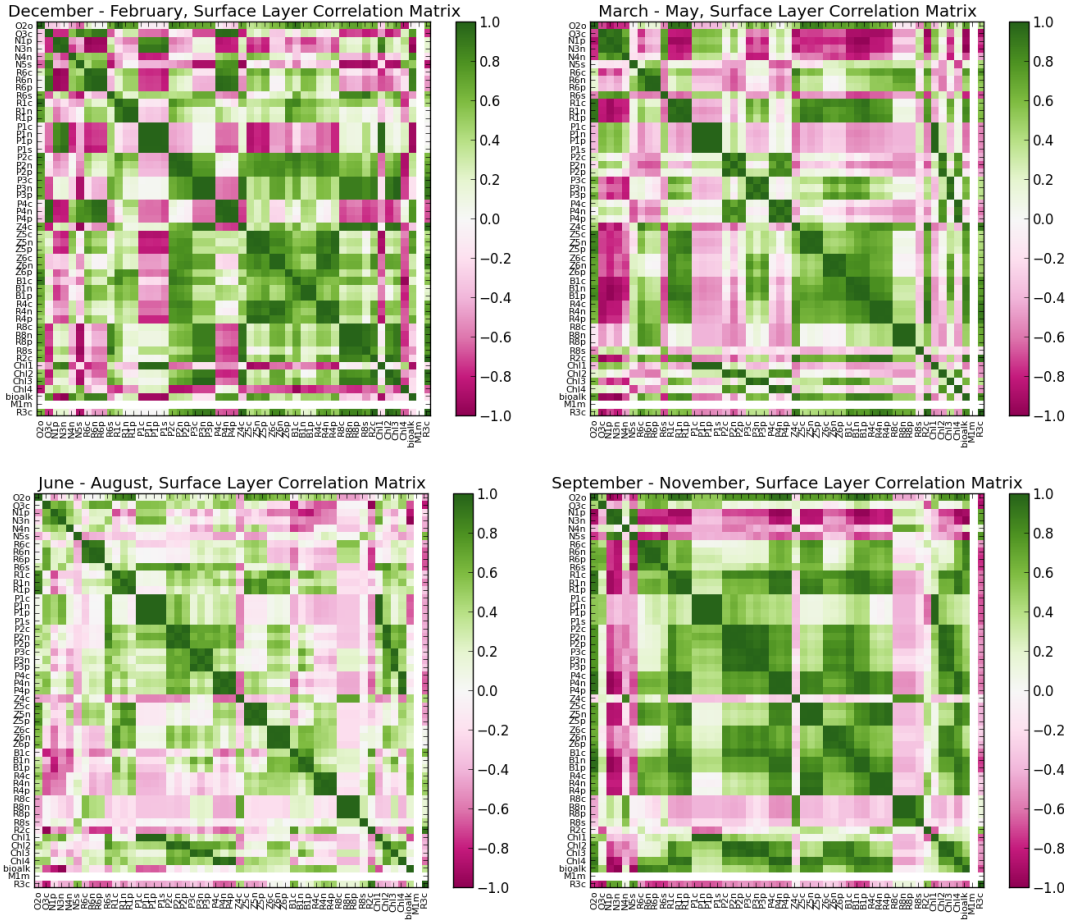

Figure 3.2. A visual representation of the correlation matrices for the 51 variables considered in the Q matrix: Winter (top-left), Spring (top right), Summer (bottom-left), Autumn (bottom-right). The variable names are given by their codes in ERSEM; e.g. N = nutrient types, P = phytoplankton types, Z = zooplankton types, Chl = chlorophyll types, R = dissolved and particulate organic carbon; B =bacteria, O = gas compounds

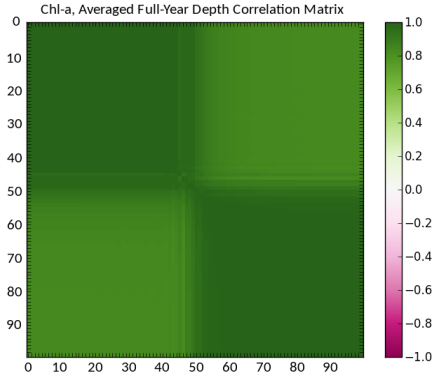

Figure 3.3. One year correlation for the total chlorophyll variable compared at different depths, where 0 is the surface layer and 99 is the bottom layer in the model. This shows that there are two distinct regions in the water column, which are separated by the mixed layer depth. The x and y-axes represent the depth layers within the model. Within each region chlorophyll is approximately uniform.

The final matrix was computed at the surface layer and used throughout the water column. It is argued that it is preferable to use correlations based on a point above the mixed layer depth (such as the surface) rather than at a deeper layer, because most of the carbon fluxes that are relevant in this project are stronger at the surface, e.g. primary production, grazing, air-sea carbon fluxes. However, it is recognised that this approach may have limits for other fluxes that occur at greater depths, such as the sinking of the particulate organic carbon and the bacterial production and respiration.

Therefore, the TEs were applied using a Q matrix that incorporates constant correlations shown in Figure 3.1. The ensemble simulations use this Q matrix to define the directions of the multivariate stochastic perturbations representing the model error; however the magnitude of the perturbations are still controlled by adjusting the value of the standard deviation of the Q matrix (Qsd) (see section 2.3.4). This parameter was used for inflating the dispersion of the ensemble members, while preserving their biogeochemical reliability. In particular, a multiplication factor of Qsd = $1x10^{-8}$ was used. It should be noted that as Q is derived from the covariance of the states rather than the errors, these are expected to be much larger than the covariance of the errors in the model equations. This explains the need for such a low value for Qsd.

A final note on the Q matrix is that it was used in a square root form ($Q^{1/2}$). This technique has been used in many EnKF applications as it can be used to reduce the sampling errors associated with the forecast step (Raanes et al., 2015), and by using the symmetric square root approach the mean is not altered (Evensen, 2009).

3.2.3 Observation errors

This simulation of the true state of surface chlorophyll was used to obtain model-generated observations of ocean-colour data (for the year 2008 only). This was achieved by randomly perturbing the simulated chlorophyll at pre-determined observation timesteps, which involved sampling from a Gaussian distribution which was adjusted such that the standard deviation was comparable to the error of real data. The error of chlorophyll data was assumed here to be equal to 30%, which is a value often used for ocean-colour in open-ocean waters (Brewin et al., 2017).

To provide a constant standard deviation for the observation error covariance matrix (R), the mean value of a set of L4 data from 2002-2010 was computed. 30% of this value was then set as the standard deviation for R (0.148 mg Chl-a m^{-3}).

3.2.4 ETKF Specific Parameters

For the ETKF, the main parameter that required tuning was the inflation factor. It should be noted while the implementation of this filter in EMPIRE was the LETKF, localisation was not used as a factor as the localisation length was set to 100 to represent the 100 depth layers in the physical model.

The inflation factor is used to increase the spread of the ensemble. The value of this parameter was set up by assessing the performance of iterative ETKF simulations where the value of the parameter was incrementally increased. This performance was determined based on the average difference between ensemble mean and truth (the absolute error), with the lowest value representing the best performance. The best simulation from these tests was used as the final ETKF result.

It was found that increasing the inflation factor by almost any amount resulted in an increase of the absolute error of the simulations, so the final ETKF results used an inflation factor of zero. This result is likely due to the increased frequency of the clipping of unrealistic negative BGC values when the ensemble is inflated, which in turn increases the positive model bias. It was concluded from this that the inflation factor would not be used as a tool to influence ensemble dispersion, and so the Q matrix along with the parameter Qsd were used in its place. This was deemed an acceptable alternative as this matrix was already tuned to represent model error in the SE ensemble, and was therefore helpful for consistency.

3.2.5 IEWPF Specific Parameters

For the IEWPF, the parameters needed for tuning are related to the nudging, which include the nudging factor and a control on when the nudging occurs.

The nudging factor is used to force the simulation towards a future observation. The value of this parameter was determined through various trial runs and a comparison of the absolute error, in a similar iterative procedure to that used for the inflation factor for the ETKF (section 3.2.4). This is set as a fixed value that persists throughout the assimilation.

The nudging factor can have a detrimental effect if it is either too high or too low, by either pulling the ensemble too strongly towards the observations or not directing them enough, and so there is a middle value that achieves the best overall result. The magnitude of this optimal nudging factor, as shown by the lowest average absolute error, was found to be a value of 1×10^5. This was based on a series of tests that examined the IEWPF runs while incrementing the nudging factor by a factor of 10 in each test.

The location in time of the nudging was also decided from different iterative simulations. The best value for this, determined by examining the absolute error for the IEWPF and changing the location of the nudging between analysis timesteps in increments of 10% (of the distance between analysis steps), was determined to be at 40% of the distance between analysis steps. This is 2.2 days for the pseudo-observations of ocean colour assimilated at interval of 5 days in the TEs, meaning that there is a 2.2 day period after an analysis step before nudging takes place.

3.3. Results

By using the set-up described in the previous section, the TEs were conducted, which simulated a representation of "true" BGC variables, generated pseudo observations of chlorophyll, and then assimilated this data in an attempt to reproduce the truth. A comparison of the performance of the ETKF and IEWPF methods will be presented for each carbon flux.

The results of the twin experiments indicate that each DA method was able to reproduce the seasonal cycles of the "true" carbon fluxes in the system, as shown by Figure 3.4. The average RMSD values between ensemble mean and truth (Table 3.1) show that DA generally performed better than the stochastic ensemble, with a few exceptions, most notably for the IEWPF. The RMSD in Table 3.1 is the primary metric to assess each DA method's performance (see chapter 2.4.1). In this table the statistics for the SE simulation are included as a benchmark.

The table shows that on annual average the IEWPF was better than the SE for two of the fluxes and the observed surface chlorophyll concentration. The ETKF made improvements on four carbon fluxes and the observed variable. The ETKF also outperformed the IEWPF for the surface chlorophyll concentration, the air-sea carbon flux, the net ecosystem production and the net bacterial production. However, the ETKF did not perform as well as the IEWPF for the zooplankton predation, and the sinking of all particulate organic carbon. Therefore, while the ETKF shows the best overall performance, the strength of each method is situational. The ETKF generally performed better for fluxes evaluated at the surface layer and for variables with a close relationship to the observed variable. Also, the IEWPF performed better for fluxes evaluated at lower depths and for variables with an indirect relationship to the assimilated chlorophyll.

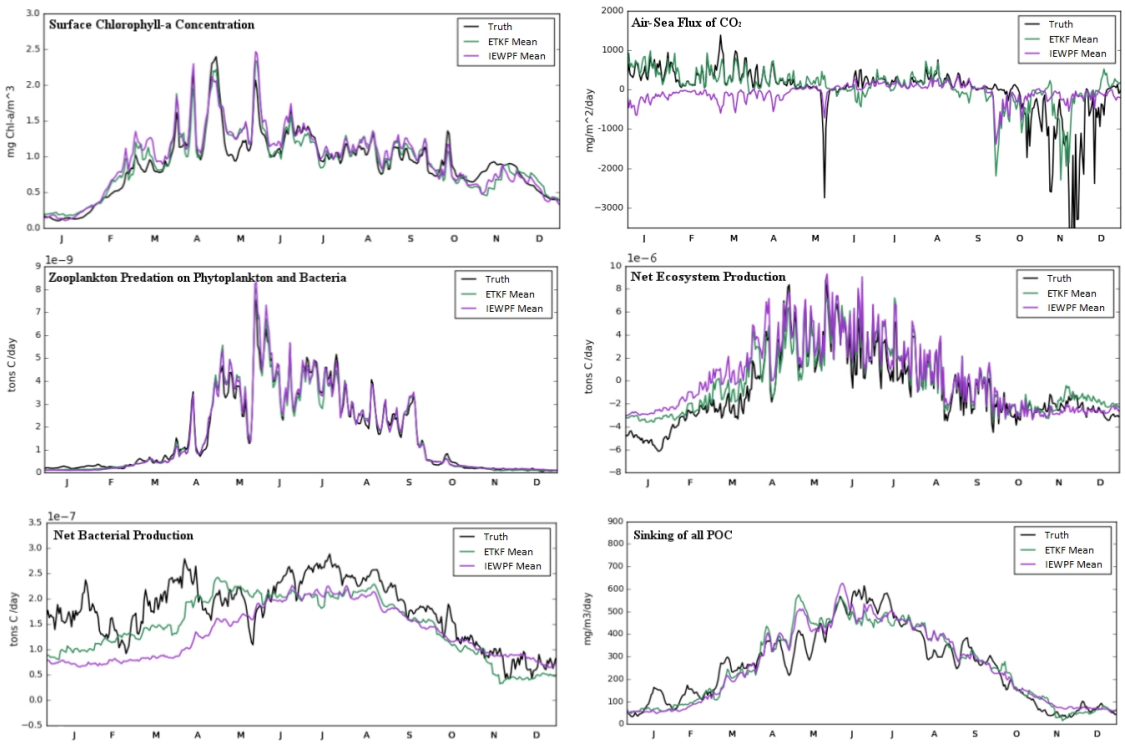

Figure 3.4. Ensemble Means vs. Truth for the six key fluxes. The units for each variable are shown on the y-axis. The x-axis is time, indicated by months. Note that gross primary production minus respiration is the net ecosystem production.

Carbon Flux	Depth	SE	ETKF	IEWPF
Surface [Chl] (Observed Variable)	Surface (0 metres)	0.092	0.056 (- 39%)	0.061 (- 33%)
Air-sea CO_2 Flux	Surface (0 metres)	182	161 (- 11%)	221 (+ 21%)
Zooplankton Predation	Surface (0 metres)	8.5×10^{-11}	8.4×10^{-11} (- 2.0%)	7.9×10^{-11} (- 6.5%)
Net ecosystem Production	Sum of All Layers (0-50 metres)	6.17×10^{-8}	4.71×10^{-8} (- 24%)	6.20×10^{-8} (+ 0.49%)
Net Bacterial Production	Sum of All Layers (0-50 metres)	2.20×10^{-8}	1.91×10^{-8} (- 13%)	2.50×10^{-8} (+ 14%)
Sinking of all POC	Bottom Layer (50 metres)	21.0	22.2 (+ 6.0%)	20.7 (- 1.4%)

Table 3.1. Root Mean Square Deviation (RMSD) between mean and truth for each assimilation technique compared to a stochastic ensemble with the same number of ensemble members. The colours mean indicate the ranking of the performance of each method – green: best, orange: middle, red: worst. The percentages show the decrease from the SE as a proportion of the value for the SE.

The annual evolutions for both DA methods, shown in Figure 3.5, reveals that the ensemble mean for the ETKF fits more tightly than the IEWPF to the true surface chlorophyll concentration (at the surface), which is the observed variable, as well as the air-sea carbon flux, net ecosystem production and net bacterial production. The largest improvement the ETKF makes over the IEWPF is seen for the air-sea flux, where the trajectory of mean ensemble flux is much closer to the simulated truth in Figure 3.4. The IEWPF estimates of the air-sea flux are less skilled, and even mistake the direction of the flux at the start of the year. Overall, the IEWPF only outperforms the ETKF in the case of the sinking of POC at the deepest layer in the model, which is where the ETKF does not improve on the stochastic ensemble (although the difference is relatively small). The IEWPF does perform better towards the end of the run in many cases, as shown for the net ecosystem production and net bacterial production in Figure 3.4, but suffers overall from straying too far from the truth at the start of the year.

In general, while the ETKF performs better, there is a notable difference in where the methods perform strongest - the ETKF generally performs much better for the fluxes taken close to the surface, but the IEWPF performs best (or degrades far less than the ETKF) for the flux at the bottom layer. This shows that the differences in the depths at which variables and fluxes are considered is important to the performance of these methods, and this will be discussed in the following section.

3.4. Discussion

The results showed that the assimilation of the pseudo-observations of ocean colour outperformed the uncertain model simulation, the SE, in estimating the seasonal cycle and annual average of the true carbon fluxes. It also emerged that the spread of the chlorophyll ensemble, as well as the depth at which the DA performance is to be evaluated, are crucial factors in explaining the different performance of the methods. These factors will now be discussed.

3.4.1 Analysis of the Observed Variable

The two assimilation methods operate in different ways, which is best shown by the graphs for the ensemble of chlorophyll concentration values simulated by the different methods (see Figure 3.5, left). The stochastic ensemble (SE) illustrates what the ensemble looks like without assimilating the data, which is displayed here so that the adjustments due to assimilation are made clear.

The ETKF has a reduced dispersion compared to the SE, and ensures that the truth is mostly centred within the ensemble. This makes it a very accurate method for the estimation of chlorophyll. The ensemble overestimates the data in some areas, most notably in March which is suspected to be due to the simulation of an unobserved peak of diatoms. Otherwise there are very few areas beyond this point where the ensemble performs inadequately.

The IEWPF resembles the structure of the SE closely, in both the magnitude of ensemble dispersion as well as the trajectory for the mid-parts of the run. This implies that the IEWPF overestimates the chlorophyll observations during the summer. The features of the nudging parameter applied in the simulations are evident from the midway points between each observation, characterised by sharp decreases of the ensemble spread. The role of the re-sampling step in

a)

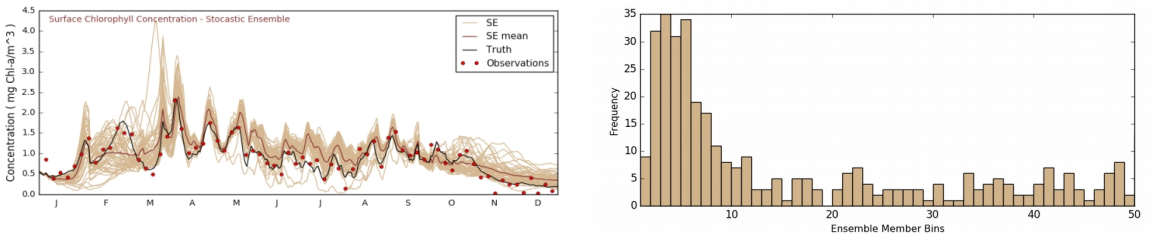

b)

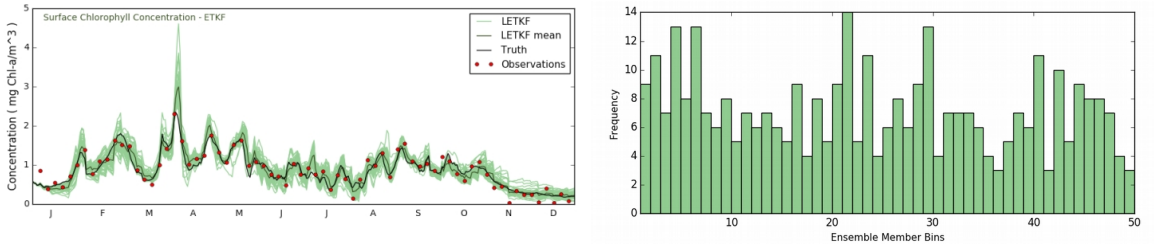

c)

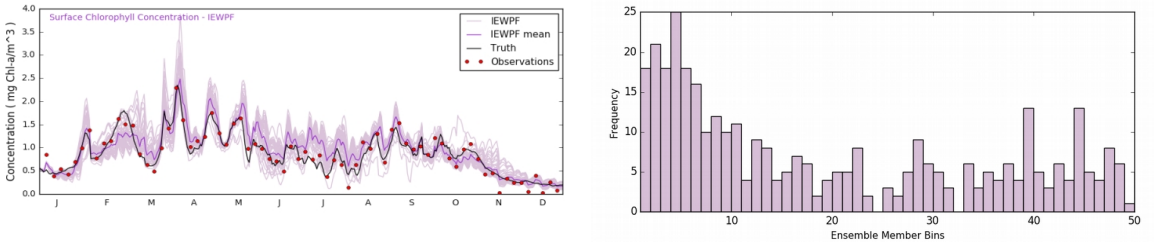

Figure 3.5. Each ensemble method plotted alongside truth and observations for surface chlorophyll for 2008 (left). A rank histogram for each ensemble comparing the spread of the ensemble to the location of the truth within the ensemble (right).

reducing the ensemble inflation is indicated by the slight narrowing of the ensemble at each analysis step.

Both the ETKF and the IEWPF bring the ensemble closer to the observations than the SE, which is to be expected as the SE is given no information about the observations. The ETKF brings the ensemble mean about ten times closer to the observations than the IEWPF (the average difference between the observations and the ensemble mean was 0.06 for the ETKF compared to 0.54 for the IEWPF). It also avoids strong nudges towards observations that deviate strongly from the model trajectory.

The quality of the ETKF compared to the IEWPF is also evident in Figure 3.5: the ETKF ensemble is able to track the truth sufficiently and does so with a lower spread than the IEWPF. Therefore, the ensemble mean is also closer to the truth throughout the year (Figure 3.5) as well as on an annual average (Table 3.1).

Figure 3.5 (right) shows rank histograms for each ensemble in the case of the simulated surface-layer chlorophyll concentration. As described in the Methods, rank histograms show when the ideal ensemble will be centred on the truth (flat columns), while a skew towards low (or high) values represents positive (or negative) bias of the ensemble with respect to the truth.

The stochastic ensemble fails to show a flat histogram, and instead has a peak skewed towards low ranked values. This means that the truth ranks low among the ensemble, i.e. most of the ensemble members are above the truth and so the ensemble has a positive bias). The origin of this bias is suspected to be a result of the truth simulation taking a relatively high value within the distribution of the initial conditions in the SE, which results in the ensemble taking an overall higher trajectory that the truth. Note that while this bias could have been reduced by selecting a more centred value from multliple runs, it is considered a better test of each method to see how each they correct for a truth that lies at the limits of the ensemble. For the SE, there is no assimilation, and therefore no means by which the ensemble can account for this lower-valued state and so most ensemble members will remain above the truth for the full run. Note that this is in contrast to what is encountered in more chaotic systems, such as in atmospheric models, where the information from initial conditions is quickly forgotten.

The ETKF however takes the ensemble down towards the lower-valued truth

from assimilation at an early stage in the run. The comparative flatness of the histogram confirms that the spread of the ensemble encompasses the truth for the majority of the run, indicating an unbiased representation.

The IEWPF improves on the SE as it lowers the frequency of occurrences that most of the ensemble are above the truth. However, it is still is unable to shift the trajectories to sufficiently encompass the truth, as the particles typically resume the regimes they take in the stochastic ensemble. This results in a rank histogram resembling that of the stochastic ensemble, with a minor reduction in the bias.

These histograms show that the ETKF has produced the most appropriate ensemble for the observed variable with a suitable adjustment for the position of the truth compared to the ensemble. This suggests that the ETKF method was better suited than the IEWPF method for surface chlorophyll because the whole ensemble surrounds the truth more closely throughout the year. As a consequence, it is argued that the ETKF is expected to be more skilled at simulating the variables and fluxes that are directly linked to phytoplankton and are also evaluated at surface, such as the air-sea flux and the net ecosystem production. Figure 3.4 appears to support this in the case of the air-sea flux.

3.4.2 Analysis of Unobserved Fluxes

To re-cap: the results in Table 3.1 show that on an annual average, the ETKF was more skilled than the IEWPF, but Figure 3.4 suggested that the skill was variable in time. This is confirmed in figure 3.6, which now shows the plotted difference between mean and truth from the daily averages for all five of the fluxes of interest (note that table 3.1 simply shows the average values of the plots in this figure). These graphs can be used to examine the specific time

frames in which a method is performing especially well, or poorly for each carbon fluxes.

The DA methods typically performed better than the SE almost throughout the whole year, as the difference between SE mean and the truth is mostly higher than the DA methods, particularly for chlorophyll. The IEWPF struggles for some of the fluxes, such as the air-sea flux and the net bacterial production, and the ETKF also under-performs in the summer for some fluxes such as the zooplankton predation. Overall, the ETKF has a more consistent improvement, but both methods are capable of making improvements over the SE, confirming that ocean colour assimilation can improve the simulation of carbon fluxes.

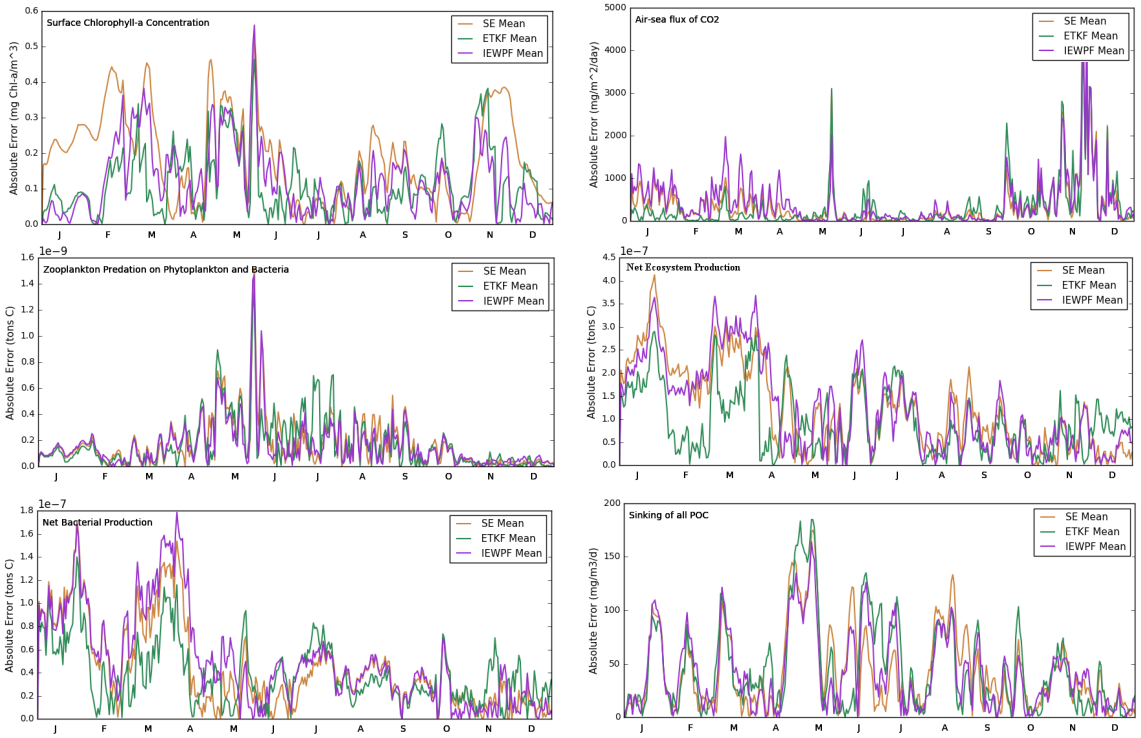

Figure 3.6. The absolute value of the difference between the ensemble mean and the truth (absolute error). These values are shown for the Stochastic Ensemble simulation (SE), the ETKF and the IEWPF, plotted over the full assimilation period. The errors are shown for the surface chlorophyll concentration and the five fluxes previously discussed.

Expanding on the individual performance of DA methods, it is clear that the superior performance shown by the ETKF for the surface chlorophyll concentration, air-sea flux, net ecosystem production and net bacterial production (evident from Table 3.1) is largely due to its ability to adjust to the truth during the summer (Figure 3.6). The air-sea carbon flux is interesting in that it appears to be the winter season where the ETKF performs better, which is likely due to the seasonal dependence on the mixed layer depth (discussed in the following section).

It is also interesting to see that the locations at which the ETKF is less effective for the remaining fluxes is also during the summer. This is the season where non-linear dynamics among variables become more evident, due to phytoplankton blooms, crossing the limits of the linear assumption in the ETKF analysis.

The IEWPF performs better than the ETKF in the cases of zooplankton predation and sinking of POC. This is mainly due to the decrease in skill for both of these fluxes by the ETKF, rather than an accurate representation by the IEWPF. The IEWPF trajectory still remains fairly close to the one of the SE. It can be seen from Figure 3.6 that unlike the surface chlorophyll concentration, there is no clear point in the run at which the IEWPF improves significantly on the SE estimates of the biogeochemical fluxes.

3.4.3 Influence of the mixed layer depth (MLD)

A significant factor that influenced the results of the twin-experiments is the temporal evolution of the mixed layer depth (MLD). An explanation of MLD and a plot of its annual evolution at station L4 is provided in section 2.2.3.

The relevance of the MLD evolution was suggested by the preliminary analysis of the model error in the set-up (Figure 3.2) and was confirmed by the results of the SE and DA simulations (Table 3.1 and Figure 3.4).

As shown previously, the BGC variables simulated at the bottom and surface layers have a stronger correlation in the winter season. However, in the spring and summer seasons the water column is stratified, which implies a weaker correlation among variables simulated at the bottom with respect those at the surface. In particular, there are weaker correlations with respect to the surface chlorophyll concentration, which is the variable assimilated. A weaker summer correlation is expected to result in the weakening of the ETKF due to its linear assumptions.

Therefore, it is mainly in the summer, when the location of the MLD is within the modelled water column, that the non-linear behaviour is exhibited. In fact, this is when the ETKF performed more poorly with respect to the SE for the sinking of POC, while the skill was comparable in the remaining part of the year. This is explained in Figure 2.4 which examined the different degrees of correlation in stratified and non-stratified seasons.

This analysis has allowed us to better assess the limits of the ETKF when examining the influence of ocean colour DA on the variables in deeper layers. The results from this experiment reinforce the idea that the non-linear DA problem can vary in time as the MLD position evolves throughout the year.

3.4.4 Influence of the error covariance matrix Q

Another factor to consider is that the approximations involved in the construction of the Q matrix are likely to have a stronger negative impact on the IEWPF than the ETKF.

All updates for the IEWPF are directly related to the form of the Q matrix, in both the nudging term and the analysis step. As the Q matrix is unrepresentative of the seasonal and mixed-layer variations demonstrated in 3.2.1, the IEWPF is fully unable to incorporate these dynamics as the variables are updated following the time-averaged Q matrix.

The ETKF however generates the covariance matrix directly from the ensemble members at the analysis step. The structure of the Q matrix will have some influence on this, but in general the ETKF will be able to capture some of the model dynamics that will be inherent in the propagation of the ensemble members. The ensemble will see the mixed-layer variations, so is expected to do better below the mixed layer depth than the IEWPF. It is also expected to perform very well for any variable that has a close linear relation to the observations, which is supported by its performance in the cases of the air-sea flux and the net ecosystem production.

From this, it should be considered that the IEWPF has the capacity to improve by a greater amount than the ETKF if a dynamic Q matrix was used that reflects the time-varying physics and biogeochemistry of the system. Therefore, there may be potential for the IEWPF to outperform ETKF if a more advanced setup of the Q matrix is achieved.

3.5. Conclusion

These TEs provide evidence that assimilation of surface chlorophyll concentration into the ERSEM-GOTM model can improve the representation of carbon fluxes in an ideal system, and by extension the assimilation of real ocean colour data can also be expected to benefit the simulation. It has been shown that the simulation of the air-sea carbon flux, the zooplankton predation and the net ecosystem production can all be improved through assimilating surface chlorophyll concentration. Since these fluxes are important components of the BCP, one can argue that this can also be improved by assimilating ocean colour. The improvement to the net bacterial production also indicates that the understanding of the MCP may also benefit from ocean colour assimilation. Therefore, our twin experiments support assimilating ocean colour to investigate the relative importance of the MCP and BCP in the ocean and their contributions to the global carbon budget.

While it is concluded that the ETKF performs better than the IEWPF in this experiment, it appears that to some extent the IEWPF has some minor advantages. To achieve the best results for surface layer variables, or variables with a somewhat linear correlation to the surface chlorophyll concentration, the ETKF is expected to produce more reliable results. However, the IEWPF may be more reliable for ensuring an improvement has been made for some relatively uncorrelated variables. However, it was noted that this improvement may be relatively insignificant. In general, the ETKF made a stronger adjustment for all variables, which often results in a more accurate representation but also results in a greater degree of misrepresentation for the variables with a low correlation to surface chlorophyll.

The TEs could have been improved through the use of a covariance matrix that varies with depth according to the mixed layer depth and the seasonal

variations, as it appears to be a significant contributor to the difference in each DA methods performance. As discussed in section 3.4.4 this may particularly benefit the IEWPF. Also, the number of ensemble members used as well as the number of time-steps between observations has not been investigated here due to the computational costs, but they may be significant factors for investigation in a future analysis.

Chapter 4

Ocean Colour Assimilation at Station L4

4.1 Overview

This chapter describes the multi-annual assimilation of ocean colour data into ERSEM at the coastal station L4 in the Western English Channel. The objective of this is to use ocean colour DA to improve the model simulation and understanding of BGC variables and carbon fluxes in a coastal marine ecosystem characterised by relatively high nutrient concentrations.

The chosen DA method was the ETKF as it outperformed the IEWPF in representing the carbon fluxes in the Twin Experiments (TEs; see Chapter 3 for details). The application at station L4 used a configuration of the ETKF tuned in the TEs, with a few extra modifications that were needed to address spurious trends in the long-term simulations and to accommodate the irregular availability of ocean colour data.

The core results are presented here in two parts: firstly, an evaluation of the assimilation performance in estimating station L4 biogeochemistry, by comparing the output with in situ data (chlorophyll and nutrients) and applying the quantitative skill metrics (see Chapter 2); and secondly, an evaluation of the revised estimates of the carbon fluxes that are associated with the biological and microbial carbon pump (BCP and MCP) after assimilation at station L4.

The discussion of the results will focus on the model performance and on the mean value of the unobserved flux estimates in relation to previous literature estimates of the biogeochemical patterns at the study site. Then, the ability of the

assimilated ocean colour data to represent the chlorophyll concentration at station L4 and the sensitivity of the results to the definition of the observational and model errors will be assessed.

The final section of this chapter will present some concluding remarks, highlighting the advantages and potential limits of assimilating ocean colour into marine models to simulate biogeochemistry in coastal, nutrient-rich sites such as station L4.

4.2 The study site: Station L4

Station L4 is a coastal long-term monitoring site in the Western English Channel (R. Harris, 2010). Figure 4.1 illustrates the location of this site. It is one of several sites included in the Western Channel Observatory (WCO) monitoring program, and has been extensively monitored through both remote sensing and in-situ data retrievals. The site was initially monitored by the UK Marine Biological Association (MBA), but has been sampled weekly by the Plymouth Marine Laboratory (PML) since 1988, providing high-frequency data for core variables such as phytoplankton biomass and pigments, zooplankton biomass, inorganic nutrient concentrations, temperature and salinity.

The site is seasonally stratified throughout the summer period (typically late-April up until September), and is affected by tidal currents with surface speeds of up to $0.6ms^{-1}$ (Smyth et al., 2009). The site is nutrient-rich in winter but surface waters experience nutrient depletion during the reduced vertical mixing in the summer. There is also a considerable influence of weather conditions and cloud cover, which constrains the availability of remote sensing data. The nutrient availability of this site is affected by the riverine run-off by the River Tamar after periods of heavy rainfall (P. Rees et al., 2009), which was particularly noticeable

in 2007 where a period of heavy summertime rainfall contributed to the development of haline stratification at station L4. The chlorophyll seasonality at station L4 are characterised by a spring and autumn phytoplankton blooms (S. Groom et al., 2009).

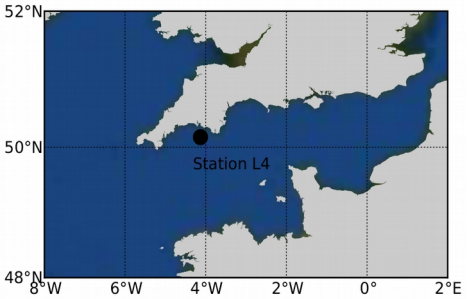

Figure 4.1. The location of Station L4 in the English Channel: 50° 15.00' N, 4° 13.02' W.

There have been many previous modelling efforts at station L4, some of which provide a baseline for comparison with the results presented in this thesis. For example, Lewis et al., 2007, evaluates an ERSEM-POLCOMS model simulation (POLCOMS includes GOTM to model vertical turbulence) through comparison to an in-situ time-series of temperature and nutrients. Polimene et al., 2015, used GOTM-ERSEM to examine the role of the nutritional status of phytoplankton in the formation of the spring bloom, by simulating carbon to nutrient ratios in diatoms at station L4. Some relevant DA examples at station L4 includes Ciavatta et al., 2011, which looks at remotely sensed ocean colour assimilation using ERSEM-POLCOMS, and Ciavatta et al., 2014, which compares assimilation of optical properties with chlorophyll assimilation.

Observational analysis of carbon flux estimates have also been made at station L4, including Litt et al., 2010, who calculated the net air-sea fluxes using the differences in partial pressure of CO_2 (pCO_2) between the ocean and atmosphere observed at station L4 (see Figure 4.2 for results). This study helped to show that station L4 is useful for understanding BCP contributions to the carbon cycle at

coastal marine sites, along with various other studies relating to phytoplankton dynamics, such as Tarran et al., 2015, who examine the seasonal cycles of the nano- and pico-plankton community at station L4. Recently, the site has also been used for conducting studies relating to the MCP due to the bacterial information available at station L4. Tait et al., 2015, for example, examines benthic bacterial responses to the spring bloom at station L4, and Stern et al., 2015, studied microbial biodiversity from water samples at station L4 (among other sites). This study demonstrated that the bacterial community is a crucial driver of the plankton community and biological fluxes at station L4.

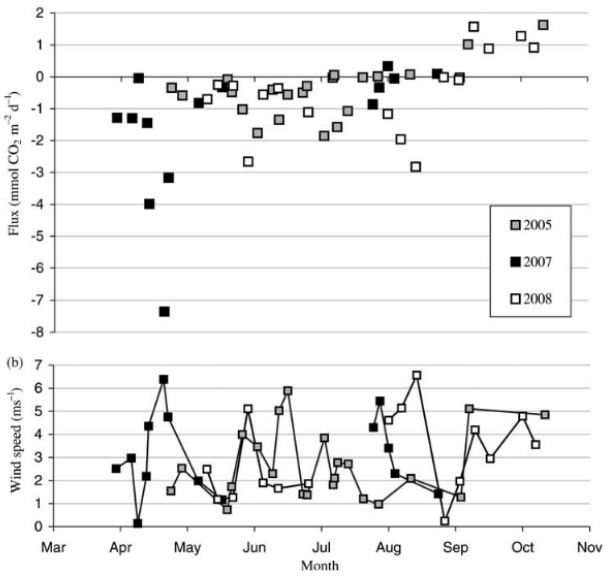

Figure 4.2. Inter-seasonal variability of air-sea CO_2 fluxes during 2005, 2007 and 2008, as reported by Litt et al., 2010. The peaks indicate various phytoplankton dynamics present in the system.

4.3 Set-up of the assimilative system

4.3.1 GOTM-ERSEM

Most parts of the model set-up were derived from Butenschon et al., 2016, and were similar to the application in the TEs (Chapter 3). These include: the selection of the 51 model state variables, the physical parameters used for initialisation and the computation of the five carbon fluxes of interest: air-sea carbon flux, zooplankton predation, net ecosystem production, net bacterial production and sinking of POC. The simulation spans a nine-year period from 2002 to 2010.

The meteorological surface forcing data were acquired from the European Centre for Medium-range Weather Forecasts (Allen et al., 2004). GOTM was set-up to nudge data of weekly temperature and salinity profiles at station L4 for a better simulation of the physical processes (e.g. vertical mixing) at the study site (see also Chapter 2.2 of the Methods).

The remotely sensed chlorophyll-a observations of this site used in the assimilation were extracted as 5-day composites from a global ocean-colour product delivered by the Climate Change Initiative – Ocean-Colour (OC-CCI) Project of the European Space Agency (see Section 2.5).

4.3.2 ETKF Set-Up

The set-up of the ETKF in these simulations exploit the set-up tuned in the TEs (Chapter 3), and so it was also applied with 50 members.

The model configurations uses 100 vertical layers to represent the L4 depth of 50 m, so the localisation factor was set to 100 units. The inflation was unused, as the

scaling factor applied to the Q matrix was used to parametrise the model error, i.e. the dispersion of the model ensemble determined by the stochastic perturbations with covariances defined by Q. This Q matrix is constructed from matrices representing the correlations between variables, and is then scaled according to an input scalar factor. For this application, a further control, the clipping of very low values, was added in the code to prevent the production of negative values of the biogeochemical variable resulting from the stochastic sampling when a variable reaches a low value. A threshold value was set to $1x10^{-10}$, below which the perturbation is recalculated with a different random number until it exceeds this value.

The observational error of the ocean colour data was set up to correspond to 30% of the average value of the chlorophyll concentrations, as it was in the TEs, and similarly to previous applications of data assimilation with real ocean-colour observations (e.g. Natvik and Evensen, 2003).

4.3.3 EMPIRE

Modifications were also required within the EMPIRE system. The main change with respect to the TEs was to rewrite the parts of the EMPIRE input-output code which relied on receiving a set of observations at regular time intervals (e.g. every five days in the TEs). For the TEs, this was not a problem as the observations were artificially generated and so the frequency of their production could be controlled. However, in the real data sets there are certain observations missing due to technical complications or restrictions, such as cloud cover that prevents the satellite detection of ocean colour. Therefore, the EMPIRE code was modified to process a list containing the irregular dates at which observations were available, and could therefore identify the points at which an analysis step was necessary.

An additional task, though not strictly within EMPIRE, was the conversion of the data stored in the ESA OC-CCI files into a similar format as the pseudo-data produced by a truth simulation in EMPIRE. This required the production of binary files with names indicating the timesteps within the model that correspond to the time at which each observation was retrieved.

4.3.4 Assimilative and benchmarking simulations

The model simulation and assimilative reanalysis at station L4 are extended over a period of nine years, initialised at the beginning of 2002 and finishing at the end of 2010. Forcing functions and validation data for this period were available from Butenschon et al. (2016).

The length of the simulated period is much longer than the one in the TEs described in Chapter 3, where the simulation spanned 2 years only. One of the challenges posed by the increased length of the simulation was the emergence of unconstrained trending in the ensemble for certain variables, particularly the nutrients. These trends were always positive and are believed to be the result of the clipping from negative to positive values of certain ensemble members. This clipping had been included in the code to avoid unrealistic negative values of the biogeochemical variable when applying stochastic perturbations (see Section 4.3.2). However, this has the drawback of accumulating positive values over long time periods, typically leading to a significant spurious trend after the first two years of simulation.

To prevent this issue, the ensemble is subject to a re-initialisation at the beginning of each year, where the ensemble members reassemble around pre-set initial values; these are then perturbed stochastically to initialise the ensemble by

representing the uncertainty on initial conditions of the model state variables.

In more detail, the pre-set initial values are computed from a preliminary model simulation, which is identical to the model run without assimilation and is presented as the "reference" in subsequent figures. These values were calculated in two stages: (1) by performing a preliminary model simulation in the years 2002-2009, using the initial conditions in Butenschon et al. (2016) for 2002, and then (2) by computing the average value of each variable on the first of January in the years 2003-2009, averaged along the water column.

The scalar values obtained for each variable in (1)-(2) above were used to initialise the profile of the variable at the beginning of each year of the final reference model simulation. However, in the assimilation simulation, the scalar values obtained for each variable in (1)-(2) were used as mean values of the Gaussian distributions from which the initial conditions of the ensembles were sampled randomly at the beginning of each year.

This approach to reinitialise the simulation annually implies that the reference and reanalysis simulations should not be considered as an unconstrained nine-year simulations, but rather an aggregation of runs for each year individually. The further implication is that such simulations are useful to investigate the biogeochemical seasonal cycles and their inter-annual variability, rather than the long-term trends.

More refined approaches could be applied in future applications to avoid spurious trends in the assimilative simulations, and this will be explored in the discussion.

4.4 Results

4.4.1 Simulation of the Ocean Colour Surface Chlorophyll

The reanalysis and stand-alone model simulation of the ocean-colour derived surface chlorophyll concentration is shown in Figure 4.3. This figure compares the reanalysis output with the assimilated ocean colour data, and shows the reference model simulation without assimilation.

The RMSD between the output and observations is lower for the ETKF than the reference simulation, which is expected as the ETKF is updated by the observations whereas the reference simulation is not.

Considering the time evolution of outputs and data, the chlorophyll observations are more variable than the model and assimilation outputs, and they typically take on higher values during the late summer and autumn period which are underestimated by the model. The autumn bloom in particular is consistently below the observations for both the model and reanalysis.

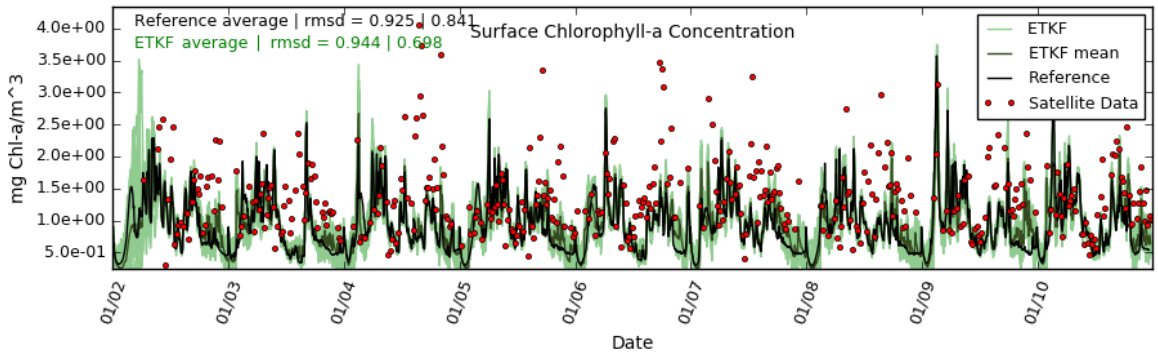

Figure 4.3. A plot of the ETKF ensemble and assimilated data (red) for surface chlorophyll-a concentration. The light green lines represent each ETKF ensemble member, the dark green line is the mean of the ensemble and the black line is the stand-alone model simulation (referred to as the reference). The values in the top left of this graph show the average value (left) and RMSD between the observations (right) for each simulation.

The dispersion of the ETKF ensemble also varies on an annual cycle, with a much narrower range of values taken by the ensemble members during the summer of each year. The reanalysis is also typically higher and closer to the data than the reference during this period.

The main inter-annual differences for both the model and the observations come from the variability in the sizes of the peaks. This is particularly the case for the data, which appears to have a variety of peak sizes that are often formed by just a few observations.

The seasonal cycles and their interannual variability represented by the ETKF mean and the reference simulation are overall comparable. However, some differences are evident. For example, the reanalysis during the autumn-winter period in 2009 is noticeably higher in comparison to the previous years, whereas the reference simulation shows very little variation in this period from other years. It appears that the autumn-winter period in most years is the main time frame in which the reanalysis achieves a better fit to the data than the reference.

Unfortunately the spread is under-dispersive compared to the spread of the data set, implying an under-representation of the observation errors. This results from implementing the same Q matrix as that used in the TEs, which was adjusted to accommodate a 30% uncertainty in the observations. The parameters were kept the same in this chapter as the TEs to maintain enough consistency to apply the results from Chapter 3 to the discussion here, but it is acknowledged that this leads to an under-dispersion in comparison to the data set here due to potentially higher errors in the observations at this site.

4.4.2 Simulation of in-situ Biogeochemical Observations

Figure 4.4 compares the time evolutions of the ETKF ensemble with the in situ data (chlorophyll and nutrient concentrations), as well as the reference model run. In most cases, the reanalysis mean is closer to the data than the reference, suggesting a better biogeochemical simulation by assimilating ocean colour. This is confirmed by the lower RMSD values reported in the plots. Improvements are more evident for chlorophyll and nitrate (0.62% and 1.17%, respectively), less for silicate (0.56%), while the simulation of phosphate degraded (6.67%). These changes are displayed in table 4.1. The RMSD time averaged changes between the reference and reanalysis simulations were relatively small, but differences between the two simulations were evident in some of the simulated seasons and years.

For the in-situ chlorophyll the time evolution of the in situ observations resembles, to a certain extent, the one of the ocean colour observations (Figure 4.3). The seasonal cycle of the data is characterized by low concentrations in winter, peaks in spring that then decrease in summer and reappear in autumn. However, this typical cycle can change with the year, in particular the amplitude of the spring blooms. The model outputs, including the reference but in particular the reanalysis, were capable of reproducing the typical seasonal cycle as well as its inter-annual variability. The low winter and summer values are, in general, well represented by the outputs, e.g. winter 2003/2004 and summer 2010. However, the model is less skilled in representing abrupt spring blooms and the inter-annual variability of their amplitude. For example, the spring bloom was largely underestimated in 2003, while an unobserved bloom was simulated in spring 2009. Overall, the variability of the data was much larger than that of the outputs.

Though both the reference and reanalysis simulations represented the general features of the observed time series, some differences are clear. Crucially, in several instances the reanalysis was closer to the un-assimilated in situ data evident also at a simple visual inspection. This is the case, for example, in Autumn 2005, 2007 and 2008. In a few other circumstances, the assimilation of ocean colour brought the model simulation away from the observations, e.g. autumn 2009. However, the overall benefit of ocean colour assimilation in reproducing in situ chlorophyll observations at station L4 is indicated by the decreased value of the RMSD in Figure 4.4.

For the nutrients: the time evolution of the observations and model runs exhibits an annually repeating pattern. The seasonal cycles are characterised by peaks in winter and periods of low concentrations in summer, converse to the chlorophyll concentration. The shape of the reference run and the ensemble also tend to show fewer individual peaks aside from the peak seen in the winter. The in-situ data shows more variation in peak sizes than the model run which is not captured by the reanalysis. There is a degree of inter-annual variability which is shown by the in-situ data but is not fully captured by the model. The most evident example of this are the high-valued peaks typically seen in the years 2003-2006, where the data is more scattered, which are not present in the later years. There are also periods of very low concentration in the summer for the in-situ data, which is consistently overestimated by the model run. Due to this overestimation, the model generally performs better during the winter periods.

It is also evident from Figure 4.4 that the surface simulations of the nutrients present some discontinuities at the beginning of each year (see e.g. winter 2003/2004). This is due to the annual reinitialisations performed using constant initial values averaged throughout the water column and the period 2002-2003 (described in Section 4.3.4). This helped to prevent long-term trending due to the readjustment of low values.

Variable	Reference Average Value	Reanalysis Average Value (% Difference)	Reference RMSD	Reanalysis RMSD (% Difference)
Chlorophyll	0.94 mg/Chl-a/m^3	0.93 mg/Chl-a/m^3 (- 1.06%)	1.122	1.115 (- 0.62%)
Nitrate	4.89 mmol/m^3	4.85 mmol/m^3 (- 0.82%)	2.56	2.53 (- 1.17%)
Phosphate	0.34 mmol/m^3	0.35 mmol/m^3 (+ 2.94%)	0.15	0.16 (+ 6.67%)
Silicate	2.30 mmol/m^3	2.30 mmol/m^3 (- 0.02%)	1.77	1.76 (- 0.56%)

Table 4.1. Comparison of the average values for the reference and reanalysis. The number in brackets is the percentage difference between the reanalysis and the reference.

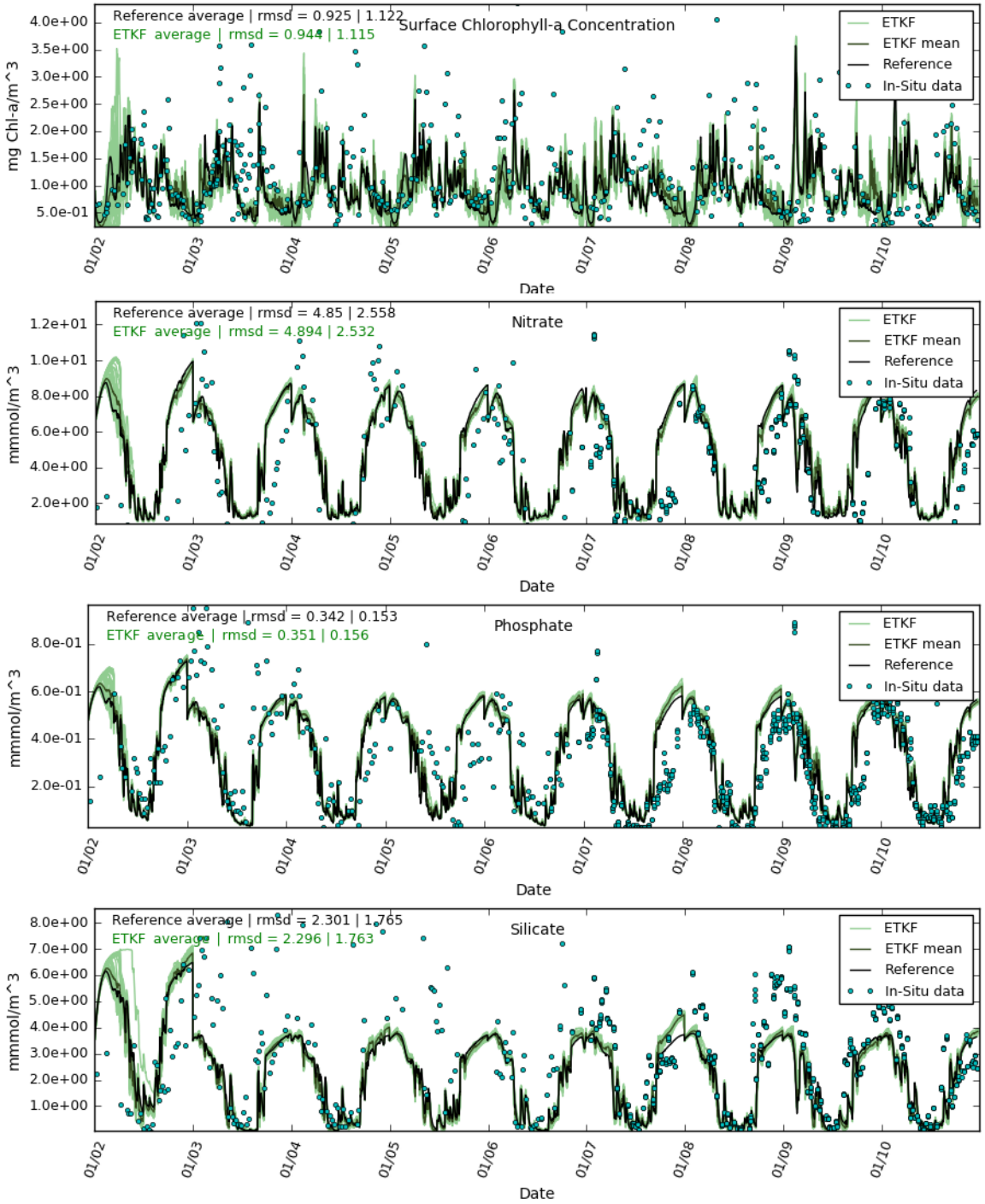

Figure 4.4. A plot of the ETKF ensemble (green) and in situ data (blue) for surface chlorophyll-a concentration and the three modelled nutrients. The light green lines represent each ETKF ensemble member, the dark green line is the mean of the ensemble and the black line is the stand-alone model simulation. The values in the top left of this graph show the average value (left) and RMSD between the observations (right) for each simulation.

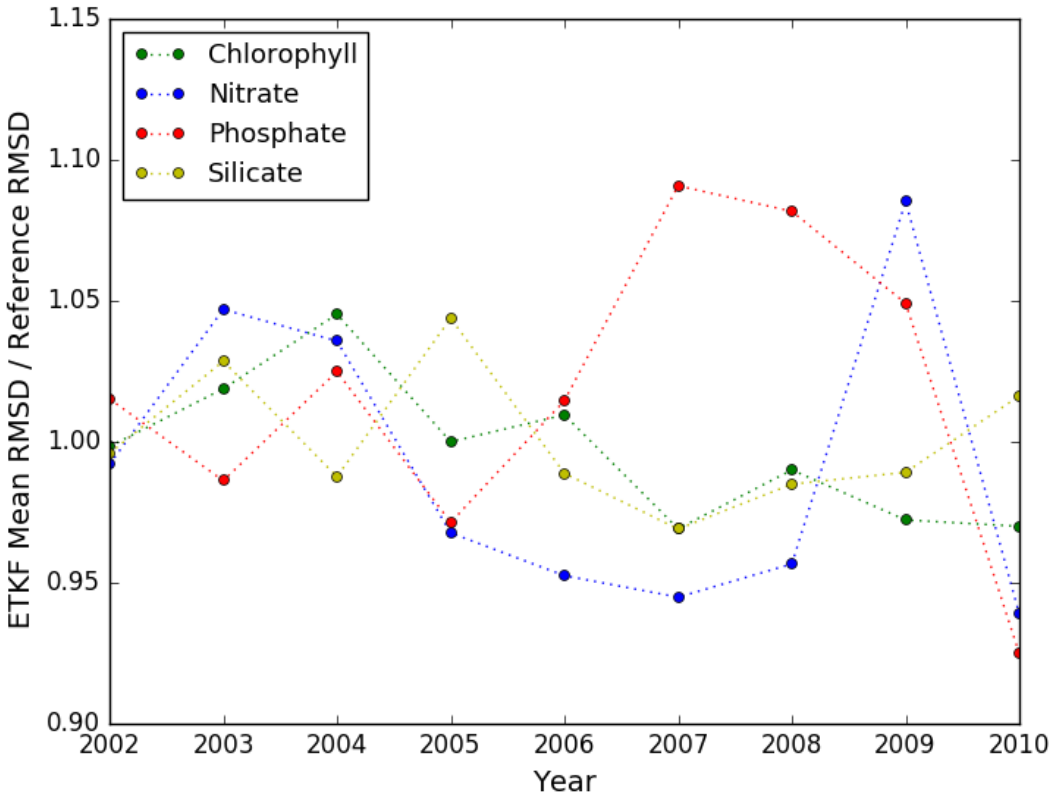

Figure 4.5. Ratio of the data-output RMSD for the ETKF reanalysis mean ("Ensemble Mean RMSD") and reference simulation ("Reference RMSD") computed at each year of the simulation period. Values below one indicate that the reanalysis outperformed the reference simulation

While the reanalysis outperformed the reference simulation on average, with the exception of phosphate (Table 4.1), Figure 4.5 shows that the performance of the ETKF had a large degree of interannual variability. Changes were scattered around the 1-valued threshold until 2005, where the variations became more systematic. In the last period of simulation, the reanalysis outperformed the reference simulations of nitrate at each year, with the exception of 2009. Also silicate and chlorophyll data were simulated better by the reanalysis in the second period of simulation, in general. On the contrary, phosphate deteriorated from 2006 till 2009, and this was not balanced by the low reanalysis RMSD in 2010, explaining the overall deterioration in Table 4.1. The figure also shows that while the differences between the RMSD values for chlorophyll and silicate were small, the robustness of the small changes in chlorophyll was highly variable compared to silicate.

4.4.3 Simulation of Carbon Fluxes

In Figure 4.6, the reanalysis output is plotted alongside the reference model simulation of carbon fluxes that are of interest to the biological and microbial carbon pumps at station L4. Table 4.2 shows the average values for each of these fluxes, taken by the reference and reanalysis simulations.

The air-sea flux of CO_2 is negative in both the simulations, indicating that the simulated system is a source of CO_2 to the atmosphere. Both the simulations represent a seasonal cycle characterized by a negative peak in winter (indicating outgassing) and a positive peak in summer (indicating ingassing). Within each cycle, there are a large number of individual peaks indicating large variations on the time-scale of days. This cycle shows some differences between years, in particular the large downwards peak in 2007 is seen in the reanalysis.

The time evolution for the zooplankton predation is characterized by peaks in the summer and low values in winter. There are numerous internal peaks seen within the summer periods that can vary in frequency between years, for example the two simulated blooms in 2003 are not observed in some other years. The winter period is mostly smooth and does not show much variation.

The net ecosystem production is consistently negative, indicating that CO_2 is released into the water through overall respiration in greater amounts than it is taken from the water by photosynthesis. The seasonal cycle characterized by low negative values in the summer and highly negative values in winter. It closely resembles the graph for zooplankton predation in terms of the differences between internal peaks for each year, but with the values inverted.

The sinking of POC is typically higher valued in the summer than in the winter, and shows a large number of individual peaks with a similar frequency to those seen in the air-sea flux. The height and frequency of these peaks vary across each year.

The net bacterial production is characterized by peaks in summer and low-values in winter. As with many of the other fluxes, small peaks are observed during the summer period with very few seen in winter. Note that here there is a large shift observed at the beginning of each year, but this is due re-initialisation and does not appear to influence the overall simulation.

The largest carbon flux changes made by the reanalysis with respect to the reference simulation are the sinking of POC and air-sea flux, the first of which increases while the second decreases. The remaining fluxes do not change significantly, especially the zooplankton predation which undergoes a very minor reduction.

The ensemble dispersion also varies on an annual cycle for many of the fluxes, similar to the case for surface chlorophyll. This is most prominent for the air-sea flux and the net bacterial production, with a large ensemble spread observed after the beginning of each year for the air-sea flux, and during the winter period for net bacterial production. This is likely to be related to the re-initialisation at the start of each year.

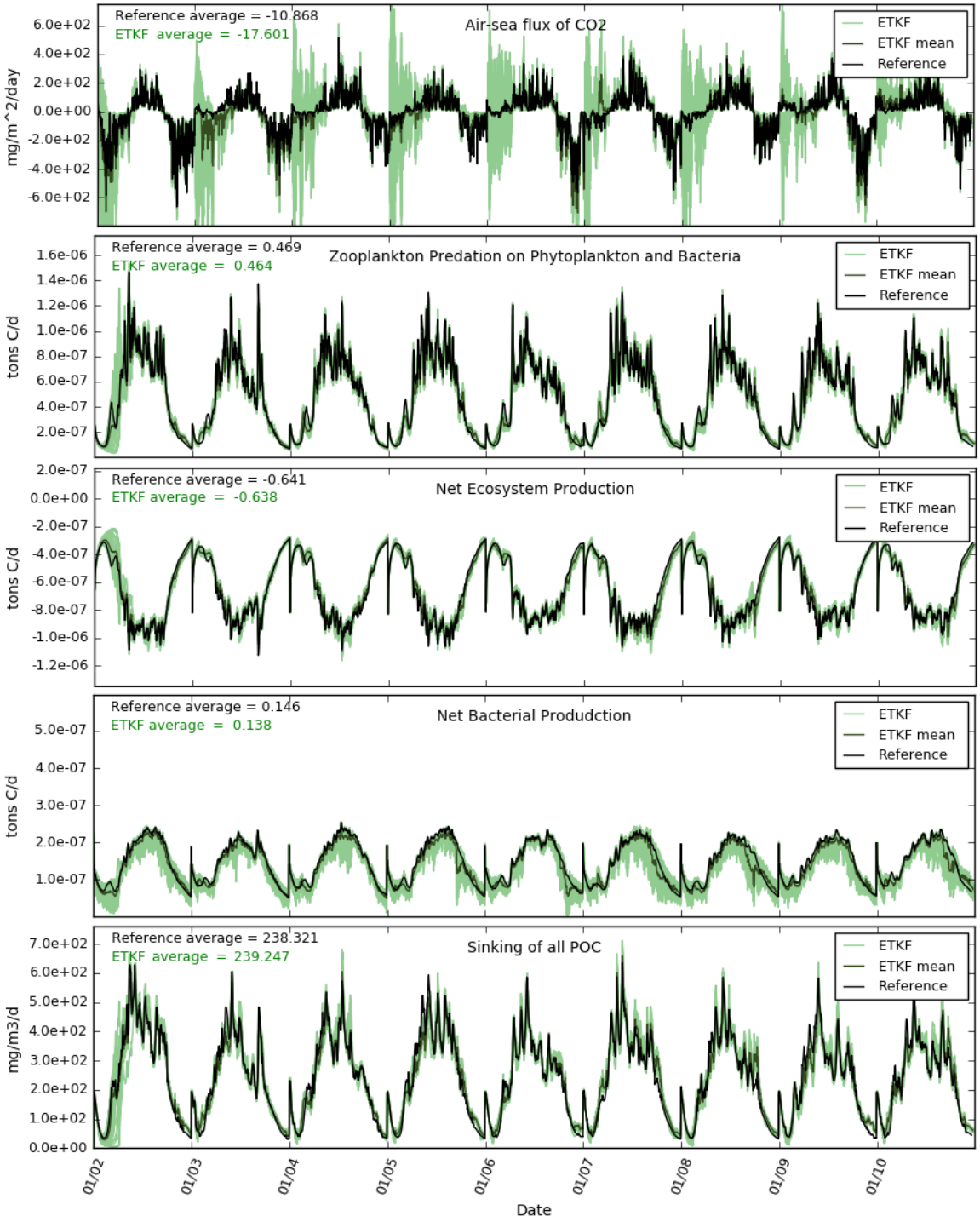

Figure 4.6. Plots of the ETKF ensemble against the model for each of the five carbon fluxes of interest. The light green lines represent each ETKF ensemble member, the dark green line is the mean of the ensemble and the black line is the stand-alone model simulation. The average values displayed in the top left of each plot indicate the average values of the reference and ensemble mean throughout the whole run. The percentage in brackets indicates the change in the average value expressed as a percentage of the average reference value.

Carbon flux	Depth	Reference Average Value	Reanalysis Average Value (% Difference)
Air-sea flux	Surface	-10.9 mg C/m^2/day	-17.6 mg C/m^2/day (- 38.3%)
Zooplankton Predation	Sum of All Layers	46.9 mg C / day	46.4 mg C / day (- 1.06%)
Net Ecosystem Production	Sum of All Layers	-64.1 mg C / day	-63.8 mg C / day (+ 0.47%)
Net Bacterial Production	Sum of All Layers	14.6 mg C / day	13.8 mg C / day (- 5.48%)
Sinking of all POC	500m	238.3 mg C/m^3/day	239.3 mg C/m^3/day (+ 0.42%)

Table 4.2. Comparison of the average values for the reference and reanalysis. Negative values represent outgassing. The number in brackets is the percentage difference between the reanalysis and the reference.

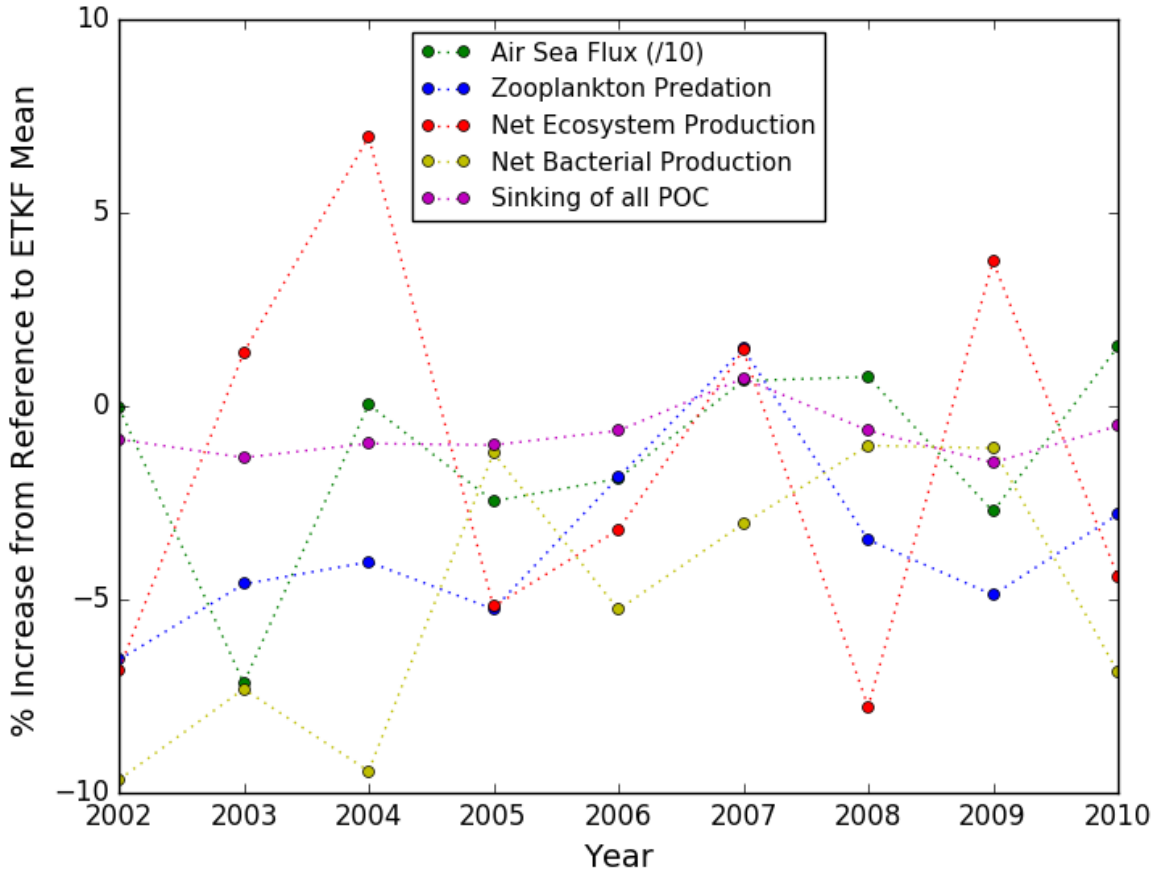

Figure 4.7. Percentage changes of the reanalysis carbon fluxes with respect to the reference simulation. A positive value indicates an increase in value and a negative value indicates a decrease. Changes to the air-sea flux have been reduced by a factor of ten to increase the visibility of the changes to the other fluxes.

Figure 4.7 shows the percentage difference between the reference and reanalysis for each year. The changes to the air-sea flux are the largest, but are divided by a factor of 10 to fit into the plot. The figure shows that the changes of the fluxes are generally consistent between each year. The clearest examples of this are the sinking of POC, the zooplankton predation and the net bacterial production, that were consistently lower in the reanalysis than in the reference simulations (excluding 2007 for zooplankton predation). Also the air-sea flux was lower in most years, with some exceptions such as 2007 and 2009. Despite this, the changes in the net ecosystem production have a marked interannual variability, with different signs in subsequent years. With the exception of the air-sea flux, most of the updates are relatively small as they do not exceed a 10% increase or decrease.

4.5 Discussion

Overall, the reanalysis improves the model simulation of surface chlorophyll concentration derived from ocean colour (Figure 4.3), which is validated from in situ observations (Figure 4.4). On average, assimilation of ocean colour also improved the nitrate and silicate, but deteriorated phosphate (Figure 4.4). However, the performance of the reanalysis with respect to the reference simulation has a degree of interannual variability (Figure 4.5). In terms of the fluxes, the largest impact of assimilation was seen for the air-sea flux and net bacterial production, while the zooplankton predation received the least impact in the multi-annual average (Figure 4.6; Table 4.1). The sign of the changes in the fluxes were substantially consistent throughout the different years of the simulation window (Figure 4.7). The outcome of these are broadly related to the model's capability in representing the biogeochemistry at L4, the reliability of the ocean colour data and the properties of the ETKF. The statements in this overview are explored further in the following subsections.

4.5.1 Impact on the simulation of the Biogeochemical Variables

For the observed variable, surface chlorophyll-a concentration, there was lower RMSD (Figure 4.3) between the ETKF mean and the observations compared to the reference and observations. This is to be expected and serves as a confirmation that the assimilation scheme was successfully implemented, which is similarly argued in Triantafyllou et al., 2007, and again in more depth by Gregg et al., 2009.

A notable feature in Figure 4.3 is that chlorophyll data is fairly consistently underestimated by both the reference and the reanalysis in the summer regions. In Ciavatta et al., 2011, these summer peaks are in fact overestimated, which is likely to be due to differing initial conditions for the model simulation. However, in both cases, blooms in the autumn period are underestimated which can be attributed to the difficulty of the ERSEM model in simulating sudden blooms. This is particularly relevant in late summer and early autumn as the phytoplankton community at station L4 is dominated by dinoflallates. Most of the dinoflagellates species are mixotrophs (Stoecker, 2017), but ERSEM represents them alongside other microphytoplankton which are autotrophs, resulting in a failure to accommodate these peaks appropriately in the current model setup. While this issue remains present in both this application and that of Ciavatta et al., 2011, the set-up here achieves a better RMSD between reference and in-situ data, suggesting a potential improvement over the previous station L4 set-up.

Aside from the assimilated ocean colour data, there was also a slight improvement obtained for the estimation of the in-situ data of surface chlorophyll, shown in Figure 4.4. These observations refer to the same property retrieved from the satellite observations. However the two data sets did not match in time for most of the observations, and a different number of

observations were available for each. The two data sets are shown superimposed in time in Figure 4.6 which illustrates the variations in their trajectories. This is further revealed in Figure 4.8, which shows only the points in each data set that occur at about the same time within a 24-hour period. The relatively high RMSD and low correlation between in situ and ocean colour chlorophyll data means that the assimilation of ocean colour observations may adjust the reanalysis far away from the in situ observations for particular analysis steps. As these situations appear to be in the minority it appears that overall the in situ and ocean colour data were in relative agreement. However, the discrepancy between the two data sets is sufficient to explain the relatively low value of the improvement of the RMSD of in situ chlorophyll.

The most noticeable shortcoming of both the simulation and reanalysis compared to in-situ chlorophyll, is that the peaks are poorly represented. Butenschon et al., 2016, which also provides a comparison between simulated chlorophyll concentration and in-situ data at station L4, also found that the simulation was unable to capture the peaks in the data. One of the suggested reasons they provided for this was the lack of consideration of physical and biogeochemical impacts of the lateral processes in a 1D setting. It is assumed that this argument applies to the simulation shown. Another issue is that ERSEM was parameterised for a general marine system, and so it fails to capture some of the dynamics specific to L4 (Blackford et al., 2004) (Butenschon et al., 2016).

Improvements to the RMSD between mean and in situ data is less prominent for the nutrients. The RMSD was only reduced by 0.03 $mmol/m^3$ for nitrate and 0.01 $mmol/m^3$ for silicate, which is a rather small change. Furthermore, the RMSD was in fact higher in the case of phosphate by 0.01 $mmol/m^3$, suggesting that the reference run may be a better representation of the phosphate evolution.

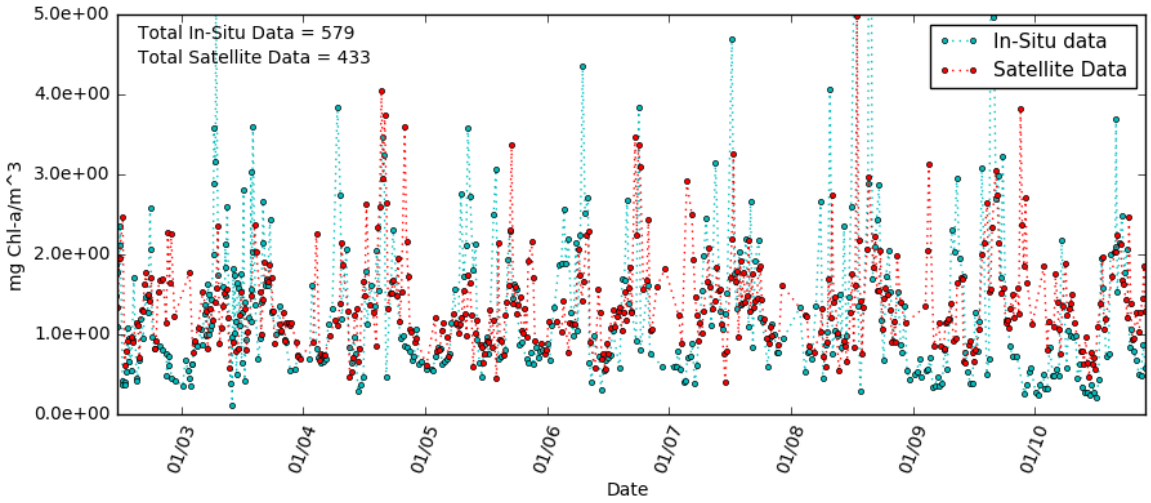

Figure 4.8. A plot of the in situ data and satellite data for surface chlorophyll-a concentration, plotted across the same 8-year period used in the assimilation. The dotted lines show the difference between adjacent plots and are included to illustrate the approximate trajectory represented by each set of data.

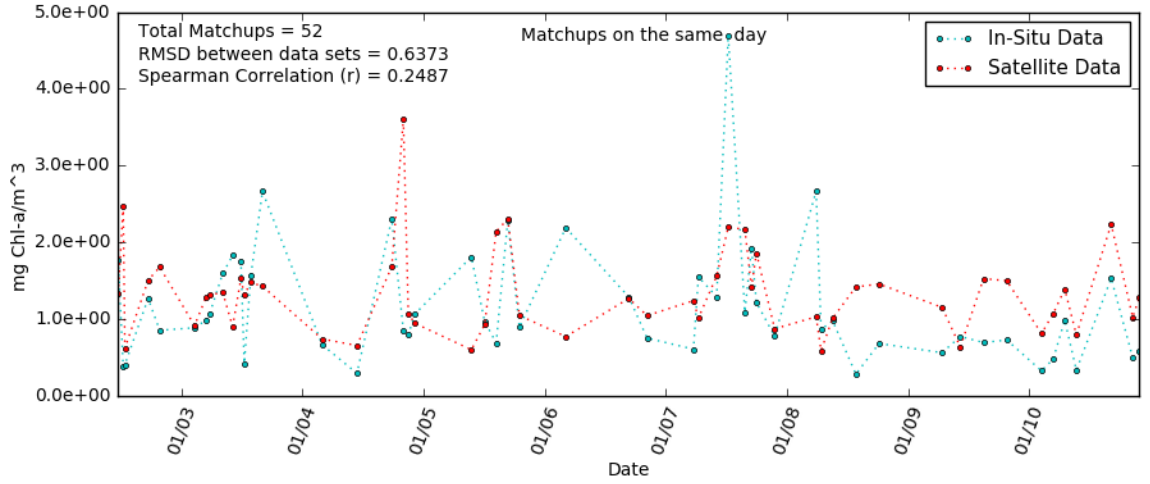

Figure 4.9. A plot of the in situ data and satellite data for surface chlorophyll-a concentration, which shows only the observations that occur within the same 24-hour period. Additional information is displayed in the top left of this figure.

To understand this, it is worth noting that the difficulty in capturing the trends of independent in-situ nutrient data is also present in previous applications of ocean color assimilation. For example, Fontana et al., 2009, found that assimilation took their hindcasts away from ammonia as well as nitrate concentrations (in cases below the surface layer). Nerger and Gregg, 2007, also reported that representation of the nitrate concentration (and some other nutrients) were often

degraded with respect to the model predictions. For the specific case of phosphate, which showed a deterioration for the reanalysis here, it is evident from Figure 4.4 that an overestimation in 2008 and 2009 occurred. Also, it could be the case that because phosphate was already sufficiently captured by the reference model, correcting the bias for phytoplankton increased the phosphate uptake by phytoplankton, deteriorating the optimal previous situation. This remains an issue in other up-to-date studies, such as Ciavatta et al., 2018, which found that PFT assimilation also deteriorated nitrate in ERSEM.

It is also important to note that the relative small changes in the values of the RMSD for the whole simulation period is consistent with the marked interannual variability of the reanalysis performance with respect to the reference simulation (Figure 4.6). However, the improvements are more systematic in the second part of the simulation window, with the exception of phosphate which deteriorated each year. This indicates the need for higher time-resolution metrics (such as the annual RMSD) to understand the full potential an asismilation system.

4.5.2 Impact on the simulation of the Biogeochemical Fluxes

The overall success of the results obtained for the biogeochemical variables allows us to consider the reanalysis estimates of the unobserved carbon fluxes with some confidence on their reliability (Figure 4.5; Table 4.1). This section will begin with a discussion of the causal relationship between the fluxes relating to the influence of the ocean colour DA, and will then discuss the overall quality of the reanalysis and implications for the BCP and MCP.

The starting point for interpreting the DA adjustments made to each flux comes from the increase in total chlorophyll-a concentration. This increase is due to assimilating satellite data which are at higher values on average than the reference run, and this eventually led to the changes seen in the average values for the fluxes. A diagram outlining the effects of the assimilation on the average value of each flux is shown in Figure 4.10, with links between the fluxes. A table summarising the effects of assimilation on other quantities is displayed in Table 4.3, which the following paragraphs will make use of to explain these changes.

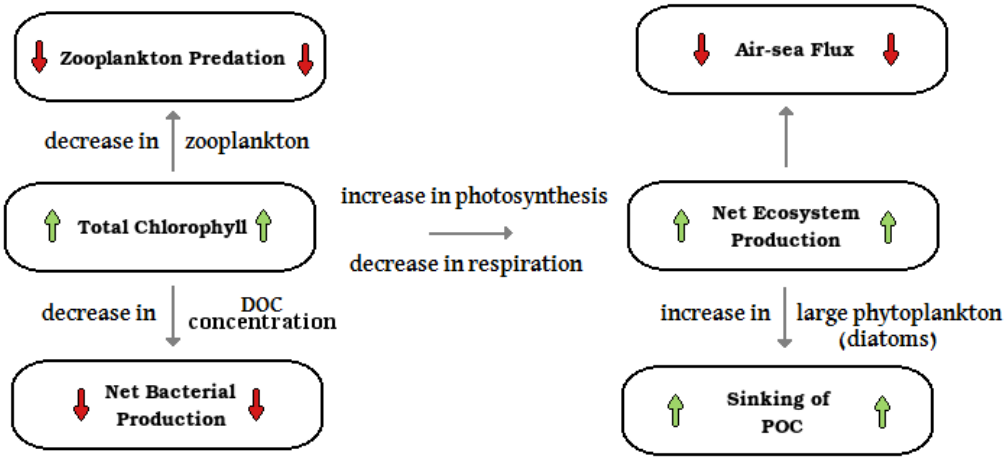

Figure 4.10. Diagram illustrating the impact of the assimilated total chlorophyll increase from DA on the carbon fluxes. Green arrows pointing up indicate an increase and red arrows pointing down indicate a decrease.

Fluxes	Change from Reference Average to ETKF Average
Air-sea flux	- 38.26%
Zooplankton Predation	- 1.06%
Net Ecosystem Production	+ 0.47%
Net Bacterial Production	- 5.48%
Sinking of all POC	+ 0.42%
Phytoplankton Biomass	
Diatoms	+ 5.18%
Nanophytoplankton	- 19.3%
Picophytoplankton	+ 3.13%
Microphytoplankton	- 15.0%
Zooplankton Biomass	
Mesozooplankton	- 0.82%
Microzooplankton	+ 0.94%
Heterotrophic Nanoflagellates	- 1.18%
Dissolved Organic Carbon	
Labile DOC	- 0.37%
Semi-Labile DOC	- 1.51%
Recalcitrant DOC	+ 0.74%
C:Nutrient Ratios	
C:N in Diatoms	- 0.96%
C:P in Diatoms	- 4.84%
C:S in Diatoms	- 0.04%
C:N in Labile DOM	- 0.65%
C:P in Labile DOM	- 1.15%
Respiration	
Phytoplankton Respiration	- 0.38%
Zooplankton Respiration	- 0.36%
Bacteria Respiration	- 0.16%
Additional	
Zooplankton Predation on Phytoplankton Only	+ 0.66%
Zooplankton Predation on Bacteria Only	- 2.83%
Phytoplankton Excretion to DOC	- 0.99%

Table 4.3. A summary of the changes made to the average value of various outputs in ERSEM, expressed as percentages of the reference value.

Net Ecosystem Production: the average value increased by a small margin (+0.47%), which translates to a slight decrease in the carbon output from this flux. As explained previously, this flux relates to the combined effects of photosynthesis by phytoplankton and respiration by each microorganism. For the photosynthesis, an increase is expected due to the increase in the large-type phytoplankton biomass (diatoms), which the model introduces after the rise in chlorophyll concentration that follows from the assimilation. As Table 4.3 shows, the increase in phytoplankton mainly takes the form of diatoms. It should be noted that while there is also a decrease in biomass for smaller phytoplankton

types, nano- and microphytoplankton, their masses are small by comparison and therefore do not make a significant contribution the overall biomass. The increase in overall phytoplankton biomass results in an increase in carbon intake from photosynthesis. Furthermore, the overall respiration of phytoplankton zooplankton and bacteria was slightly reduced after assimilation due which results for the shifts in the PFT and ZFT biomass. Therefore, there is less carbon output which further reinforced the reduction of this flux.

Net Bacterial Production: the average value decreased (-5.48%) which is explained by the decrease in DOC concentration and availability (Table 3.4). The overall reduction in labile and semi-labile DOC means that there are less substrates available for bacterial breakdown. There was also a small reduction in the DOC excretion by phytoplankton, which produce DOC for bacteria. This reduced production of DOC is triggered by the reduction of the carbon to nutrient ratios for diatoms, due to the influence of changing the stoichiometric ratio on the rate of conversion of CO_2 into DOC. While the average of the net bacterial production flux appears to change more than most of the other fluxes by the assimilation, the large shifts imposed by the re-initialisation (which are prominent in Figure 4.5) may be a significant factor for this.

Air-sea flux: the average value decreased (-38.26%), suggesting that the ocean is releasing more CO_2 than predicted by the stand-alone model. The extent of this change is inflated strongly by the timing of the downwards peak in the reanalysis at the start of 2003 which is not present in the reference run. However, even when excluding the first two years from this calculation, a decrease of 15.66% remains (see Figure 4.11). The apparent decrease in this flux is a somewhat unexpected result as it should correlate with respect to the net ecosystem production due to it also sharing contributions from primary production and respiration.

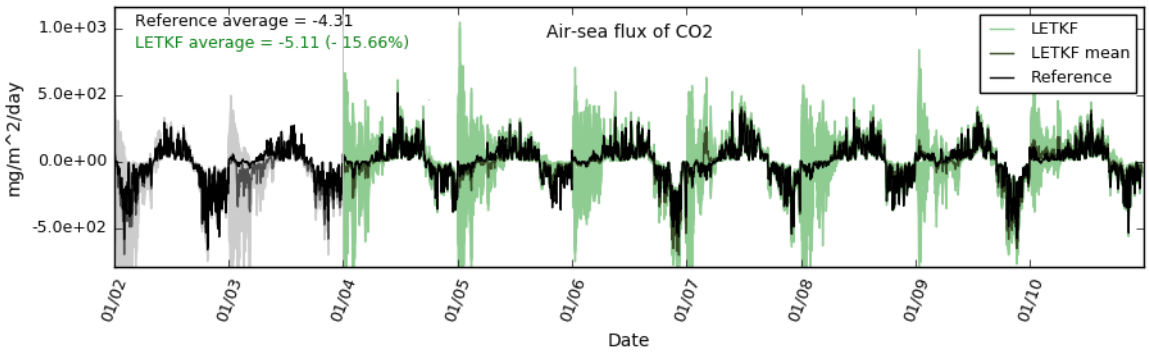

Figure 4.11. Calculation of the reference and assimilation mean for the air-sea flux while excluding the first two years.

It should also be noted that this flux exhibits large variations in spread, shown in Figure 4.5. During the summer and early-autumn periods the ETKF mean remains similar to that of the model, but shows a very large spread of ensemble members in the winter period. Such a large uncertainty might be related dynamics to the produced the annual re-initialization of the model state variables.

By comparing this flux (Figure 4.5) to the findings in Litt et al., 2010 (Figure 4.2), which was derived through pCO_2 observations at station L4, it is evident that some shared seasonal patterns are present. For example, the largest negative peak of air-sea flux is seen for 2007 in both this assimilation and in the observations of Litt et al., 2010, suggesting that ocean colour assimilation may be beneficial with respect to this flux.

Zooplankton predation: the average value decreased by a small amount (-1.06%). The overall decrease can be explained by the fall in the biomass of most zooplankton types which results from the reduction of phytoplankton types that act as prey for these zooplankton. Therefore, there will clearly be a lower amount of grazing by zooplankton as there is a smaller concentration of the overall zooplankton present in the water column. The relatively low extent of this update

may also be due to the cancelling effect of the simultaneous rise in phytoplankton grazing and fall in bacteria grazing which are shown as separate values at the bottom of Table 4.3.

An interesting result from Figure 4.6 is that many of the changes for the zooplankton predation can be linked to the timing of changes to the net ecosystem production. In general, zooplankton predation appears to be inversely linked to the net ecosystem production, which is likely due to the inter-relationship between the zooplankton and phytoplankton biomass. These updates are typically located in the spring period. During the spring period in 2007, the assimilation was influenced by the observed phytoplankton bloom as it increased from the reference, which indicates an improvement. The ability of the assimilation to capture this will have made a beneficial impact on the simulated low trophic web (zooplankton biomass and predation).

Sinking of POC: the average value increased by a small margin (+0.42%). This implies that more POC is being exported on to the sediment. This update is likely due to the extra diatom biomass which produces more particulate organic matter that is subject to sinking. This is not contradicted by the reduction in smaller types of phytoplankton as they are not typically large enough to sink themselves and instead produce fast sinking POC.

4.5.3 Impact on the simulation of the Carbon Pumps

There are implications of the ETKF representation of carbon fluxes in relation to the BCP and MCP shown by the results in Figure 4.5. But, as mentioned before, station L4 is a shallow water site and therefore does not incorporate pumping into the deep ocean. This makes it difficult for a full BCP representation in this set-up, and this should be taken into account in the proceeding comments.

The net ecosystem production, which was the flux most reliably updated by the assimilation according to the TEs (see section 3.4.2), is shifted upwards overall after assimilation by 0.4% (Table 4.3). This may suggest that there is an increased significance of the BCP contribution in the site, due to the additional primary production. There are also many apparent changes made to the bacterial production of recalcitrant DOC (+ 0.74%), which can be seen as an indicator of the influence of ocean colour DA on the simulation of the MCP. The intra-annual changes in the net bacterial production suggests a variation in the dominance of the MCP relative to the BCP throughout the year, as the amount of bacterial decomposition tends to deviate from the reference in the winter periods.

Another interesting result is the zooplankton predation representation, which shows the most variation between the ETKF and the reference simulation model during the spring bloom period each year. The location of many of the changes can be linked to the location of changes to the net ecosystem production, which is likely due to the inter-relationship between the zooplankton and phytoplankton biomass. This suggests that the assimilation improves the representation of phytoplankton contributions during spring, where the observations are helpful in driving the reanalysis towards towards the observed the diatom bloom.

The effects of the MLD dynamics discussed in the TE chapter are most relevant to the sinking of POC. The TEs showed that in the summer periods, this performance of this flux is less reliable, which is likely due to the non-linearity of the relationships between surface and bottom dynamics when the water column is not fully mixed. Therefore, the increase in POC sinking shown by the assimilation may be affected by the uncertainty induced by the onset of the seasonal stratification. As a consequence the ETKF is less effective in improving the simulation of POC fluxes in summer at station L4, which is explored in the next section.

4.5.4 Impact of the ETKF Hypothesis and Set-up

As stated in prior chapters, one of the aims of this thesis is to explore the consequence of the linear assumption of Ensemble Kalman Filter methods within the BGC modelling context, and the difficulty this might present in such non-linear models (van Leeuwen, 2010). This is because the transition throughout the year from a mixed water column to a stratified water column may approximately represent the transition from a spatially non-linear to linear environment (see TE discussion for more details). Therefore, the Gaussian assumptions made within Ensemble Kalman Filter should be more valid during the mixed water column period.

In the context of the biogeochemical analysis at L4, limitations of the linear assumption might become particularly relevant in the late spring and summer periods. In these seasons, the complex production dynamics are at their highest. Additionally, the physical system is split in two by stratification, which weakens the linear link between variables at the surface and the deepest layers.

Through a close examination of Figure 4.3, it is also evident that the reduced RMSD achieved by the reanalysis is mainly achieved in the winter periods, which is where the chlorophyll concentration is clearly above the reference run and therefore closer to the observations. This, along with similar observations for some of the fluxes, can be viewed as evidence of the ETKF showing the most improvement during the periods of high "spatial linearity" (i.e. homogeneity of the biogeochemistry) along the water column. It should be noted however that there is likely a mixture of other factors, such as the failure to capture particular ecosystem dynamics specific to the summer period, as suggested earlier in section 4.5.1.

This application may have improved though the use of a dynamic Q matrix, which could alter throughout the run to account for dynamics that influence the cross-correlations between variables. As discussed in Chapter 3, the potential success of the ETKF may have been greater with respect to the nutrients and fluxes such as the POC sinking. Another improvement could be made by eliminating the need for the annual reinitialisation in the set-up, as this has a strong influence on the results at the start of each year.

4.6 Conclusion

The results of the reanalysis simulations present some evidence that the assimilation of ocean colour can improve our representation of the biogeochemical variables and fluxes at station L4. The result of the decreased air-sea flux and increased sinking of POC implies that certain relevant carbon fluxes may be impacted by the assimilation.

However, these updates are often very small, which is likely to be due to the large observational errors placed on the assimilated chlorophyll data. The overall chlorophyll trajectory is therefore not very sensitive to the assimilation at station L4. It is also difficult to ensure that the updates made are always improvements, especially due to the discrepancies between the in-situ and satellite data sets for chlorophyll.

Overall, the calculations of the carbon fluxes are influenced by the ocean colour assimilation, but are also heavily restrained by the large observation errors present for the current data sets. There will be benefits from ongoing research efforts in developing ocean-colour algorithms for optically complex coastal areas, which will reduce the uncertainties of products available for data assimilation in coastal waters.

Note that a further discussion of the inter-annual variability of the seasonal cycle of the carbon fluxes shown by the assimilation at station L4 is included in Chapter 6, which will compare the results of the station L4 assimilation to that of Bermuda Atlantic Time-Series Study (BATS), which is presented in the next chapter.

Chapter 5

Ocean Colour Assimilation at BATS

5.1 Overview

This chapter describes the multi-annual data assimilation of ocean colour data into ERSEM-GOTM configured for the open ocean station BATS (Bermuda Atlantic Time-Series Study). The objective of this is to improve the simulation and understanding of BGC variables and carbon fluxes in an oligotrophic site in the open ocean, using the same ocean colour DA method that was applied at station L4 (Chapter 4).

While the set-up is similar to the one described in the previous chapter, there are a few essential changes. These changes apply to the initial conditions, observation uncertainties and the exclusion of some phytoplankton functional types to account for the different ecosystem features at the BATS site. Section 5.3 will describe these changes in more detail.

The results presented here include the impact of assimilation on total chlorophyll (section 5.4.1), a comparison of the output with in situ data of chlorophyll and nutrients (section 5.4.2) followed by an evaluation of the revised assimilative estimates of carbon fluxes that are associated with the biological and microbial carbon pump (BCP and MCP) at BATS (section 5.4.3).

The discussion of the results will focus on the model performance and on the mean value of the unobserved flux estimates in relation to previous literature estimates of the biogeochemical patterns at the site (section 5.5).

5.2 The study site: Bermuda Atlantic Time-Series Study

BATS was initiated in 1989 as a broad study of the physical, chemical and biological ocean processes throughout the 4500m deep water column (Philips et al., 2007). It is one of the two main island-based sites examined in the U.S. Joint Global Ocean Flux Study (JGOFS), along with the Hawaiian Ocean Time Series (HOTS). The location of the BATS site is in the western North Atlantic subtropical gyre, illustrated in Figure 5.1.

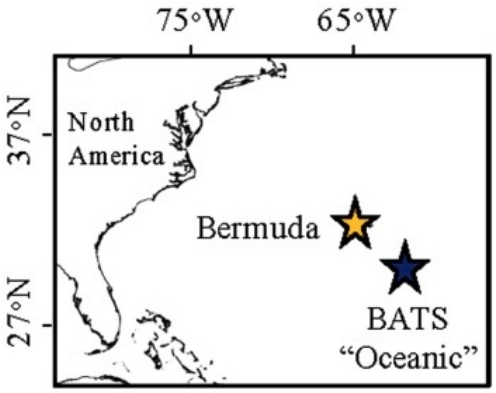

Figure 5.1. The location of the BATS study site: 31° 40' N, 64° 10' W.

BATS has been used to examine the causes of seasonal and inter-annual variability in ocean biogeochemistry (Michaels et al., 1996). Since 1989, there have been nearly monthly cruises to the site, which has helped to create comprehensive data sets useful for inter-annual and decadal climate variability studies.

The site is characterised as an open-ocean site and is nutrient poor (oligotrophic) (Steinberg et al., 2001). The typically low concentrations of nutrients leads to very low concentrations of diatoms and dinoflagellates (Steinberg et al., 2001), which greatly diminishes the prominence of the spring bloom of these groups compared to those seen in nutrient-rich marine environments. Nutrients are available at the surface during winter where the subtropical mode water (STMW) is subject to

deep winter mixing (Worthington, 1976), which results in mixed layer depths between 150-300m. In the summer, the region is subject to high-pressure that prevents further frontal passage and leads to a shallow mixed layer depth, often less than 20m (Steinberg et al., 2001). The typical profiles of temperature and the mixed layer depth from 1989-1997 are illustrated in Figure 5.2.

The ecosystem is also impacted by tropical meteorological events. Low-salinity layers form due to heavy rainfall which can stimulate bloom formation (Michaels et al., 1993). Also, tropical storm activity in the summer and early autumn results in strong winds which change the thermal and physical structure by deepening the mixed layer depth and bringing nutrients to the upper layers, fuelling the phytoplankton blooms (Nelson et al., 1998).

Seasonal and inter-annual dynamics of the carbon fluxes within the water column and the atmospheric interface at BATS have been examined in previous studies. For example, Bates et al., 1996 looked at the total carbon dioxide in the surface layer of BATS for the years 1989-1993, shown in Figure 5.3. They found that there were seasonal variations between about 2010 and 2065 $\mu molkg^{-1}$ in these years. Characteristic seasonal patterns in total CO_2 were evident from these observations, including a maximum in the winter-spring from mixed layer total CO_2, a sharp decrease in spring-summer reaching a minimum in the summer, and a rise in mixed layer total CO_2 during autumn.

The inter-annual dynamics of the biogeochemistry has also been examined through other carbon fluxes in previous studies such as Steinberg et al,. 2001. Figure 5.4. shows these dynamics for primary production and POC at a variety of depths. While some annually recurring features can be identified, these plots typically show large variations in the sizes of most of the peaks between years.

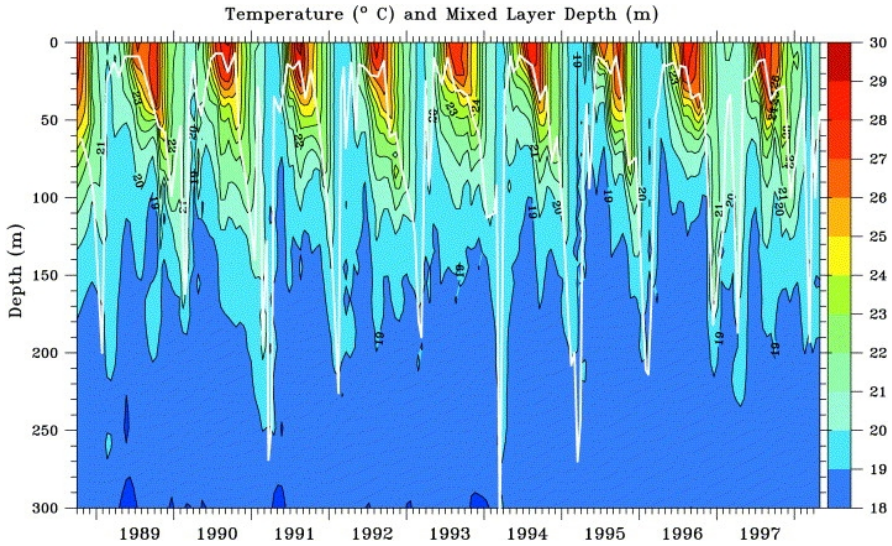

Figure 5.2. Contour plot of temperature with a 1 degrees C contour level. The mixed-layer depth is shown by the white line. Figure is taken from Steinberg et al., 2001.

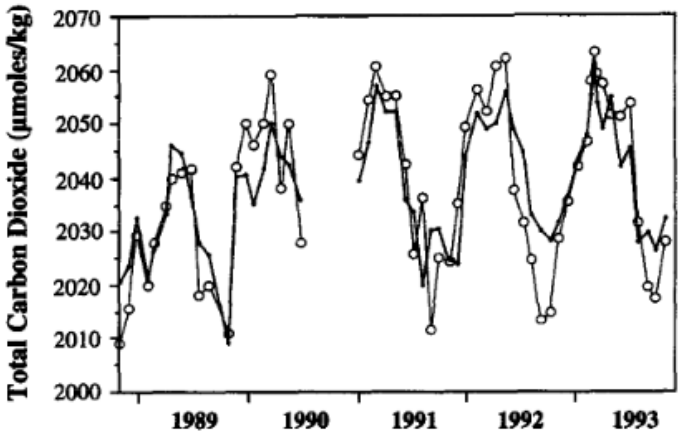

Figure 5.3. Total CO_2 taken monthly at the surface during the first five years of BATS sampling, taken from Bates et al., 1996.

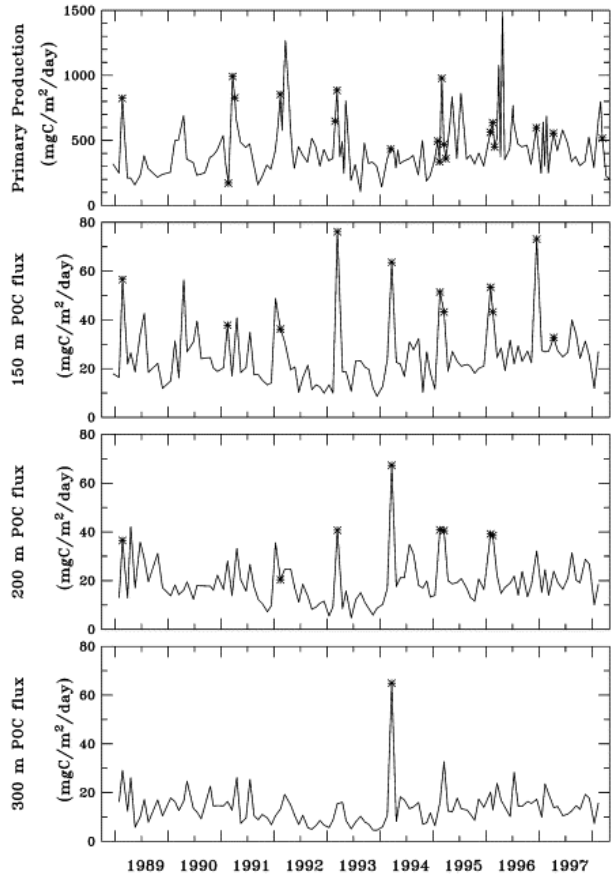

Figure 5.4. Integrated Primary Production from 0 – 140m (top), compared to particulate organic carbon measurements at three depths: 150m, 200m, and 300m, taken each month. Figure is taken from Steinberg et al., 2001.

Previous modelling studies at BATS include Doney et al., 1996, which used a nitrogen-based 1D biologically-physical model based on the site and found success in capturing features of the annual chlorophyll distribution, depth-integrated chlorophyll and primary production that were present in BATS data. More recent modelling efforts include Le Clainche et al., 2010 and Polimene et al., 2011, which have been helpful in explaining various observations in further depth, such as the dimethyl-sulfide summer accumulation at BATS.

Data assimilation at BATS has also been explored. An early example of this is Spitz et al., 1998, which used variational adjoint assimilation to estimate the optimal parameters of a mixed-layer ecosystem model in the upper ocean. A

more recent study that assimilated BATS data is Mattern et al., 2010, which applied both the Ensemble Kalman FIlter (EnKF) and Sequential Importance Resampling (SIR) filter to a physical-biological model including GOTM. This study assessed its results by using a cross comparison of data assimilative and deterministic simulations from a two-year period, and concluded that the predictive skill of the system could be enhanced using the Ensemble Kalman Filter with ensemble sizes of 20 members or greater (which supports the use of 50 in the application of this thesis). A key result of the study by Mattern et al., 2010, was that the estimates of surface chlorophyll and particulate organic carbon were improved compared to a stand-alone model run.

5.3 Set-up of the assimilative system

The set-up of the model and assimilation system is mostly the same as that used in the TEs (Chapter 3) and the station L4 assimilation (Chapter 4). However, there are necessary changes that were required to accommodate the model to the characteristics of the BATS ecosystem and to assimilate the ocean-colour observations retrieved for BATS. An overview of the set-up and changes will now be outlined for both the model (GOTM-ERSEM) set-up and the DA framework (EMPIRE) set-up.

5.3.1 GOTM-ERSEM

The fundamentals of the model set-up were the same as in the TEs, but with the exclusion of some phytoplankton variables to accommodate certain differences from station L4. The same five carbon fluxes were examined here: air-sea carbon flux, zooplankton predation, net ecosystem production, net bacterial production and sinking of POC.

The configuration used for the water column, parameters, initial conditions, and atmospheric forcing for the marine model (GOTM-ERSEM) at BATS was drawn from a previous model application at the same site by Butenschon et al. (2016). The assimilated ocean-colour data were extracted as five-day composites from the ocean-colour CCI-OC product.

The model simulation at BATS spanned the years 1998-2007, based on the availability of forcing data within this range. The initial conditions were also changed from those used for station L4 to better fit the BATS site, with a notable change being the reduction of nutrient concentrations, which were tuned to fit the average values of available in-situ data. The annual reinitialisation that was

employed in the assimilation at station L4 to prevent runaway trends was also used here, but was based on initial values more appropriate for the BATS site.

Another alteration is that two of the four phytoplankton functional types, diatoms and microphytoplankton (i.e. dinoflagellates), were excluded from both the reference simulation and the reanalysis. This exclusion was made to reflect the reports of very low concentrations of diatoms and dinoflagellates (Steinberg et al., 2001). Preliminary simulations with ERSEM at BATS performed for this study also led to the extinction of the diatoms and dinoflagellates, prompting this change.

A further point relating to GOTM in this set-up should be mentioned. The depth levels were defined as 100 vertical layers as in the station L4 application, but here this represent a depth of about 500 metres, compared to 50 metres at station L4. The choice of a deeper threshold ensures that the expected position of the mixed layer depth, which can reach depths up to 300 metres (see Figure 5.2.), is still contained by the model.

5.3.2 Assimilation and EMPIRE

The set-up of the ETKF was also based on the configuration that was tuned in the TEs (Chapter 3), which includes 50 ensemble members.

The model configurations uses 100 vertical layers to represent the BATS depth of 500m (and so each layer represents a greater depth compared to station L4), so the localisation factor was set to 100 units for consistency. The inflation was again unused, and the Q matrix was constructed from matrices representing the correlations between variables, scaled according to an input scalar factor. The clipping control is also present to prevent negative values of the biogeochemical

variable resulting from the stochastic sampling when a variable reaches a low value. A threshold value was set to $1x10^{-10}$, below which an alternative perturbation is used.

An important change made in EMPIRE which relates to the data assimilation was that the observation errors were reduced from those used in the station L4 assimilation. As before, this was a number that represented about 30% of the value of the chlorophyll concentration by looking at the average chlorophyll value of the available data. Because the BATS data had lower values, the magnitudes of the observation errors were reduced. This should also approximately account for the reduced error in observations due it being an open ocean site, and therefore without the uncertainty contributions seen at a coastal site from riverine inputs of coloured dissolved organic matter (CDOM) and re-suspension of sediments.

5.4 Results

5.4.1 Simulation of the Ocean Colour Surface Chlorophyll

The reanalysis simulation and the model simulation of the ocean-colour derived surface chlorophyll concentration are shown in Figure 5.5. This figure compares the reanalysis output with the assimilated ocean colour data, and shows the reference model simulation without assimilation. The RMSD between the output and observations is lower for the ETKF than for the reference simulation, which is expected as the ETKF is updated by the observations. The surface chlorophyll concentration shown here is modelled from just two phytoplankton functional types: pico- and nano- phytoplankton.

In terms of the temporal evolution of the observations and the assimilation output, the chlorophyll observations are followed closely by the trajectory of the ETKF ensemble mean. There are some notable exceptions to this, which includes the lower values of the spring peaks in the reanalysis that is most evident in the years 2000 and 2001. Generally, the reanalysis fits the data well in winter. The reference simulation remains below from the observations at almost all periods.

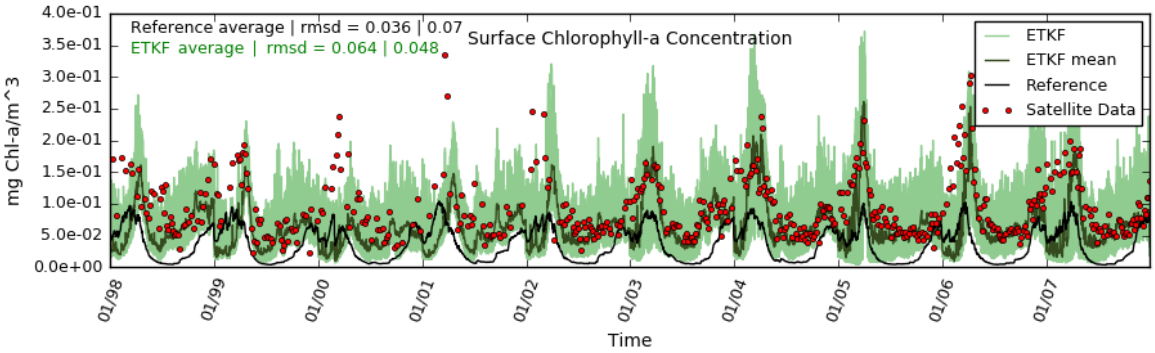

Figure 5.5. A plot of the ETKF ensemble and assimilated data (red) for surface chlorophyll-a concentration. The light green lines represent each ETKF ensemble member, the dark green line is the mean of the ensemble and the black line is the stand-alone model simulation (referred to as the reference). The values in the top left of this graph show the average value (left) and RMSD between the observations (right) for each simulation.

The ensemble spread is highly variable and includes most of the observations within its range, with the spring period of 2000 and 2001 being exceptions to this. The range of ensemble values does not vary significantly on an annual cycle, although the spread is broader from spring 2002 onwards, indicating an increased uncertainty of the estimates.

The main inter-annual differences for both the model and the observations comes from variability in the peak sizes rather than the peaks' location in time. The observations show a wider variety of peak sizes that often consist of only a few data, such as the high peak in 2001 form from only two observations.

The seasonal cycles and their interannual variability represented by the ETKF mean and the reference simulation show some differences. There are many points early in each year where the ETKF takes on values lower than the reference, and during these periods the reference is closer to the spring blooms shown in the data. Also, while the reduction in chlorophyll in the summer is shown by both the assimilation and reference run, they become very close to zero in the case of the reference, which contrasts with the higher chlorophyll concentration seen in the autumn period. For the assimilation output, the magnitude of the chlorophyll concentration remains fairly consistent over the summer-autumn transition period.

Compared to the ensemble spread for the chlorophyll-a concentration at station L4, the dispersion is much better fitted to the data set, with only a few major outliers during the spring bloom period. This suggests that the assignment of observation errors of 30% is more appropriate at the BATS site compared to station L4.

5.4.2 Simulation of in-situ Biogeochemical Observations

Figure 5.6 compares the time evolutions of the ETKF ensemble with in situ data (chlorophyll, nutrient concentrations and primary production), as well as the reference model run. These plots are split into two depth layers which includes surface layer in-situ data of chlorophyll and primary production and data taken at a depth of approximately 100 metres for chlorophyll, nitrate and phosphate. Note that silicate is excluded here due to the omission of diatoms in the simulation. It's useful to consider nutrient concentrations at these depths for skill assessment purposes because the observed concentrations were below the analytical detection limit at the surface. Chlorophyll at 100 metres is also included to evaluate this, and to capture the capability of the system in simulating the deep chlorophyll maximum which is typically observed at ocean open sites (Varrela et al., 1992). Overall, the assimilation improved the simulation of the BGC data compared to the reference simulation. Table 5.1 summarises the metrics used to assess this.

For the surface data, the reanalysis ensemble mean is closer to the data than the reference for both the chlorophyll and primary production, suggesting a better biogeochemical simulation by assimilating ocean colour. This is confirmed by the lower RMSD values reported in the plots, which is about a 4% reduction in RMSD for surface chlorophyll, and a 9% reduction in RMSD for net primary production.

For the surface in-situ chlorophyll data, there is a much higher range of variability compared to the reanalysis mean (Figure 5.3). The data often takes very low values in the summer period which was difficult for the simulation to capture. There are also relatively high data in the years 2003 and 2004, which is not captured by the reanalysis or reference, but was also not evident in the

satellite data. The seasonal cycle of both the chlorophyll and primary production data is typically characterized by two peaks in spring and autumn and lower values in winter and summer during the simulated time window. The amplitude of the spring blooms shows the most variation within this cycle. Both the reference and the reanalysis were capable of reproducing the typical seasonal cycle as well as its inter-annual variability. The reference is in general less skilled in representing abrupt spring blooms and the inter-annual variability of their amplitude, resulting in the underestimation of spring blooms consistently seen in both the ocean-colour and in-situ surface chlorophyll data at BATS. Overall, the benefit of ocean colour assimilation in reproducing in situ surface chlorophyll observations at BATS is indicated by the decreased value of the RMSD in Figure 5.6.

The net primary production at the surface is underestimated by both the reference and reanalysis, and is largely similar in its evolution to chlorophyll. It is improved in the reanalysis case due to the overall increase resulting from the assimilation. The reduction of RMSD from reference to reanalysis is proportionally larger than in the chlorophyll case, indicating a more reliable representation due to the assimilation. There is a high amount of inter-annual variability in both the data and the simulations, which is comparable to previous findings on the primary production shown in Figure 5.4.

For the data at 100 metres, the reanalysis ensemble mean is slightly closer to the data than the reference for two cases, chlorophyll and nitrate, while approximately the same for phosphate, suggesting a slight improvement to the deep layer simulation by assimilating ocean colour. The improvement in RMSD values are about 1%, 0%, and 6% for chlorophyll, phosphate and nitrate respectively.

For the 100 metre chlorophyll data, the reanalysis is shifted upwards slightly due to the effects of surface chlorophyll increase. However, the spread does not sufficiently include the data, suggesting an underestimation of the deep chlorophyll maxima.

Variable	Reference Average Value	Reanalysis Average Value (% Difference)	Reference RMSD	Reanalysis RMSD (% Difference)
Chlorophyll (Surface)	0.036 mg/Chl-a/m^3	0.064 mg/Chl-a/m^3 (+ 77.8%)	0.278	0.267 (- 4.12%)
Net Primary Production (Surface)	2.74 mg C/m^3 / day	5.09 mgC/m^3 / day (+ 85.6%)	6.225	5.713 (- 8.96%)
Chlorophyll (100 metres)	0.012 mg/Chl-a/m^3	0.015 mg/Chl-a/m^3 (+ 25%)	0.539	0.534 (- 0.93%)
Phosphate (100 metres)	0.052 mmol/m^3	0.053 mmol/m^3 (+ 1.89%)	0.018	0.018 (+ 0%)
Nitrate (100 metres)	0.238 mmol/m^3	0.302 mmol/m^3 (+ 21.2%)	0.53	0.501 (- 5.79%)

Table 5.1. Comparison of the average values for the reference and reanalysis. The number in brackets is the percentage difference between the reanalysis and the reference.

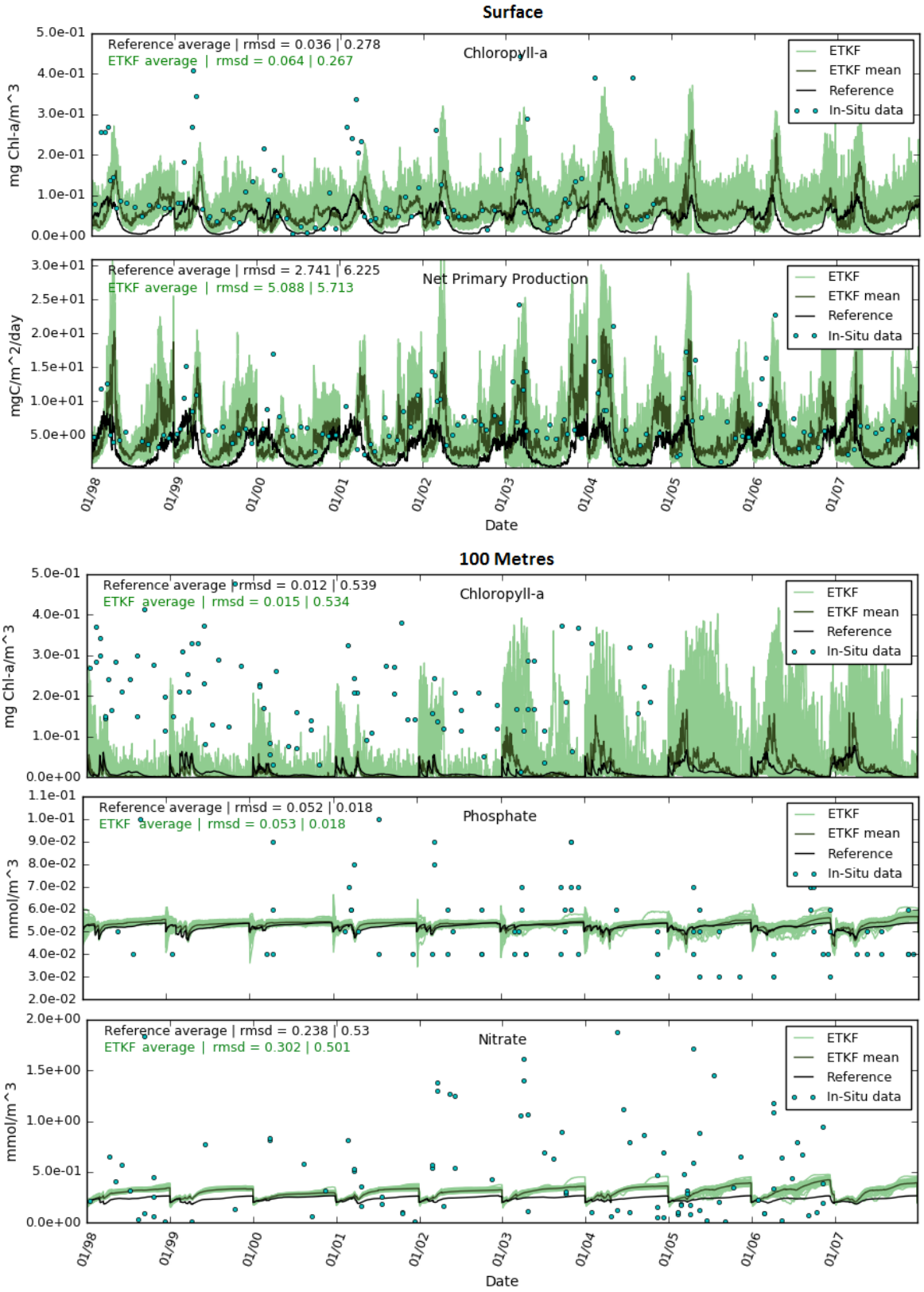

Figure 5.6. A plot of the ETKF ensemble (green) and in situ data (blue) for chlorophyll-a concentration, net primary production and two modelled nutrients. The top two plots are taken from the surface layer, the remaining three plots are taken from a depth of 100 metres. The light green lines represent each ETKF ensemble member, the dark green line is the mean of the ensemble and the black line is the stand-alone model simulation. The values in the top left of this graph show the average value (left) and RMSD between the observations (right) for each simulation.

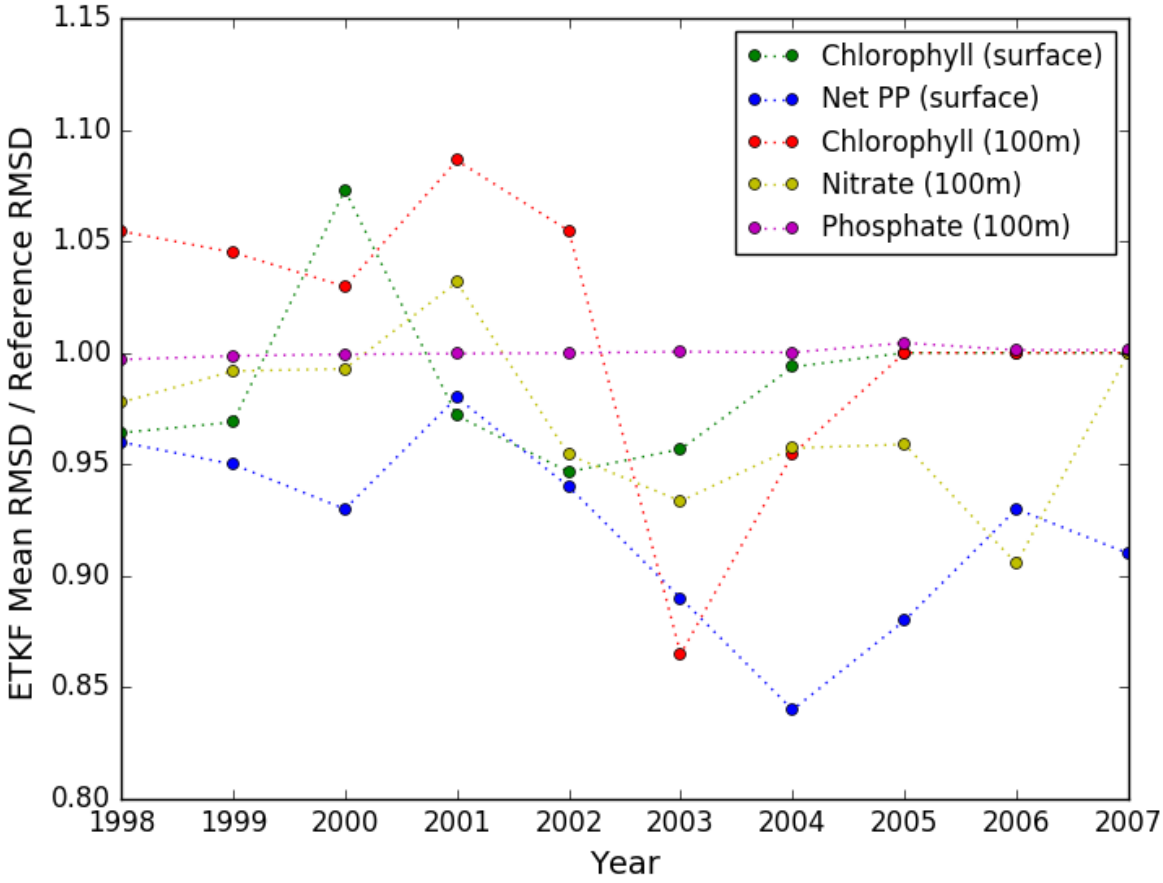

Figure 5.7. Ratio of the data-output RMSD for the ETKF reanalysis mean ("Ensemble Mean RMSD") and reference simulation ("Reference RMSD") computed at each year of the simulation period. Values below one indicate that the reanalysis outperformed the reference simulationThere is no value shown when there is no data available, e.g. for chlorophyll at 100m from 2005-2007.

For the nutrients: the time evolution of the observations and model runs exhibit an annually repeating pattern, but this is typically constrained to very low values. The peaks shown in the model simulations are very small in comparison to the in-situ data, despite having comparable average values. Nitrate shows the most impact of the assimilation with multiple years showing a high-valued reanalysis compared to reference, which results in a lower RMSD due to the typically high valued in-situ data. The modelled phosphate does not appear to be influenced significantly due the low concentrations involved.

In general, the nutrient concentrations are slightly higher-valued in the summer period than the winter period, which is in contrast to the chlorophyll

concentration at the same depth. The reference run and reanalysis do not show any discernible peaks, and the low availability of the data also makes these peaks somewhat difficult to identify, due to being comprised of only a few data. The data shows far more variation in each case compared to that of the ensemble.

It is also evident from some of the plots in Figure 5.6, particularly for deep layer chlorophyll and nitrate, that some of these simulations exhibit the discontinuities at the beginning of certain years. This is again due to the annual reinitialisations performed using constant initial values.

Figure 5.7 shows the differences in the RMSD between each run and the in-situ data for each year. The reanalysis improved the simulation of the in situ data for most variables at each year. The clearest example is the surface net primary production, with the RMSD ratios always below 1. The simulations of surface chlorophyll and nitrate at depth were almost constantly improved by the reanalysis, with the exception of one year in each case (2000 and 2001 for surface chlorophyll and nitrate, respectively). However, chlorophyll at 100 metres was deteriorated by the reanalysis in the first part of the simulation (1998-2003) and was improved markedly in 2 subsequent years. The reanalysis and reference simulation of phosphate had comparable errors at each year, but the significance of this results is affected by the low number of data available for this parameter in the first part of the simulation (shown in Figure 5.6) Unlike at Station L4, the differences between the reference and the reanalysis are mostly consistent, as the plots are usually remain above or below a value of 1.

The poor performance of the assimilation at the deeper layers is suspected to be due in part to the problem of representing very low concentrations with an ensemble for positive-definite variables. It is also reflective of the difficulty of the ETKF to provide consistent results throughout the full water column, as discussed in the results in Chapter 3.

5.4.3 Simulation of Carbon Fluxes

In Figure 5.6, the reanalysis output is plotted alongside the reference model simulation of carbon fluxes that are of interest to the biological and microbial carbon pumps at BATS. Table 5.2 shows the average values for each of these fluxes, taken by the reference and reanalysis simulations, and states the depths at which each flux has been considered.

The air-sea flux of CO_2 is negative in both the simulations, indicating that the simulated system is a source of CO_2 to the atmosphere. Both the simulations represent a seasonal cycle characterized by a negative peak in winter (indicating outgassing) with some very minor positive peaks in summer (indicating ingassing). Within each cycle, there are a large number of individual peaks indicating large variations on the time-scale of days. This cycle shows some differences between years, but in general the amplitudes of these peaks are similar. Note that due to the large shifts in values at the beginning of each year, the average values shown in Figure 5.6 were calculated excluding the first three months of each year to exclude the effect of the reinitialisations from these estimates.

The time evolution for the reference simulation of zooplankton predation is consistently low-valued with respect to the reanalysis, with the exception of reinitialisation peaks at the beginning of each year. For the reanalysis there is a clear region in which higher values are taken by the ensemble throughout the years 2003-2004, and there are peaks around the autumn period for almost every year. The ensemble spread during the peaks is very high compared to the mean, indicating that the increase in the mean is influenced by just a few members. During the early stages of each year, the ensemble is mostly at slightly lower values than the reference.

The net ecosystem production is consistently positive, indicating that CO_2 is taken from the water by photosynthesis in greater amounts than it is released into the water through overall respiration. The seasonal cycle is characterized by high values during the spring period, with steady positive values in the summer and low positive values at the beginning of each year. The reanalysis takes on higher values in almost every period except for the low-valued winter regions. Apart from a notably reduced spring peak in the year 2000, there is not much inter-annual variability, as each year exhibits a similar pattern.

The net bacterial production is characterized by peaks in spring and lower values for the remaining parts of each year. The average value of this flux outside of the spring period is very close to zero. As with many of the other fluxes, small peaks are observed throughout the year. The assimilation mean deviates from the reference in a number of places, and a relatively large spread is seen in the ensemble which extends both above and below the typical reference values.

The sinking of POC is typically high valued in the spring and at its lowest during the summer, and shows a large number of small peaks throughout the year. The height of these peaks is quite variable for the reanalysis, but does not seem to vary by much for the reference. The ensemble is mostly higher-valued than the reference with a few exceptions at the start of each year for the first few years. There is very little inter-annual variability outside of the variation in peak size during spring for the reanalysis.

The largest proportional carbon flux changes made by the reanalysis with respect to the reference simulation is the zooplankton predation, with a considerable increase of almost 72% of the average value for the reference run. The remaining fluxes apart from the air-sea flux also receive a considerable increase. Despite a few periods where the reanalysis takes on lower values than the reference, the average value of each carbon flux shown here is increased by the assimilation.

Carbon flux	Depth	Reference Average Value	Reanalysis Average Value (% Difference)
Air-sea flux	Surface	- 1081 mg C/m^2/day	- 946 mg C/m^2/day (+ 12.5%)
Zooplankton Predation	Sum of All Layers	0.002 mg C / day	0.006 mg C / day (+ 200%)
Net Ecosystem Production	Sum of All Layers	3.70 mg C / day	8.32 mg C / day (+ 125%)
Net Bacterial Production	Sum of All Layers	0.021 mg C / day	0.041 mg C / day (+ 95.2%)
Sinking of all POC	500m	1.85 mg C/m^3/day	3.79 mg C/m^3/day (+ 105%)

Table 5.2. Comparison of the average values for the reference and reanalysis. Negative values represent outgassing. The number in brackets is the percentage difference between the reanalysis and the reference.

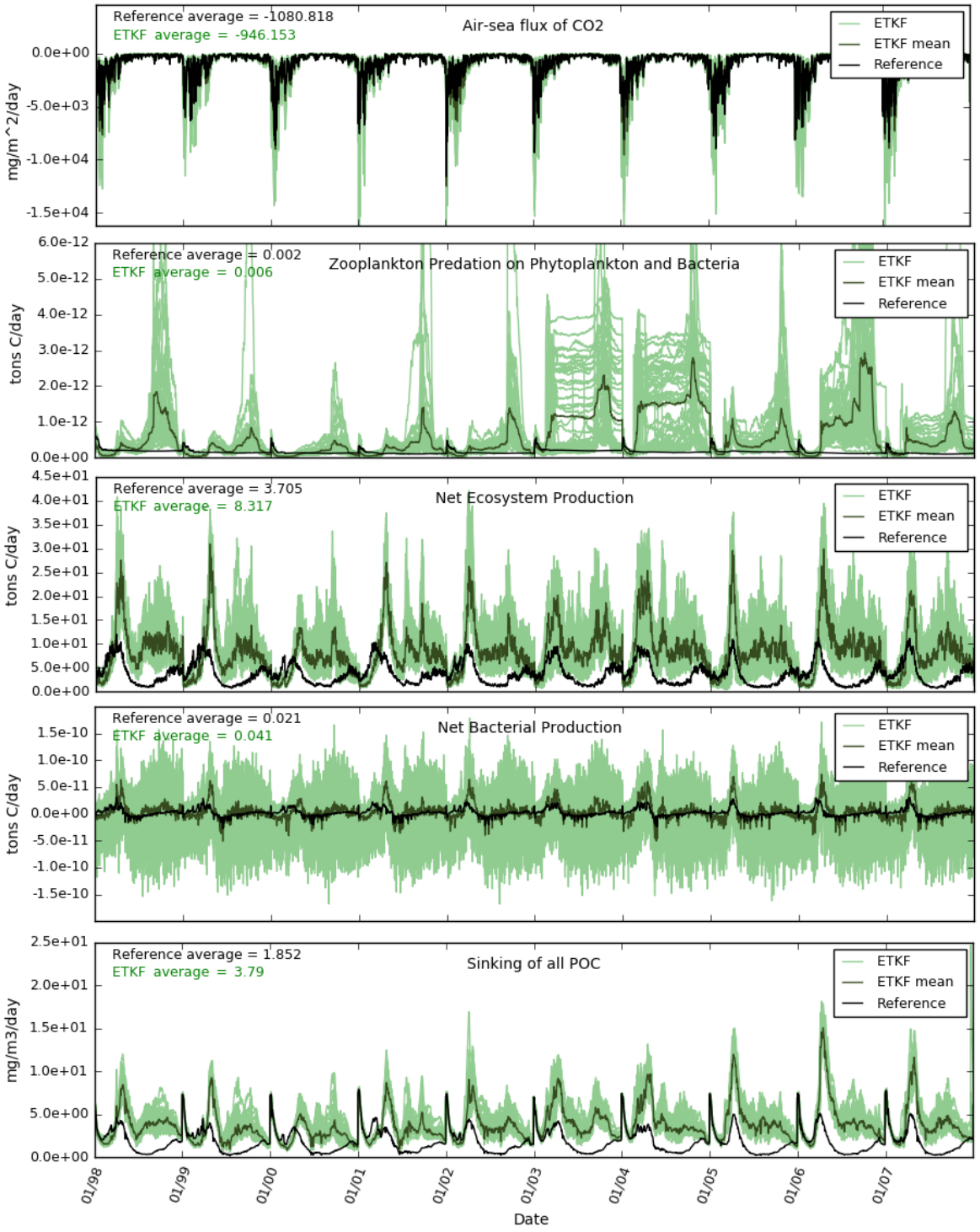

Figure 5.8. Plots of the ETKF ensemble against the model for each of the five carbon fluxes of interest. The light green lines represent each ETKF ensemble member, the dark green line is the mean of the ensemble and the black line is the stand-alone model simulation. The average values displayed in the top left of each plot indicate the average values of the reference and ensemble mean throughout the whole run. The percentage in brackets indicates the change in the average value expressed as a proportion of the average reference value. The average values calculated for the air-sea flux were made while excluding the first three months of each year.

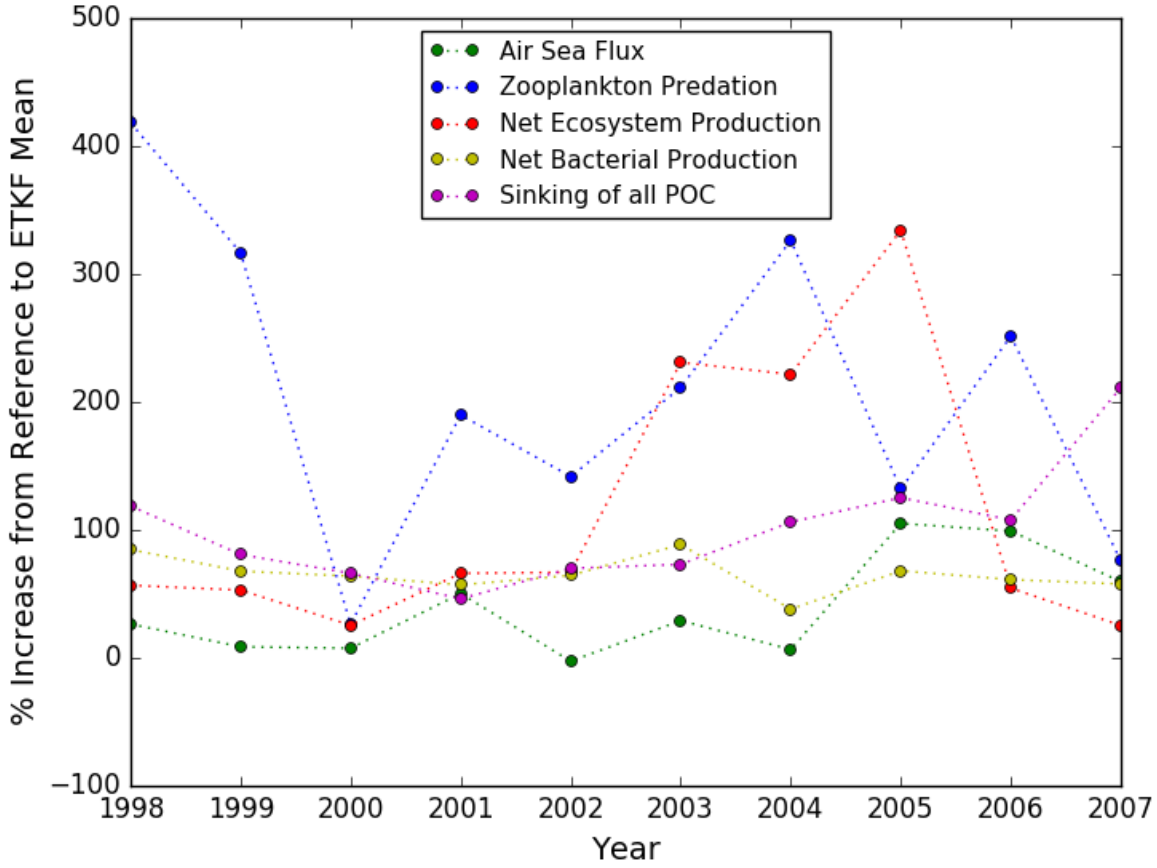

Figure 5.9. Percentage changes of the reanalysis carbon fluxes with respect to the reference simulation. A plot of the percentage increase from Reference to LETKF mean for each year. A positive value indicates an increase in value and a negative value indicates a decrease.

Figure 5.9 shows the percentage difference between the reference and reanalysis for each year. From this figure, it is clear that the fluxes are increased at almost all stages of the run, with one exception for the air-sea flux (2002). The zooplankton predation and net ecosystem production experience the largest variations between values, with some values exceeding 300% of the value in the reference run. These changes were overall much larger than those for station L4.

5.5 Discussion

Overall, the reanalysis improved the model simulation of surface chlorophyll concentration derived from ocean colour (Figure 5.5), and in-situ observations (Figure 5.6). Further comparison to in-situ data (averaged over the multi-annual simulation window) suggests that the assimilation of ocean colour also improved the unassimilated deep-layer nitrate and surface-layer primary production, but showed results for deep chlorophyll and phosphate comparable to the reference runs (Figure 5.6). Crucially, such improvements were consistent during every year of the simulation window, for most of the variables (Figure 5.7). The largest proportional impact of assimilation on the fluxes was seen for the zooplankton predation, while the air-sea flux was impacted the least (Figure 5.7; Table 5.1). These outcomes are related to the model's capability in representing the biogeochemistry at BATS, the reliability of the ocean colour data and to the properties of the ETKF. The following subsections explain these points in more depth in a similar format to Chapter 4.

5.5.1 Impact on the simulation of the Biogeochemical Variables

For the observed variable, surface chlorophyll-a concentration, there was lower RMSD (Figure 5.5) between the ETKF mean and the observations compared to the RMSD between the reference and observations. The reason for this improvement is influenced strongly by the relatively low observation errors of the assimilated ocean-colour data, which were consistent with the open-ocean location of the BATS site.

The observed chlorophyll peak values are consistently underestimated by both the reference and the reanalysis. This is related to both the difficulty of the ERSEM model in simulating sudden blooms, and the exclusion of diatoms and

dinoflagellates in the simulations.

There was also an improvement to the estimation of in-situ data of surface chlorophyll, shown in Figure 5.6. In general, the improvement of the reanalysis is due to the consistent underestimation of the reference run for the typical concentration values. As the run is increased by assimilating higher-valued satellite observations, is it also closer to this much sparser data set of in-situ chlorophyll concentration, as the values in this data are also much higher than the reference. Despite this, the in-situ data peaks are still not captured by the reanalysis run, for the same reason that the model could not capture the peaks of phytoplankton blooms.

The result of the reduction in the RMSD between mean and in situ data for the surface net primary production is likely due to the close relationship between this flux and the chlorophyll. Like the chlorophyll plots, the primary production is understimated consistently by the reference, and so the reanalysis fits the data better by increasing the phytoplankton biomass through the increase in chlorophyll after assimilation.

For the in-situ data taken at 100 metres, the improvements are less obvious, but still present. As there is a full range of simulated layers separating this depth and the surface layer where the assimilated data is retrieved, it is expected that assimilation will struggle to influence the deeper layer as strongly as the surface. The reanalysis is drawn towards the deep chlorophyll data similarly to the case at the surface layer, but to a much lesser extent. The reanalysis of nitrate is also increased which supports the fact that the in-situ data is, on average, located above the reference simulation, whereas the distribution is more even around the reference in the case of phosphate. The reason for the lack of updates from the average in-situ data values for the nutrients is likely due to a combination of the

initialisation of the simulation, which is already based on similar data, and the absence of significant dynamics for trajectories to deviate from this value. However, the variation in location of the nutrient data does suggest that some dynamics may have been difficult to simulate at these depths.

Figure 5.7. consolidates some of these comments as almost all of the variables are improved as the past 2002. However, it is important to note that the accuracy of many of these improvements is reduced due to the relatively small sample size of data in these years An important outcome shown in Figure 5.7. is the ability of the reanalysis to improve the RMSD for net primary production across all years suggesting a robust improvement in its representation with the assimilation.

5.5.2 Impact on the simulation of the Biogeochemical Fluxes

The overall success of the results obtained for the biogeochemical variables allows us to consider the reanalysis estimates of the unobserved carbon fluxes with some confidence on their reliability (Figure 5.7 and Table 5.2). This section will begin with a discussion of the causal relationship between changes in the reanalysed fluxes driven by ocean-colour DA. Then, the overall quality of the reanalysis and its implications for the BCP and MCP simulation will be discussed in the next section.

The increase in the assimilated total chlorophyll-a concentration is the initial driver of the changes to each of the fluxes. The total chlorophyll increases due to assimilating satellite data which are at higher values on average than the reference run. The corresponding increase of phytoplankton biomass and production has cascading effects throughout the simulated ecosystem processes and carbon fluxes. A diagram outlining the effects of the assimilation on the average of each flux is shown in Figure 5.8, with links between the fluxes.

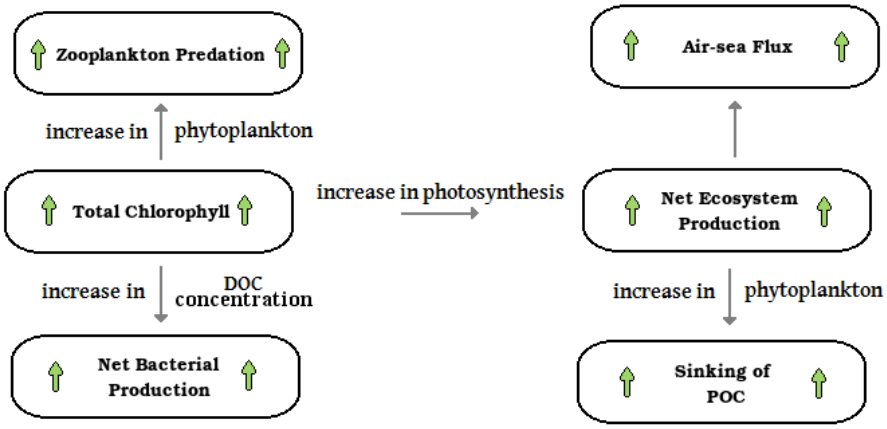

Figure 5.8. Diagram illustrating the impact of the total chlorophyll increase from DA on the carbon fluxes. The green arrows pointing up indicate an increase in the flux as defined by the model output, which is the case for each flux in this DA application.

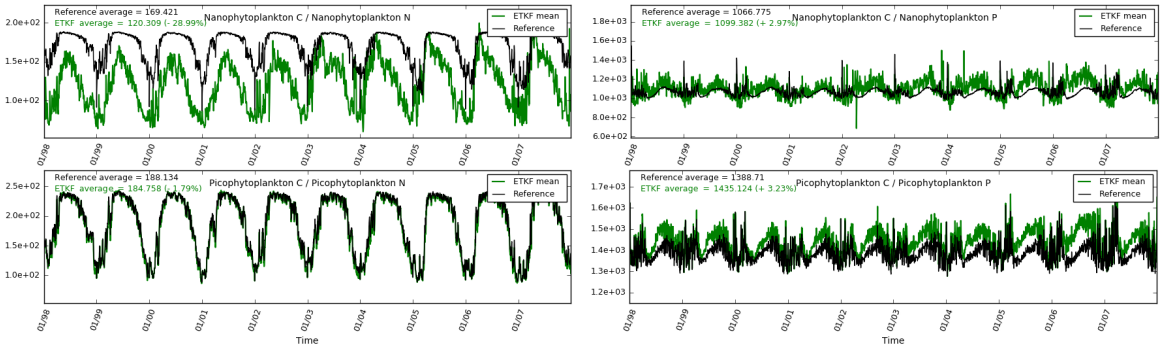

Figure 5.9. A comparison of reference and reanalysis mean for carbon to nutrient ratios for the two phytoplankton functional types used in the BATS simulation.

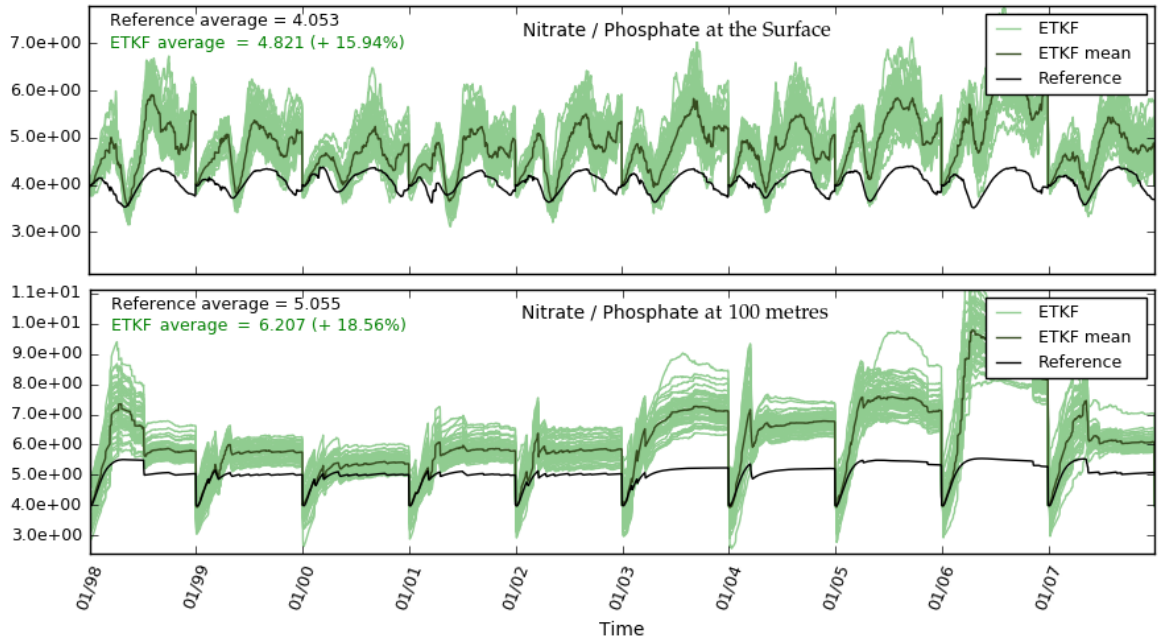

Figure 5.10. Evolution of nitrate to phosphate ratio in the reference and reanalysis ensemble in the BATS simulation. The surface layer is plotted at the top, with a corresponding plots at 100 metres plotted below.

Carbon Fluxes	Change from Reference Average to ETKF Average
Air-sea flux	+ 12.46%*
Zooplankton Predation	+ 200%
Net Ecosystem Production	+ 125%
Net Bacterial Production	+ 95.2%
Sinking of all POC	+105%
Phytoplankton Biomass	
Diatoms	0%
Nanophytoplankton	+ 2.51%
Picophytoplankton	+ 71.2%
Microphytoplankton	0%
Zooplankton Biomass	
Mesozooplankton	- 12.86%
Microzooplankton	+ 10.04%
Heterotrophic Nanoflagellates	+ 20.3%
Dissolved Organic Carbon	
Labile DOC	+ 59.75%
Semi-Labile DOC	+ 65.73%
Recalcitrant DOC	+ 65.23%
C:Nutrient Ratios	
C:N in Nanophytoplankton	- 28.99%
C:P in Nanophytoplankton	+ 2.97%
C:N in Picophytoplankton	- 1.79%
C:P in Picophytoplankton	+ 3.23%
C:N in Labile DOM	+ 1.23%
C:P in Labile DOM	+ 3.73%
Respiration	
Phytoplankton Respiration	+ 60.82%
Zooplankton Respiration	+ 31.47%
Bacteria Respiration	+ 63.86%
Additional	
Zooplankton Predation on Phytoplankton Only	+ 53.43%
Zooplankton Predation on Bacteria Only	+ 94.91%
Phytoplankton Excretion to DOC	+ 56.83%

Table 5.3. A summary of the changes made to the average value of various outputs in ERSEM, expressed as percentages of the reference value. *The air-sea flux calculation shown here ignores the first three months

Net Ecosystem Production: the average value increased considerably (125%), which translates to a decrease in the carbon output from this flux. This can be explained from the increases in phytoplankton biomass for the two phytoplankton functional types included here, which implies an increase in the simulated gross primary production that overwhelmed the respiration from phytoplankton, zooplankton and bacteria (see Table 5.3). The increase in phytoplankton results in an increase in primary production, which is evident from the plot in Figure 5.6,

and this has a major impact of the overall ecosystem production. However, respiration is also increased by a very large amount (60.82% for phytoplankton) which is expected to somewhat counteract the primary production, making the extent of this change surprising. This can be accounted for by the decrease in overall carbon to nutrient ratios (from Figure 5.9, which shows a large decrease in carbon to nitrate ratios following the increase to nitrate), resulting lower release of carbon by phytoplankton.

Net Bacterial Production: this increased on average by 95.2% which results from the overall increase in DOC availability shown in Table 5.4. As there is more DOC present in the system, there are more substrates available for bacterial breakdown. The large increase in DOC excretion by phytoplankton was likely a mechanism for this change which follows from the large increase in picophytoplankton biomass.

Air-sea flux: the average value decreased (12.46%), indicating that the ocean is releasing less CO_2 to the atmosphere than predicted by the stand-alone model. The lower rate of outgassing at BATS is explained by the increase of the net ecosystem production, by an increased net uptake of carbon dioxide by the primary producers. However, the changes to this flux are small in comparison to the other fluxes at BATS, both in average value and in the ensemble distribution.

Zooplankton predation: the average value increased by a significant amount (200%). Here it is important to notice that this increase was driven by large increases to the flux seen in the years 2003-2004, shown in Figure 5.7. The cause of this change correlates to a large increase in the nanophytoplankton biomass in the same years. The increase can only be related to the smaller zooplankton groups because the mesozooplankton decreases, shown in Table 5.3. However, as the overall zooplankton biomass increases, there is a larger amount of zooplankton

preying on phytoplankton and bacteria. Most of the flux is in the form of bacteria predation, which increases by 94.91%, and suggests that the increase in this flux and the net bacterial production are largely due to an increased biomass of bacteria (which drives an increase in the MCP).

Sinking of POC: the average value increased by a large amount (105%). This implies that much more POC is being exported to the deeper layers. For BATS, this is difficult to explain as diatoms and dinoflagellates are excluded in the simulation, which are the larger type of phytoplankton and will produce larger and faster-sinking POC compared to the other types. However, it could be that the increases to the overall zooplankton biomass are responsible for this change. Most of the spring peaks in the first half of the run are just below 100 mgC/ m^2/day, which is in agreement to the typical peak value shown in figure 5.4. for the POC flux reported by Steinberg et al., 2001.

There are differences between the impact on the fluxes for BATS compared to station L4 despite an increase in chlorophyll in both cases. This is predominantly due to the reduction of large components of phytoplankton in the case of BATS which increases zooplankton predation on the smaller phytoplankton types. This is reflected Table 5.3., where the biomass of mesozooplankton decreases while the biomass of microzooplankton and heterotrophic nanoflagellates increases. The increase in DOC produced from this types of zooplankton drives the increase in net bacterial production, which is not observed at station L4. The difference in the change to the air-sea flux between these sites is not as obvious which is because the decrease in air-sea flux is an unexpected result (as stated in section 4.5.2). It is suspected that the reinitialisation at the start of each year plays a role in reinforcing the very large negative peaks that are present for the air-sea flux at station L4.

5.5.3 Impact on the simulation of the Carbon Pumps

There are implications of the ETKF representation of carbon fluxes in relation to the BCP and MCP shown by the results in Figure 5.7 as well as Figure 5.9.

The net ecosystem production, which was the flux most reliably updated by the assimilation according to the TEs (see section 3.4.2), received a largest increase in the BATS assimilation, increasing by 55.45% (Table 5.3). This suggests an increase in the significance of the BCP contributions at the BATS site, due to a higher rate of primary production.

For the MCP, the increase in net bacterial production and in recalcitrant DOC concentration (65.23%) suggests an increase in the prominence of the MCP at BATS. This means that the assimilation at BATS resulted in a slight increase the MCP to BCP ratio.

Ocean colour assimilation also implied an increase in the C:N ratio in phytoplankton, as the biomass increased without a reduction in phytoplankton nitrate. A high (i.e. unbalanced) C:N ratio increases the exudation of DOC in ERSEM (Butenschon et al., 2016), which potentially boosts the MCP (Jiao et al., 2014).

5.6 Conclusion

The results of the reanalysis simulations presents evidence that the assimilation of ocean colour can improve our representation of the carbon fluxes at BATS. The relatively larger extent of the flux changes at the BATS site suggests that DA had a stronger impact on the simulations at the open ocean site than at station L4.

The large values of these updates may be due to a combination of reasons, including, (1) the lower observational uncertainty of the assimilated chlorophyll data at BATS compared to station L4, (2) the low values of the nutrient concentrations that may result in more extreme dynamic consequences from small modifications to some the variables, and (3) the larger number of sources of uncertainty that the open ocean site BATS presents (as explained in section 5.2).

Overall, the calculations of the carbon budget are significantly influenced by the BATS ocean colour assimilation. The large update to the net bacterial production may show that DA enhances MCP dynamics with respect to the reference model simulation. In particular, assimilation increased the phytoplankton C:N ratios, which may contribute to the increase in the MCP. This mechanism is the focus of next chapter.

Chapter 6

Comparison between the Carbon Pumps at Station L4 and BATS

6.1 Overview

This chapter will focus on the final aim of this thesis, which is to establish an understanding of the processes behind the two biologically driven carbon pumps from the ocean-colour data assimilation reanalyses at station L4 and BATS. This will be performed using the ensemble mean of the ETKF reanalyses presented in the previous two chapters. At this point, it is assumed that assimilation has provided a reliable representation of the system, justified from the validation using in-situ data and by comparison to predictions in the literature (see Chapters 4 and 5), and so no further discussion of the assimilation methods will be included in this chapter.

The main hypothesis to be examined is that the ratio between the microbial carbon pump (MCP) and the biological carbon pump (BCP) increases as nutrient concentrations decrease (see literature review in section 1.3) Due to the large differences in nutrient concentrations between station L4 and BATS, this study is suitable for exploring this concept in depth. As a reminder, this pumps-to-nutrient hypothesis was formulated by Jiao et al., 2010 and 2014, on the basis of established conceptual frameworks, and was supported by Polimene et al. (2017), through model simulations of an idealised marine system.

In this chapter, this hypothesis is tested for the first time through data-assimilated model simulations of real systems, at station L4 and BATS. For these

sites, it is expected that the oligotrophic conditions at BATS will increase the ratio microbial-to-biological carbon pumps by both: increasing the carbon-to-nutrient concentrations in the phytoplankton cells, which increases the production of recalcitrant dissolved organic matter (MCP) (Polimene et al., 2017), and decreasing the production of large phytoplankton, i.e. decreasing the sinking of POC (BCP). This will be tested by comparing the ratios between the reanalysed biological and microbial carbon pumps at both sites, as well as comparing the underlying drivers of these pumps, such as the nitrate concentrations and the phytoplankton C:N ratios

This chapter will first outline the methods, stating the depth layers and outputs used in the calculation of the results shown here. Then, there will be an in-depth look at the differences between the pumps at both sites and the mechanisms behind these differences. Finally, the seasonal differences of the pump ratios at station L4 will be examined, to investigate if the dominance of each pump can shift throughout the year due to the seasonal cycle of the marine ecosystem.

6.2 Methods

The MCP and BCP were calculated according to the approach outlined in Polimene et al. (2017). The MCP was quantified as the total release of semi-labile and semi-refractory dissolved organic carbon by the ERSEM bacteria functional group, integrated from the surface to a selected depth. The BCP was quantified as the vertical flux of total particulate carbon across a cross-section of the water column, at a selected depth.

The analysis in this chapter is focussed on examining the total quantities throughout a range of depths, rather than at the surface. For station L4, each output is calculated up to a selected depth of 50 metres to include the full water column, with the sinking of POC calculated at this depth. For BATS, the depth selected was 100 metres, which does not include the full range of depths simulated, but is the depth that is often used to evaluate carbon export in the open ocean (Legendre et al., 2015).

The ratio MCP:BCP is computed to compare the relative importance of the two pumps at station L4 and BATS. The normalized MCP* and BCP* were also computed by dividing MCP and BCP by the gross primary production (GPP). The asterisk notation used throughout this chapter indicates a division of these pumps by the GPP. Using these normalised quantities allows for a comparison of the relative importance of the MCP and BCP at the sites (and seasons) with respect to the different amounts of organic matter available for degradation and sinking, and will therefore be referenced extensively throughout the chapter.

The nutrient regime of station L4 and BATS were characterized by focusing on nitrogen. From the reanalyses, nitrogen was on average the limiting nutrient for phytoplankton growth at both sites. This follows from the findings that the

simulated ratios of the average values of dissolved nitrogen and phosphorus were below the Redfield ratio of 16 (see Tables 4.3 and 5.3). This result was less expected in BATS, which is often limited by phosphate in the upper thermocline Polimene et al. (2017). This is suspected to be caused due to the reinitialisation performed at the start of each year in the simulation.

The phytoplankton stoichiometry (Carbon:Nitrogen) was computed by dividing the internal carbon and nitrogen concentrations summed throughout the simulated phytoplankton groups. The large phytoplankton groups were simulated only at station L4, as stated in the previous chapters. This was motivated by preliminary simulations at BATS which led to the extinction of the diatoms and dinoflagellates groups (i.e. microplankton), and is supported by the negligible concentration of microplankton observed at BATS in previous studies (Steinberg et al., 2001).

The carbon pumps, nitrate concentrations, C:N ratios and microplankton (for station L4 only) were computed by integrating the variables from the surface to 50 metres (i.e. bottom) at station L4, and 100 metres at BATS. For each variable, the time series of daily values spans the multi-annual simulations at both station L4 and BATS. These time series were used to compute scatter-plots of the annual medians of the variables (MCP, BCP, MCP:BCP and C:N) versus the annual medians of nitrate to evaluate and explain differences in the pumps related to differences in the nutrient regime at the two ocean sites. The use of medians as opposed to means is applied here to eliminate the effects of atypical behaviour for particular years, which can often be seen for the later years at BATS. Additionally, the monthly means were computed to discuss the climatologies of the variables at station L4, to evaluate and compare the seasonal variability of the two pumps.

6.3 Differences between the Carbon Pumps

The MCP has a much greater relevance at BATS than at station L4, if compared to the BCP (Figure 6.1 and 6.2 and Table 6.2). The difference of the MCP:BCP ratio is linked to the different concentration of nitrate at the two ocean sites: the MCP is comparatively more important in the oligotrophic site BATS, where the stoichiometry of phytoplankton is more unbalanced (high C:N ratio, Figure 6.3).

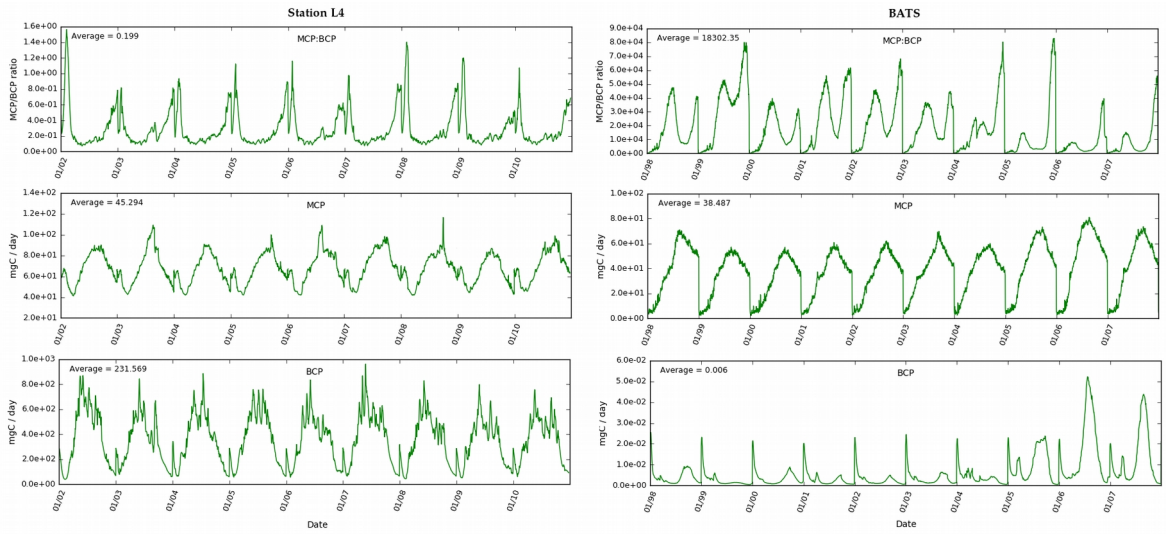

Figure 6.1. Time-Series Plots of the BCP, MCP and MCP:BCP ratio from the ocean-colour DA reanalysis at station L4 (left) and BATS (right).

	Station L4 Average	**BATS Average**
MCP:BCP	0.20	1.8×10^4
MCP	45.3 mgC / day	38.3 mgC / day
BCP	232 mgC / day	0.006 mgC / day
Nitrate	3.63×10^4 mg	747 mg
GPP	841 mgC / day	363 mgC / day
DOC	0.033 mgC	0.167 mgC

Table 6.1. The average value of each of the time-series for the carbon pumps shown in figure 6.1, as well as other relevant outputs.

Figure 6.1 shows that the MCP:BCP ratio reaches high values throughout the decadal simulation at BATS. The MCP:BCP is almost always below 1 at station L4, with the exceptions of few spikes (Figure 6.1) and the average value is about 0.2 (Table 3.1). The MCP:BCP ratio is higher at BATS though the magnitude of the MCP (and BCP) is higher at station L4 throughout the simulation. The reason for this is that the gross primary productions are much higher at station L4 than at BATS, and so there is more dissolved organic carbon available for the overall bacteria production (Table 3.1).

In terms of the time-series evolution, the peaks in the summer period present in Figure 6.1. for the BCP at station L4 represent the individual phytoplankton blooms and overall increase in primary productivity which in-turn produces more POC subject to sinking. This feature is absent in most years in the BATS time-series due to the lower availability of nutrients, and the absence of larger phytoplankton types, with some late-summer peaks shown for the last few years of the run.

The evolution of MCP is relatively similar between the two sites, with a generally smooth peak in summer and a trough in winter. While the peak-values are comparable at both sites, the winter values are typically higher for station L4, which results in the higher average value for the MCP at station L4. This is due to a much larger drop in levels of DOC released during the winter period for BATS, due to the lower biomass of phytoplankton in this period.

However, after normalization by GPP, MCP* is systematically higher at BATS than at station L4 (Figure 6.2), while BCP* remains higher at station L4. Therefore, at the oligotrophic site BATS, a much larger proportion of the gross primary production is used in bacteria transformation, rather than to the sinking of large particulate carbon.

Figure 6.3 examines the dependency of these pumps on the total nitrate. The different MCP* and BCP* and MCP:BCP correspond to different average nutrient concentrations at the two ocean sites: the MCP is comparatively higher (i.e. more important) than the BCP in low-nutrient (oligotrophic) environments. In such conditions, the resulting phytoplankton carbon to nutrient ratio is much higher (~13 at BATS shown in Figure 6.3, compared to the Redfield C:N value = 6.6).

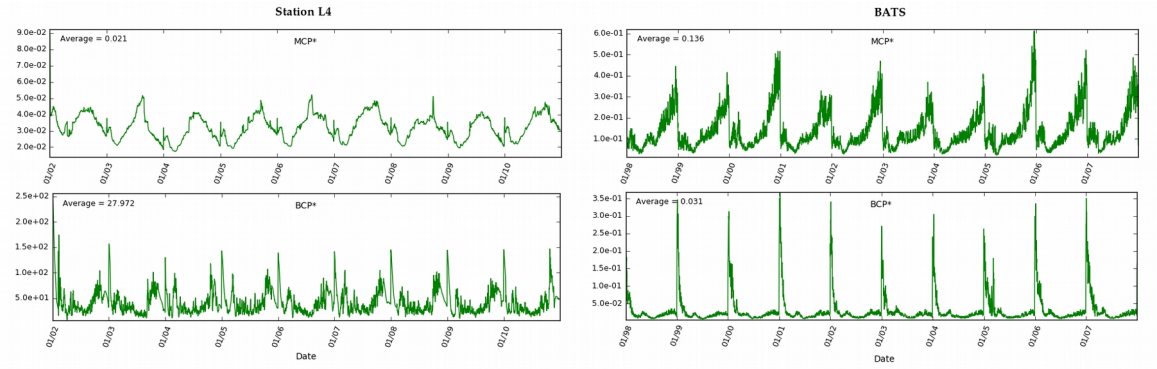

Figure 6.2 Time-Series Plots of the MCP* and BCP* from the ocean-colour DA reanalysis at station L4 (left) and BATS (right).

Both sites display a degree of spread in the magnitude of values between the median values for each year (represented by spreading along the y-axis) and a spread in nitrate values (represented by spreading along the x-axis).

These results are consistent with the conceptual diagram in Figure 6.4 and verify the general theoretical framework proposed by Polimene et al (2017). At the oligotrophic site BATS, the low nutrient concentration imbalances the phytoplankton carbon to nutrient ratio (C:N>>6.6). This leads phytoplankton to release the excess carbon, which increases the bacterial production of recalcitrant DOC, and therefore the MCP. For BATS, the simulated phytoplankton production consists of small nanophytoplankton and picoplankton production only, thus the export of POC, and therefore the BCP, is very small at a 100 metre depth. The consequence of this is that the MCP:BCP at BATS is relatively high.

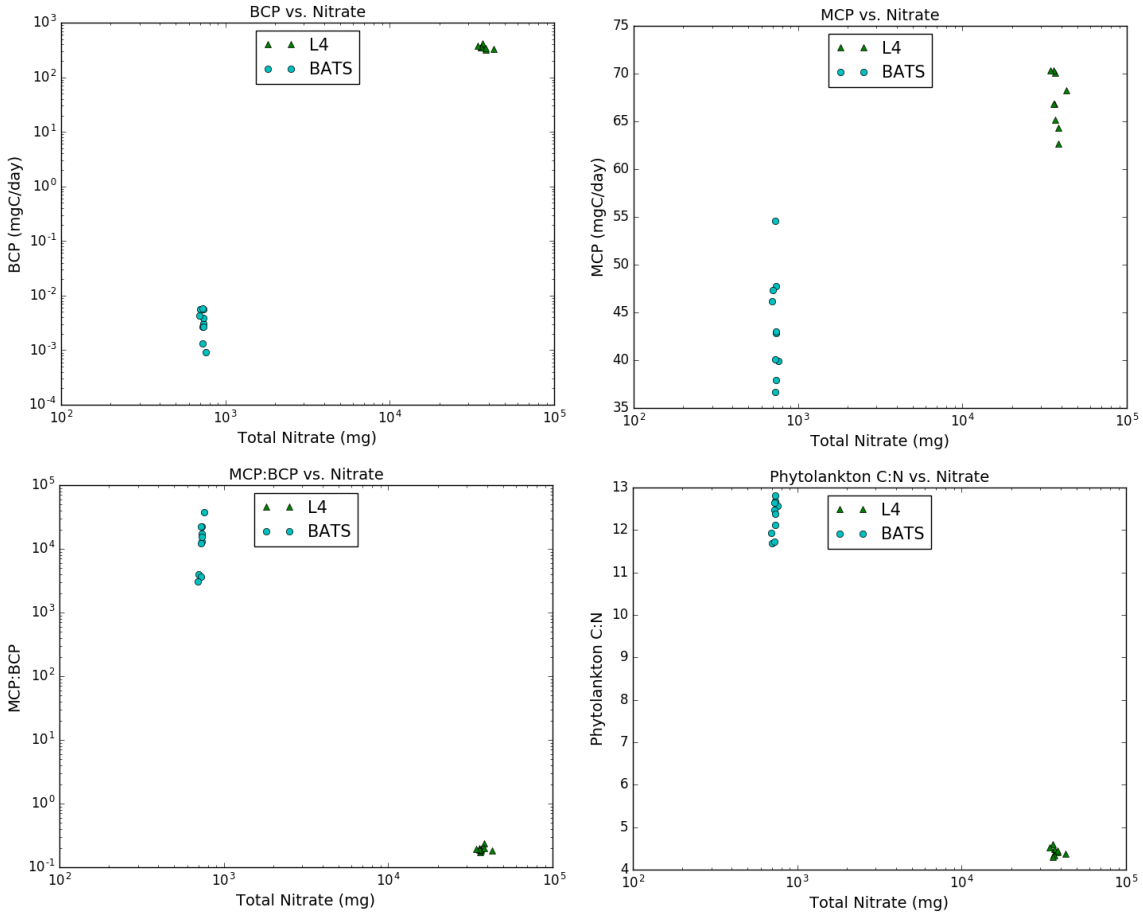

Figure 6.3. Annual-Averaged plots versus nitrate for the BCP, MCP and MCP:BCP ratio, as well as the phytoplankton carbon:nutrient ratio, taken from median value of each year. Station L4 values are represented by the green triangles, whereas BATS values are represented by the blue circles.

At station L4 the concentration of nitrate is relatively high, and therefore the C:N ratio is close to the balance value, and so the exudation of DOC, and the MCP, is relatively low. The production of large phytoplankton and their sinking is high, and so the BCP is also high. The higher downward flux of POC at the bottom, combined with a lower exudation of DOC, leads to a relatively low MCP:BCP.

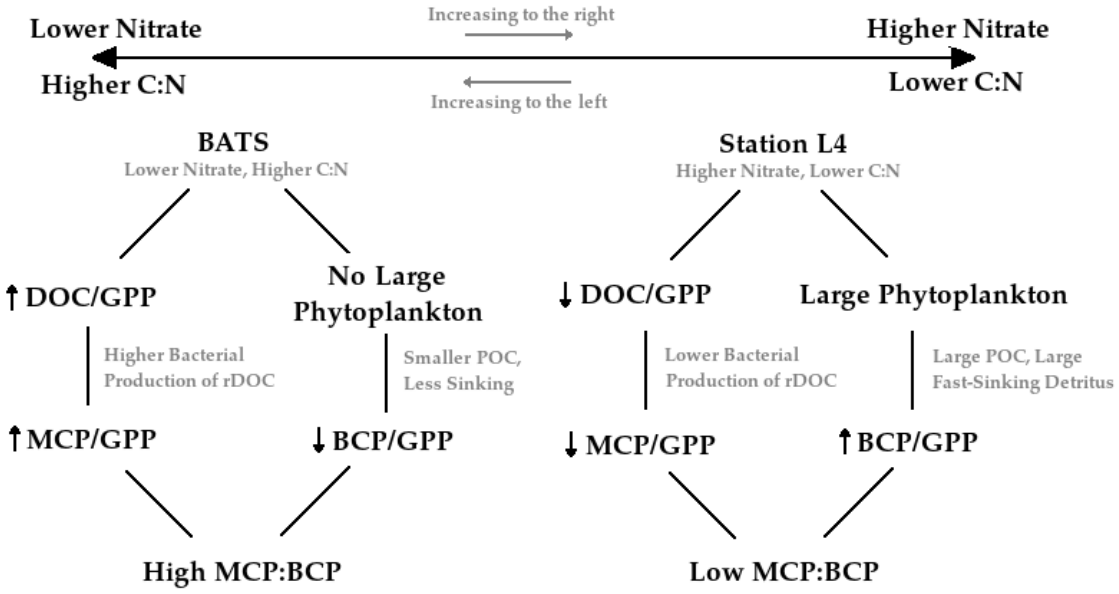

Figure 6.4 Conceptual diagram explaining the difference between MCP:BCP in relation to the trophic regimes. C:N = phytoplankton carbon to nitrogen ratio; POC = particulate organic carbon, and DOC = dissolved organic carbon, GPP = gross primary production.

6.4. Seasonal Cycle of the Carbon Pump Ratio at station L4

The conceptual diagram drawn in Figure 6.4 was tested to explain the seasonal variability of the MCP, BCP and MCP:BCP simulated at station L4. The surface waters at station L4 tend to switch between mesotrophic conditions in winter (high nitrate concentrations) to oligotrophic in summer (low nitrate concentrations), resulting in an annual cycle for the nutrient limitation. BATS is excluded here as it is characterized by oligotrophic conditions throughout the year without a clear seasonal cycle for the nutrients

Figure 6.5 shows the seasonal climatologies of carbon pumps, as well as the evolution of nitrate throughout the year. Here, the MCP:BCP climatology is consistently below 0.5 throughout the year, confirming the overall high importance of the BCP at L4 pointed out in Figures 6.1 and 6.2. Despite this, the MCP* has a clear seasonal cycle that peaks in July-August, leading to a relative maximum of MCP:BCP in the same months. This peak corresponds to a relative minimum of the microphytoplankton biomass (diatoms plus dinoflagellates) and to a summer plateau of high C:N phytoplankton ratio. On the contrary, MCP:BCP has the lowest values in spring (March to May) and early Autumn, when the microphytoplankton production peaks and the internal nutrient imbalance is slightly less severe. The GPP is typically lower in the winter as a result of light limitation rather than nitrate limitation which explains the relatively high values of BCP*=BCP/GPP in winter.

The results in Figure 6.5 are consistent with the scheme presented in Figure 6.4, indicating that the fluctuations of the external nutrient concentrations can determine phytoplankton stress and/or production, and are therefore a key driver of the seasonal variability of the MCP, BCP and MCP:BCP in a temperate coastal marine system.

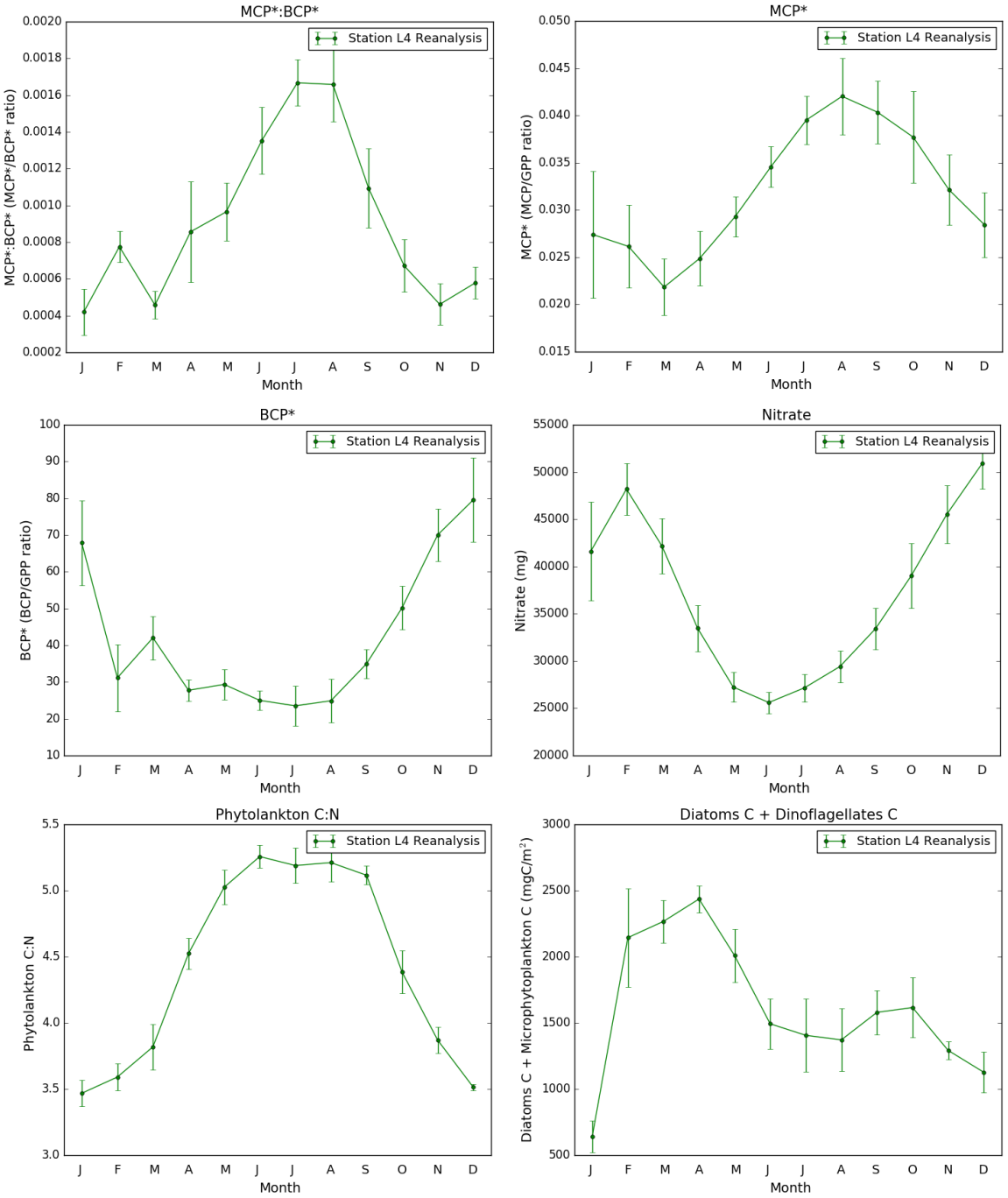

Figure 6.5 Seasonal Climatologies of MCP*:BCP*, MCP*, BCP*, Nitrate, Phytoplankton C:N, and Diatoms and Dinoflagellate Biomass.

6.5. Conclusion

The results presented in this chapter indicate that microbial carbon pump is more important than the biological carbon pump in sequestrating carbon in an oligotrophic open ocean system, if compared to a mesotrophic coastal system. In particular, these results support the hypotheses that oligotrophic conditions increase the ratio of microbial-to-biological carbon pumps by: (1) unbalancing the carbon-to-nutrient concentrations in the phytoplankton cells, i.e. increasing the production of recalcitrant dissolved organic matter (MCP) (Polimene et al., 2017); and (2) decreasing the production of large phytoplankton, i.e. decreasing the sinking of POC (BCP).

This interpretation can be used to explain the seasonal cycles of the pumps at the coastal site station L4, where stratification and primary production dynamics shifts the systems from mesotrophic to oligotrophic regimes annually.

It is argued that these results are reliable because they were obtained by post-processing the outputs of the reanalyses at the two ocean sites. Though data were not available to assess directly the skill of these pump simulations, the assimilative reanalyses were ideally the best available estimates of the "true state" of the system and were validated with large datasets of biogeochemical variables and carbon fluxes (Chapters 4 and 5).

The main aim of the analysis presented here is to compare and explain the variability of the pumps at the two sites, rather than quantify their magnitude. To this regard, there are some limitations of the results presented here. Though the concepts of MCP and BCP have been applied in the coastal zone by Jiao et al (2014), their formal definitions imply that carbon is sequestrated from the system

(below the depth of 100m, Legendre et al. 2015). Therefore this evaluation of the BCP at station L4 is an approximation to this study due to the shallowness of the site. This is because the water column is only 50m deep while experiencing full mixed in winter, and so it is affected by sediment resuspension (Smyth et al., 2009). Furthermore, ERSEM does not simulate recalcitrant dissolved organic carbon (i.e. the fraction with lifetime in the order of millennia) which is related to the MCP in a stricter sense. However, the production of semi-labile and semi-refractory dissolved organic carbon components in ERSEM have been adopted by Polimene et al (2017) as an approximation of the MCP, which is acceptable in the context of this study.

This 1D model analysis of the MCP:BCP dependency on the nutrient regime can be extended to 3D model applications. This will make possible the exploration of the variability of the pumps along the continuum of nutrient gradients and shifts in the plankton community composition of the global ocean in relation to horizontal transport processes, which were not investigated here.

Chapter 7

Conclusions

The work presented in this thesis advances the simulation and understanding of the variability of climate-relevant, biologically-driven carbon pumps in the ocean. This was achieved through applications of state-of-the-art data assimilation methods with a marine ecosystem model and ocean colour data.

This thesis has shown that ocean colour DA can be used to further our understanding of biologically driven carbon pumps in the ocean, which is especially useful in light of modern developments in the microbial carbon pump which still require development in marine models. This objective has been achieved through the real application of ocean colour DA at two distinctly different locations: station L4 (shown in Chapter 4) and BATS (Chapter 5).

The assimilative reanalysis showed that the microbial carbon pump may exceed the biological carbon pump in oligotrophic ocean regimes, due to the unbalanced phytoplankton stoichiometry in nutrient-poor waters. This was an emergent property of the ecosystem, and was underpinned by applying assimilation of ocean colour. In fact, model estimates of biogeochemical time series and carbon fluxes were improved by applying data assimilation in twin experiments (Chapter 3), mesotrophic coastal site reanalyses (L4, Chapter 4) and oligotrophic open ocean reanalyses (BATS, Chapter 5).

These findings are reviewed in the following sections. Section 7.1 will focus on the comparison of the DA methods in twin experiments, section 7.2 will highlight the impact of DA on the simulation of carbon fluxes and the understanding of the carbon pumps, and the final section 7.3 will provide suggestions for future work.

7.1 Assessing Ensemble DA Methods for Ocean Colour Assimilation

The Twin Experiments (TEs; Chapter 3) demonstrated that the assimilation of synthetic ocean colour data into the ERSEM-GOTM model can improve the model simulation of ocean carbon fluxes in an ideal system. This was achieved by assessing and comparing the performance of the Localised Ensemble Transform Kalman Filter (ETKF) and the Implicit Equal Weights Particle Filter (IEWPF), for the first time with a marine ecosystem model. In the TEs, the simulation of five carbon fluxes linked to both the BCP and the MCP were all shown to be capable of improving to some extent from assimilation, which include the air-sea carbon flux, zooplankton predation, net ecosystem production, net bacterial production and the sinking of POC.

Overall, the TEs show that ocean colour assimilation is beneficial, as both methods outperform the SE in reproducing most of the model-generated fluxes. The ETKF was overall preferable to the IEWPF in this application, because it provided better estimates for four out of the five fluxes. However, the application of the IEWPF showed that there may be some potential in outperforming the Gaussian-based ETKF in estimating a carbon flux with a highly non-linear link to the assimilated surface ocean colour (the sinking of POC).

This finding supports the view that IEWPF is capable of performing better than ETKF for a non-linear analysis, but this is overshadowed by its significant underperformance in other areas. Therefore, the potential of the IEWPF in marine ecosystems is not to be discounted, but a more in-depth implementation than the one used in this study is required. Following its overall performance in the TEs, the ETKF was the method used in the reanalyses of real marine ecosystems.

7.2 Using Ocean Colour DA to Represent Carbon Fluxes and Pumps in the Ocean

The ETKF was applied in decadal reanalyses of the biogeochemistry and carbon fluxes at the mesotrophic coastal site station L4 (Chapter 4) and the oligotrophic ocean site BATS (Chapter 5). These applications demonstrate that the assimilation of ocean colour could improve the overall simulation of independent time-series of biogeochemical data. It was also shown that substantial changes were made to the average values of the carbon fluxes, showing the potential impact of the assimilation on the simulation of the carbon pumps.

The assimilation had a large impact on the simulation of the ecosystem processes at both sites. For station L4, the increase in the total chlorophyll produced an increase in the net ecosystem production due to the increase in photosynthesis, which resulted in a slight increase in the sinking of POC due to a greater quantity of detritus produced from large phytoplankton groups. This also resulted in a reduction of the the overall zooplankton population and DOC concentration, which in turn reduced fluxes for the predation by zooplankton and the net bacterial production. For BATS, the total chlorophyll also increased, but this did not have the same impact on all of the other fluxes due to the differences in phytoplankton types.

Assimilation of ocean colour impacted the simulation of some other ecosystem and plankton features that are potentially linked to the BCP and MCP. These features include the phytoplankton blooms and the phytoplankton stoichiometry.

The assimilative reanalyses were processed in Chapter 6, providing a crucial result for this thesis. Building on the hypothesis by Jiao, and advancing the ideal modelling exercise by Polimene, it was shown for the first time in a real-system

simulation that the relative importance of the MCP and BCP is linked to the nutrient regime of marine systems because of its impact on the plankton stoichiometry. In addition, it was shown at station L4 that the MCP:BCP can shift between the seasons due to variations in the nitrate throughout the year. It should be noted that the variations in the MCP and BCP dominance are emergent properties of the simulated ecosystem, in that they are not explicitly coded in the model equations but emerge from the complexity of the model applied here.

There are some limitations for the analysis at station L4 and BATS. This includes the initialisation of variables at the start of each year, which was put in place to constrain erroneous trends but also prevents an analysis of long-term trends and inter-annual variability. Furthermore, the BCP is very approximately simulated at station L4 as it is too shallow to encompass the carbon sequestration from the system. Furthermore, the recalcitrant DOC with a full 1000-year lifetime is not simulated by the model, limiting the representation of the MCP. Another crucial limitation is in the uncertainties in the satellite data, and the difficulty in accurately characterising them, which will inevitably constrain the impact of the assimilation.

Overall, the reanalyses at these sites show evidence that ensemble DA methods can be used to improve modern understanding of the variability of climate relevant BGC processes such as the MCP and BCP. The impact that ocean colour DA is able to make on the average values of carbon fluxes, argues towards its implementation alongside updates to marine models, improving marine ecosystem understanding.

7.3 Recommendations and Opportunities for Future Work

This research opens up a lot of potential for further investigation. In terms of DA, the IEWPF could be examined further by developing the twin experiments to account for the dependency of the linearity (and non-linearity) of the ecosystem based on the seasons and depth in the water column. This could be achieved through the use of a dynamic error covariance matrix that uses different values below the mixed layer depth, and different values based on the time in the year, which would accommodate the changes in dynamics between the seasons. These updates are expected to benefit the IEWPF analysis more than the ETKF. Furthermore, there are many other DA techniques which could be examined in a similar study, in particular the LETKF with a full implementation of localisation is likely to exceed the performance of the ETKF when applied to a non-linear BGC model.

Also, the study could be extended to a 3D environment, using a 3D physical model such as NEMO. This would take into account horizontal transportation that could influence the biogeochemical variables examined in this study. Furthermore, there are a range of other sites that could be added for investigation, which would help in establishing the significance of understanding carbon pump dynamics through ocean colour assimilation on a global scale.

The accuracy of the observation errors could be improved by considering separate values for satellite-imaged ocean colour data at coastal and open-ocean sites, which was omitted in this research for simplicity. Also, a better representation of the observation errors could be achieved by exploiting the per-pixel uncertainty estimates provided by novel ocean-colour products (e.g. Jackson et al., 2017; Ciavatta et al., 2016). The representation could also be

improved through a deeper analysis of the implications of using the ocean colour – chlorophyll concentration relationship in ERSEM, which was not explored here.

Finally, data assimilation of different data sets, such as in-situ POC derived from biogeochemical carbon floats, could be useful for looking at improvements to the carbon pumps as they are more closely linked to some dynamics of the BCP and MCP. While ocean colour was chosen for this study based on its availability and relatively low observational errors compared to other data sets, there is the possibility that assimilation of other properties may have some advantages.

References

Abarbanel, H., *Predicting the future: completing models of observed complex systems*, Springer, 2013.

Ades, M., van Leeuwen, P., J., *The equivalent-weights particle filter in a high-dimensional system*, Quarterly Journal of the Royal Meteorological Society, **141(687)**, 484-503, 2014.

Akyıldız, Ö., D., Míguez, J., *Nudging the Particle Filter,* arXiv:1708.07801, 2017.

Allen, I. J., Eknes, M., Evensen, G., *An Ensemble Kalman Filter with a complex marine ecosystem model: hindcasting phytoplankton in the Cretan Sea*, Annales Geophysicae, **21 (1),** 399-411, 2003.

Allen, I. J., Siddorn, J. R., Blackford, J. C., Gilbert, F. J., *Turbulence as a control on the microbial loop in a temperate seasonally stratified marine systems model*, Journal of Sea Research, **52 (1),** 1-20, 2004.

Anderson, J., L., Anderson, S., L., *A Monte Carlo Implementation of the Nonlinear Filtering Problem to Produce Ensemble Assimilations and Forecasts*, Monthly Weather Review, **127(12)**, 2741-2758, 1999.

Baretta, J., Ebenhöh, W., Ruardij, P., *The European regional seas ecosystem model, a complex marine ecosystem model*, Netherlands Journal of Sea Research, **33(3-4)**, 233-246, 1995.

Baretta-Bekker, J. G. , Baretta, J.W., Rasmussen, E. K., *The microbial food web in the European Regional Seas Ecosystem Model, Netherlands Journal of Sea Research*, **33 (3-4)**, 363-379, 1995.

Baretta-Bekker, J., Baretta, J., Ebenhöh, W., *Microbial dynamics in the marine ecosystem model ERSEM II with decoupled carbon assimilation and nutrient uptake*, Journal of Sea Research, **38(3-4)**, 195-211, 1997.

Bates, N., R., Michaels, A., F., Knap, A., H., *Seasonal and interannual variability of oceanic carbon dioxide species at the U.S. JGOFS Bermuda Atlantic Time-series Study (BATS) site*, Deep Sea Research Part II: Topical Studies in Oceanography, **43 (2-3)**, 347-383, 1996.

Biddanda, B., Benner, R., *Carbon, nitrogen, and carbohydrate fluxes during the production of particulate and dissolved organic matter by marine phytoplankton*, Limnology and Oceanography, **42 (3)**, 506-518, 1997.

Bishop, C., H., Etherton, B., J., Majumdar, S., J., *Adaptive sampling with the ensemble transform Kalman filter. Part I: Theoretical* aspects, Monthly Weather Review, **129(3),** 420-436, 2001.

Bishop, C., H., Hodyss, D., *Flow-adaptive moderation of spurious ensemble correlations and its use in ensemble based data assimilation,* Quarterly Journal of the Royal Meteorological Society, **133 (629)**, 2029-2044, 2007.

Blackford, J. C., Allen, J. , I., Gilbert, F., J., *Ecosystem dynamics at six contrasting sites: a generic modelling study,* Journal of Marine Systems, **52 (1-4)**, 191-215, 2004.

Blackford, J. C., Gilbert, F., *pH variability and CO2 induced acidification in the North Sea*, Journal of Marine Systems, **64(1-4)**, 229-241, 2004.

Brewin, R., J., Sathyendranath, S., Müller, D., Brockmann, C., Deschamps, P., Devred, E., White, G., N. et al., *The Ocean Colour Climate Change Initiative: III. A round-robin comparison on in-water bio-optical algorithms*, Remote Sensing of Environment, **162**, 271-294, 2015.

Brewin, R., J., Hyder, K., Andersson, A., J., Billson, O., Bresnahan, P., J., Brewin, T., G., Raisos, D., E., et al., *Expanding Aquatic Observations through Recre--ation*, Frontiers in Marine Science, **4**, 2017.

Broekhuizen, N., A., Heath, M., Hay, S., Gurney, W., *Modelling the dynamics of the North Sea's Mesozooplankton*, Netherlands Journal of Sea Research, **33(3-4)**, 381-406, 1995.

Browne, P., A., van Leeuwen, P., J., *Twin experiments with the equivalent weights par ticle filter and HadCM3*, Quarterly Journal of the Royal Meteorological Society, **141(693)**, 3399-3414, 2015.

Browne, P., Wilson, S., *A simple method for integrating a complex model into an ensem ble data assimilation system using MPI*, Environmental Modelling & Soft ware, **68**, 122-128, 2015.

Buchard, H., Bolding, K., Villarreal, M., R., *GOTM, a general ocean turbulence model: theory, implementation and test cases*, Space Applications Institute, 1999.

Budyko, M., I., *Climate and Life*, Academic Press, New York, 1974.

Butenschön, M., Clark, J., Aldridge, J. N., Allen, J. I., Artioli, Y., Blackford, J., Bruggeman, J., *ERSEM 15.06: a generic model for marine biogeochemistry and the ecosystem dynamics of the lower trophic levels*, Geoscientific Model Development Discussions, **8 (8)**, 7063-7187, 2016.

Cameron, D. R., Lenton, T. M., Ridgwell, A. J., Shepherd, J. G., Marsh, R., Yool, A., *A factorial analysis of the marine carbon cycle and ocean circulation controls on atmospheric CO2*, Global Biogeochemical Cycles, **19 (4)**, 2005.

Campbell, J. W., *The lognormal distribution as a model for bio-optical variability in the sea*, Journal of Geophysical Research, **100 (C7)**, 237-254, 1995.

Caron, D. A., *Inorganic nutrients, bacteria, and the microbial loop*, Microbial Ecology, **28(2)**, 295-298, 1994.

Castellari, S., Pinardi, N., Leaman, K., *A model study of air–sea interactions in the Mediterranean Sea*, Journal of Marine Systems, **18(1-3)**, 89-114, 1998.

Chesson, J., *The estimation and analysis of preference and its relationship to foraging models,* Ecology, Wiley Online Library, 1983.

Chisolm, S. W., *Oceanography: Stirring times in the Southern Ocean*, Nature, **407**, 685–687, 2000.

Ciavatta, S. A., Torres, R., Saux-Picart, S., Allen, J. I., *Can ocean color assimilation improve biogeochemical hindcasts in shelf seas?*, Journal of Geophysical Research, **116 (C12)**, 2011.

Ciavatta, S. A., Torres, R., Martinez-Vicente, V., Smyth, T., Dall'Olmo, G., Polimene, L., Allen, I., J., *Assimilation of remotely-sensed optical properties to improve marine biogeochemistry modelling*, Progress in Oceanography, **(127)**, 74-95, 2014.

Ciavatta, S. A., Kay, S., Saux-Picart, S., Butenschön, M., Allen, J. I., *Decadal reanalysis of biogeochemical indicators and fluxes in the North West European shelf-sea ecosystem*, Journal of Geophysical Research: Oceans, **121 (3)**, 1824-1845, 2016.

Ciavatta, S., Brewin, R., J., Skákala, J., Polimene, L., de Mora, L., Artioli, Y., Allen, J., I., As similation of Ocean-Color Plankton Functional Types to Im prove Marine Ecosystem Simulations, *Journal of Geophysical Research: Oceans*, **123 (2)**, 834-854, 2018.

Dee, D., P., Uppala, S., M., Simmons, A., J., Berrisford, P., Poli, P., Kobayashi, S., Andrae, U., The ERA-Interim reanalysis: configuration and performance

of the data assimilation system, *Quarterly Journal of the Royal Meteorological Society*, **137 (656)**, 553-597, 2011.

Del Moral, P., *Nonlinear Filtering: Interacting Particle Resolution*, Markov processes and related fields, **2 (4)**, 555-580, 1996.

Doney, S., C., Glover, D., M., Najjar, R., G., *A new coupled, one-dimensional biological-physical model for the upper ocean: Applications to the JGOFS Bermuda Atlantic Time-series Study (BATS) site*, Deep Sea Research Part II: Topical Studies in Oceanography, **43 (2-3)**, 591-624, 1996.

Doron, M., Brasseur, P., Brankart, J., Losa, S., N., Melet, A., *Stochastic estimation of biogeochemical parameters from Globcolour ocean colour satellite data in a North Atlantic 3D ocean coupled physical–biogeochemical model*, Journal of Marine Systems, **117-118**, 81-95, 2013.

Doucet, A., Tadić, V., B., *Parameter estimation in general state-space models using particle methods*, Annals of the Institute of Statistical Mathematics, **55(2)**, 409-422, 2003.

Dowd, M., *Bayesian statistical data assimilation for ecosystem models using Markov Chain Monte Carlo*, Journal of Marine Systems, **68 (3-4)**, 439-456.

Dowd, M., Jones, E., Parslow, J., *A statistical overview and perspectives on data assimilation for marine biogeochemical models*, Environmetrics, **25 (4)**, 203-213, 2014.

Eknes, M., Evensen, G., *An Ensemble Kalman filter with a 1-D marine ecosystem model*, Journal of Marine Systems, **36 (1-2)**, 75-100, 2002.

Evensen, G., *Sequential data assimilation with a nonlinear quasi-geostrophic model using Monte Carlo methods to forecast error statistics*, Journal of Geophysical Research, **99 (C5)**, 10143–10162, 1994.

Evensen, G., *The Ensemble Kalman Filter: theoretical formulation and practical implementation*, Ocean Dynamics, **53(4)**, 343-367, 2003.

Falkowski, P., Scholes, R., J, Boyle, E., Canadell, J., Canfield, D., Elser, J., Gruber, N., Hibbard, K., Högberg, P., *The Global Carbon Cycle: A Test of Our Knowledge of Earth as a System*, Science, **290 (5490)**, 291-296, 2000.

Falkowski, P., Raven, J., *Photosynthesis and primary production in nature*, Aquatic Photosynthesis, 2nd ed., Princeton University, 2007.

Falkowski, P., *Ocean Science: The power of plankton*, Nature, **483 (7387)**, S17-S20, 2012.

Fasham, J. M., Ducklow, H. W., McKelvie, S. M., *A nitrogen-based model of plankton dynamics in the oceanic mixed layer*, Journal of Marine Research, **48 (3)**, 591-639, 1990.

Fontana, C., Grenz, C., Pinazo, C., Marsaleix, P., Diaz, F., *Assimilation of SeaWiFS chlorophyll data into a 3D-coupled physical–biogeochemical model applied to a freshwater-influenced coastal zone*, Continental Shelf Research, **29 (11-12)**, 1397-1409, 2009.

Ford D. A., Edwards K. P., Lea, D., Barciela, R. M., Martin, M. J., Demaria, J., *Assimilating GlobColour ocean colour data into a pre-operational physical-biogeochemical model*, *Ocean Science,* **8 (5),** 751-771, 2012.

Ford, D., A., van der Molen, J., Hyder, K., Bacon, J., Barciela, R., Creach, V., Forster, R. et al., *Observing and modelling phytoplankton community structure in theNorth Sea: can ERSEM-type models simulate biodiversity?*, Biogeosciences Discussions, 1-39, 2016.

Freidrichs, M. A., Dusenberry, J. A., Anderson, L. A., Armstrong, R. A., Chai, F., Christian, J. R., Doney, S. C., *Assessment of skill and portability in regional*

marine biogeochemical models: Role of multiple planktonic groups, Journal of Geophysical Research, **112 (C8)**, 2007.

Fukumori, I., *A Partitioned Kalman Filter and Smoother*, Monthly Weather Review, **130(5)**, 1370-1383, 2002.

Furuya, K., Hasegawa, O., Yoshikawa, T., Taguchi, S., *Photosynthesis-irradiance relationship of phytoplankton and primary production in the vicinity of Kuroshio warm core ring in spring*, Journal of Oceanography, **54 (5)**, 545-552, 1998.

Gandin, L. S., *Objective Analysis of Meteorological Fields*, Leningrad: Gridromet, 1963.

Gehlen, M., Barciela, R., Bertino, L., Brasseur, P., Butenschön, M., Chai, F., Crise, A. et al., *Building the capacity for forecasting marine biogeochemistry and ecosystems: recent advances and future developments*, Journal of Operational Oceanography, **8 (1)**, s168-s187, 2015.

Geider, R. J., *Light and temperature dependence of the carbon to chlorophyll a ratio in microalgae and cyanobacteria: implications for physiology and growth of phytoplankton*, New Phytologist, **106 (1)**, 1-34, 1987.

Geider, R. J., MacIntyre, H. L., Kana, T. M., *Dynamic model of phytoplankton growth and acclimation:responses of the balanced growth rate and the chlorophyll a:carbon ratio to light, nutrient-limitation and temperature*, Marine Ecology Progress Series, **148**, 187-200, 1997.

Gentleman, w., Leising, A., Frost, B., Strom, S., Murray, J., *Functional responses for zooplankton feeding on multiple resources: a review of assumptions and biological dynamics*, Deep Sea Research Part II: Topical Studies in Oceanography, **50(22-26)**, 2847-2875, 2003.

Giering, L. S., Sanders, R., Lampitt, R. S., Anderson, T. R., Tamburini, C., Boutrif, M., Zubkov, M. V. et al., *Reconciliation of the carbon budget in the ocean's twilight zone*, Nature, **507 (7493)**, 480-483, 2014.

Gregg, W., W., Friedrichs, M., A., Robinson, A., R., Rose, K.,A., Schlitzer, R., Thompson, K., R., Doney, S., C., *Skill assessment in ocean biological data assimilation*, Journal of Marine Systems, **76(1-2)**, 16-33, 2009.

Groom, S., Martinez-Vicente, V., Fishwick, J., Tilstone, G., Moore, G., Smyth, T., Harbour, D., The Western English Channel observatory: Optical char acteristics of station L4, *Journal of Marine Systems*, **77 (3)**, 278-295, 2009.

Hansell, D., A., *Recalcitrant Dissolved Organic Carbon Fractions,* Annual Review of Marine Science, **5(1)**, 421-445, 2013.

Harris, R., The L4 time-series: the first 20 years, *Journal of Plankton Research*, **32 (5)**, 577-583, 2010.

Heath, M., Gallego, A., *From the biology of the individual to the dynamics of the population: bridging the gap in fish early life studies*, Journal of Fish Biology, **51**, 1-29, 1997.

Hoteit, I., Triantafyllou, G., Petihakis, G., Allen, I., J., *A singular evolutive extended Kalman filter to assimilate real in situ data in a 1-D marine ecosystem model*, Annales Geophysicae, **21(1)**, 389-397, 2003.

Hoteit, I., Pham, D., *An adaptively reduced-order extended Kalman filter for data assimilation in the tropical Pacific*, Journal of Marine Systems, **45(3-4)**, 173-188, 2004.

Hunt B. R., Kostelich, E. J., Szunyogh, I., *Efficient data assimilation for spatiotemporal chaos: A local ensemble transform Kalman filter*, Physica D: Nonlinear Phenomena, **230 (1-2),** 112-126, 2007

Ishizaka, J., *Coupling of coastal zone color scanner data to a physical-biological model of the southeastern U.S. continental shelf ecosystem: 2. An Eulerian model*, Journal of Geophysical Research, **95 (C11)**, 20183–20199, 1990.

Jackson, T., Sathyendranath, S., Mélin, F., *An improved optical classification scheme for the Ocean Colour Essential Climate Variable and its applications*, Remote Sensing of Environment, **203**, 152-161, 2017.

Jazwinski, A. H., *Stochastic Processes and Filtering Theory*, Academic Press : New York, 1970.

Jiao, N. H., Herndl, G. J., Hansell, D. A., Benner R., Kattner, G., Wilhelm, S. W., Kirchman, D. L. et al., *Microbial production of recalcitrant dissolved organic matter: long-term carbon storage in the global ocean*, Nature Reviews Microbiology, **8 (8)**, 593-599, 2010.

Jiao, N. H., Robinson, C., Azam, F., Thomas, H., Baltar, F., Dang, H., Hardman-Mountford, N. J. et al., *Mechanisms of microbial carbon sequestration in the ocean – future research directions*, Biogeosciences, **11 (19)**, 5285- 5306, 2014.

Kähler, P., Bjornsten, P., K., Karin L., Antia A., *Dissolved organic matter and its utilization by bacteria during spring in the Southern Ocean,* Deep Sea Research Part II: Topical Studies in Oceanography, ***44 (1-2)***, *341-353, 1997.*

Losa, S. N., Kivman, G. A., Schröter, J., Wenzel, M., *Sequential weak constraint parameter estimation in an ecosystem model*, Journal of Marine Systems, **43 (1-2)**, 31-49.

Kalman, R. E., *A New Approach to Linear Filtering and Prediction Problems*, Journal of Basic Engineering, **82 (1)**, 35, 1960.

Kalnay, E., Toth, Z., *Removing growing errors in the analysis cycle*, Tenth conference on numerical weather prediction, 1994.

Korres, G., Triantafyllou, G., Petihakis, G., Raitsos, D., Hoteit, I., Pollani, A., Tsiaras, K., et al., *A data assimilation tool for the Pagasitikos Gulf ecosystem dynamics: Methods and benefits*, Journal of Marine Systems, **94**, S102- S117, 2012.

Le Clainche, Y., Vézina, A., Levasseur, M., Cropp, R., A., Gunson, J., R., Vallina, S., M., Vogt, M., *A first appraisal of prognostic ocean DMS models and prospects for their use in climate models*, Global Biogeochemical Cycles, **24 (3)**, 2010.

Le Dimet, F., Talagrand, O., *Variational algorithms for analysis and assimilation of meteorological observations: theoretical aspects*, **38A (2)**, 97-110, 1986.

Le Quere, C., Harrison, S. P., Prentice, C. I., Buitenhuis, E. T., Aumont, O., Bopp, L., Claustre., H. et al., *Ecosystem dynamics based on plankton functional types for global ocean biogeochemistry models*, Global Change Biology, **11 (11)**, 2016-2040, 2005.

Legendre, L., Rivkin, R. B., Weinbauer, M. G., Guidi, L., Uitz, J., *The microbial carbon pump concept: Potential biogeochemical significance in the globally changing ocean*, Progress in Oceanography, **134**, 432-450, 2015.

Lenartz, F., Raick, C., Soetaert, K., Grégoire, M., *Application of an Ensemble Kalman filter to a 1-D coupled hydrodynamic-ecosystem model of the Ligurian Sea*, Journal of Marine Systems, **68 (3-4)**, 327-348, 2007.

Lewis, K., Allen, J., *Validation of a hydrodynamic-ecosystem model simulation with time-series data collected in the western English Channel*, Journal of Marine Systems, **77 (3)**, 296-311, 2009.

Litt, E., J., Hardman-Mountford, N., J., Blackford, J., C., Mitchelson-Jacob, G., Goodman, A., Moore, G., F., Butenschon, M., et al., *Biological control of pCO2 at station L4 in the Western English Channel over 3 years,* Journal of Plankton Research, **32 (5)**, 621-629, 2010.

Losa, S. N., Kivman, G. A., Schröter, J., Wenzel, M., *Sequential weak constraint pa rameter estimation in an ecosystem model*, Journal of Marine Systems, **43 (1-2)**, 31-49, 2003.

Macedo, M. F., Duarte, P., *Phytoplankton production modelling in three marine ecosystems—static versus dynamic approach*, Ecological Modelling, **190 (3-4)**, 299-316, 2006.

Matear, R. J., *Parameter optimization and analysis of ecosystem models using simulated annealing: A case study at Station P*, Journal of Marine Research, **53 (4)**, 571-607, 1995.

Mattern, J., P., Dowd, M., Fennel, K., *Sequential data assimilation applied to a physical–biological model for the Bermuda Atlantic time series station*, Journal of Marine Systems, **79 (1-2)**, 144-156, 2010.

Mattern, J. P., Dowd, M., Fennel, K., *Particle filter-based data assimilation for a three-dimensional biological ocean model and satellite observations*, Journal of Geophysical Research: Oceans, **118 (5)**, 2746-2760, 2013.

Mellor, G., L., Yamada, T., *A Hierarchy of Turbulence Closure Models for Planetary Boundary Layers*, Journal of the Atmospheric Sciences, **31(7),** 1791-1806, 1974.

Michaels, A., F., *Overview of the U.S. JGOFS Bermuda Atlantic Time-series Study and the Hydrostation S program*, Ecological Time Series, 181-201, 1995.

Michaels, A., F., Siegel, D., A., Johnson, R., J., Knap, A., H., Galloway, J., N., *Episodic inputs of atmospheric nitrogen to the Sargasso Sea: Contributions to new production and phytoplankton blooms*, Global Biogeochemical Cycles, **7(2),** 339-351, 1993.

Moore, T., S., Campbell, J., W., Dowell, M., D., *A class-based approach to characterizing and mapping the uncertainty of the MODIS ocean chlorophyll product*, Remote Sensing of Environment, **113 (11)**, 2424-2430, 2009.

Nelson, N., B., Siegel, D.,A., Michaels, A., F., *Seasonal dynamics of colored dissolved material in the Sargasso Sea*, Deep Sea Research Part I: Oceanographic Research Papers, **45 (6),** 931-957, 1998.

Natvik, L., Evensen, G., Assimilation of ocean colour data into a biochemical model of the North Atlantic, *Journal of Marine Systems*, **40-41**, 155-169, 2003.

Nerger, L., Gregg, W., W., Assimilation of SeaWiFS data into a global ocean-bio geochemical model using a local SEIK filter, *Journal of Marine Systems*, **68 (1-2)**, 237-254, 2007.

Nightingale, P., D., Liss, P., S., Schlosser, P., *Measurements of air-sea gas transfer during an open ocean algal bloom*, Geophysical Research Letters, **27(14)**, 2117-2120, 2000.

Parslow, J., Cressie, N., Campbell, E. P., Jones, E., Murray, L., *Bayesian learning and predictability in a stochastic nonlinear dynamical model*, Ecological Applications, **23 (4)**, 679-698, 2013.

Philips, H., E., Joyce, T., M., *Bermuda's Tale of Two Time Series: Hydrostation S and BATS*, Journal of Physical Oceanography, **37 (3)**, 554-571, 2007.

Polimene, L. J., Allen, J. I., Zavatarelli, M., *Model of interactions between dissolved organic carbon and bacteria in marine systems*, Aquatic Microbial Ecology, **43**, 127-138, 2006.

Polimene, L., Brunet, C., Allen, I., J., Butenschon, M., White, D., A., Llewellyn, C., A., *Modelling xanthophyll photoprotective activity in phytoplankton*, Journal of Plankton Research, **34(4)**, 196-207, 2012.

Polimene, L., Brunet, C., Butenschon, M., Martinez-Vicente, V., Widdicombe, C., E., Torres, R., Allen, I., J., *Modelling a light-driven phytoplankton succession, Journal of Plankton Research*, **36 (1)**, 214-229, 2014.

Polimene, L., Mitra, A., Sailley, S., Ciavatta, S., Widdicombe, C., Atkinson, A., Allen, J., Decrease in diatom palatability contributes to bloom forma tion in the Western English Channel, *Progress in Oceanography*, **137**, 484-497, 2015.

Polimene, L., Sailley, S., E., Clark, D., R., Mitra, A., Allen, I., J, *Biological or Micro bial Carbon Pump? The role of phytoplankton stoichiometry in ocean carbon sequestration,* Journal of Plankton Research, **39(2)**, 180-186, 2016.

Polimene, L. J., Clark, D., Kimmance, S., McCormack, P., *A substantial fraction of phytoplankton-derived DON is resistant to degradation by a metabolically versatile, widely distributed marine bacterium*, PloS One, **12 (2)**, e0171391, 2017.

Raanes, N., P., Carrassi, A., Bertino, L., *Extending the Square Root Method to Account for Additive Forecast Noise in Ensemble Methods,* Monthly Weather Review, **143 (10)**, 3857-3873, 2015.

Redfield, A.C., *On the proportions of organic derivations in sea water and their relation to the composition of plankton*, James Johnstone Memorial Volume of the University Press of Liverpool, 176–192, 1934.

Rees, A., Gilbert, J., Kelly-Gerreyn, B., Nitrogen fixation in the western English Channel (NE Atlantic Ocean), *Marine Ecology Progress Series*, **437**, 7-12, 2009.

Ridgewell, A., Zeebe, R. E., *Past changes of ocean carbonate chemistry*, Ocean Acidifcation, Oxford University Press, 2006.

Sasaki, Y., *An Objective Analysis Based on the Variational Method*, Journal of the Meteorological Society of Japan, **36**, 77-88, 1958.

Semovski, S. V., Wozniak, B., Hapter, R., Staskiewicz, A., *Gulf of Gdansk spring bloom physical, bio-optical, biological modelling and contact data assimilation*, Journal of Marine Systems, **7 (2-4)**, 145-149, 1996.

Siddorn, J., R., Allen, I., J., *Surface heat fluxes and ecosystem function in the Cretan Sea (eastern Mediterranean): a modelling study*, Annales Geophysicae, **21(1),** 377-388, 2003.

Sigman, D. M., Haug, G. H., *The biological pump in the past*, The Oceans and Marine Geochemistry, **6**, 2003.

Simon, E., Bertino, L., *Application of the Gaussian anamorphosis to assimilation in a 3-D coupled physical-ecosystem model of the North Atlantic with the EnKF: a twin experiment*, Ocean Science, **5(4)**, 495-510, 2009.

Smyth, T., J., Fishwick, J., R., Al-Moosawi, L., Cummings, D., G., Harris, C., Kitidis, V., Woodward, E., M., et al., *A broad spatio-temporal view of the Western English Channel observatory*, Journal of Plankton Research, **32(5)**, 585-601, 2009.

Snyder, C., Bengtsson, T., Bickel, P., Anderson, J., *Obstacles to High-Dimensional Particle Filtering*, Monthly Weather Review, **136 (12),** 4629-4640, 2008.

Spitz, Y., H., Moisan, J., R, Abbott, M., R., Richman, J., G., *Data assimilation and a pelagic ecosystem model: parameterization using time series observations*, Journal of Marine Systems, **16 (1-2)**, 51-68, 1998.

Steinberg, D., K., Carlson, C., A., Bates, N., R., Johnson, R., J., Michaels, A., F., Knaps, A., H., *Overview of the US JGOFS Bermuda Atlantic Time-series Study (BATS): a decade-scale look at ocean biology and biogeochemistry*, Deep Sea Research Part II: Topical Studies in Oceanography, **48 (8-9)**, 1405-1447, 2001.

Stern, R., F., Picard, K., T., Hamilton, K., M., Waine, A., Tarran, G., A., Mils, D., Edwards, M., Novel lineage patterns from an automated water sampler to probe marine microbial biodiversity with ships of opportunity, *Pro gress in Oceanography*, **137**, 409-420, 2015.

Stoecker, D., K., Hansen, P., J., Caron, D., A., Mitra, A., Mixotrophy in the Marine Plankton, *Annual Review of Marine Science*, **9 (1)**, 311-335, 2017.

Tait, K., Airs, R., L., Widdicombe, C., E., Tarran, G., A., Jones, M., R., Wid dicombe, S., Dynamic responses of the benthic bacterial community at the Western English Channel observatory site L4 are driven by deposition of fresh phytodetritus, *Progress in Oceanography*, **137**, 546-558, 2015.

Tarran, G., A., Bruun, J., T., Nanoplankton and picoplankton in the Western Eng lish Chan nel: abundance and seasonality from 2007–2013, *Progress in Oceanography*, **137**, 446-455, 2015.

Torres, R., Allen, I. J., Figueiras, F. G., *Sequential data assimilation in an upwelling influenced estuary*, Journal of Marine Systems, **60 (3-4)**, 317-329, 2006.

Toyoda, T., Awaji, T., Masuda, S., Sugiura, N., Igarashi, H., Sasaki, Y., Hiyoshi, Y. et al., *Improved state estimations of lower trophic ecosystems in the global ocean based on a Green's function approach*, Progress in Oceanography, **119**, 90-107, 2013.

Triantafyllou, G., Hoteit, I, Petihakis, G., *A singular evolutive interpolated Kalman filter for efficient data assimilation in a 3-D complex physical–biogeochemical model of the Cretan Sea*, Journal of Marine Systems, **(40-41)**, 213-231, 2003.

Triantafyllou, G., Korres, G., Hoteit, I., Petihakis, G., Banks, A., C., Assimilation of ocean colour data into a Biogeochemical Flux Model of the Eastern Mediterranean Sea, *Ocean Science,* **3(3)**, 397-410, 2007.

Triantafyllou, G., Hoteit, I., Luo, X., Tsiaras, K., Petihakis, G., *Assessing a robust en semble-based Kalman filter for efficient ecosystem data assimilation of the Cre tan Sea*, Journal of Marine Systems, **125**, 90-100, 2013.

van Leeuwen, P. J., *Particle Filtering in Geophysical Systems*, Monthly Weather Review, **137 (12)**, 4089-4114, 2009.

van Leeuwen, P. J., *Nonlinear data assimilation in geosciences: an extremely efficient particle filter*, Quarterly Journal of the Royal Meteorological Society, **136 (653)**, 1991-1999, 2010.

Volk, T. J., Hoffert, M. I., *Ocean Carbon Pumps: Analysis of Relative Strengths and Efficiencies in Ocean-Driven Atmospheric CO2 Changes*, The Carbon Cycle and Atmospheric CO2: Natural Variations Archean to Present, 99-110, 1985.

Wakelin, L. S., Holt, J. T., Blackford, J. C., Allen, J. I., Butenschön, M., Artioli, Y., *Modeling the carbon fluxes of the northwest European continental shelf:*

Validation and budgets, Journal of Geophysical Research: Oceans, **117 (C5),** 2012.

Whitaker, J., S., Hamill, T., M., *Evaluating methods to account for system errors in ensemble data assimilation*, Monthly Weather Review, **140(9),** 3078-3089, 2012.

Worthington, L. V., *On the North Atlantic Circulation,* The Johns Hopkins Oceanographic Studies 6, 110, 1976.

Zhang, Y., Song, C., Band, L. E., Sun, G., Li, J., *Reanalysis of global terrestrial vegetation trends from MODIS products: Browning or greening?*, Remote Sensing of Environment, **191**, 145-155, 2017.

Zhu, M., van Leeuwen, P. J., Amezcua, J., *Implicit equal-weights particle filter*, Quarterly Journal of the Royal Meteorological Society, **142 (698)**, 1904-1919, 2016.

Zibordi, G., Holben, B., Mélin, F., D'Alimonte, D., Berthon, J., F., Slutsker, I., et al., *AERONET-OC: an overview,* Canadian Journal of Remote Sensing, **36**, 488-497, 2010.